Journal of Building Engineering 57 (2022) 104871

Contents lists available at ScienceDirect

Journal of Building Engineering

journal homepage: www.elsevier.com/locate/jobe

One part alkali activated materials: A state-of-the-art review

M. Elzeadani [a,*], D.V. Bompa [a,b], A.Y. Elghazouli [a]

[a] Department of Civil and Environmental Engineering, Imperial College, London, UK
[b] Department of Civil and Environmental Engineering, University of Surrey, UK

ARTICLE INFO

Keywords:
One-part alkali-activated materials
One-part geopolymers
Aluminosilicate precursors
Solid activators
Fresh properties
Mechanical properties
Durability characteristics

ABSTRACT

This article assesses the state-of-the-art for research on one-part alkali-activated materials, with particular emphasis on recent work dealing with the constituent materials, preparation methods, fresh properties, mechanical properties, and durability characteristics. The review, which covers over 170 studies, first discusses the different precursors, solid activators, admixtures, and aggregates used within such materials. Preparation techniques of one-part alkali-activated materials are then addressed, including pre-mixing treatment, mixing and curing, and 3D-printing. Reaction mechanisms and resulting binding phases are also outlined, followed by a detailed discussion on the fresh, mechanical and durability characteristics. The sensitivity of the compressive strength to different precursors and solid activators with varying chemical compositions, is examined, and predictive strength equations are proposed for common mixes. A brief comparison between the fresh, mechanical and durability characteristics of one-part and two-part AAMs is outlined, followed by a discussion on design standards as well as health and environmental aspects. The review concludes with suggestions for future research for key applications, with due consideration to the projected availability of precursors and the sustainability of solid activators. It is shown that despite the significant recent developments on one-part alkali-activated materials, further progress necessitates future research with a focus on optimising mixes made from precursors other than fly ash and blast furnace slag, as well as detailed investigations on structural members and components.

Abbreviations

AA	Alkali-activated
AAC	Alkali-activated concrete
AAMs	Alkali-activated materials
ABA	Almond-shell biomass ash
ACI	Activity concentration index
ACS	Air-cooled slag
BOF	Basic oxygen furnace
C-A-S-H	Calcium-aluminium-silicate-hydrate
CCM	Conventional concrete material
CCR	Calcium carbide residue

* Corresponding author.
E-mail address: m.el-zeadani20@imperial.ac.uk (M. Elzeadani).

https://doi.org/10.1016/j.jobe.2022.104871
Received 21 April 2022; Received in revised form 16 June 2022; Accepted 22 June 2022
Available online 27 June 2022

CHA	Coffee husk ash
CK	Cement clinker
CKD	Cement kiln dust
COV	Coefficient of variation
CoW	Concrete waste
CSA	Cotton shell ash
CW	Ceramic waste
FA	Fly ash
FASB	Fly ash sinking beads
FS	Fayalite slag
GGBS	Ground granulated blast furnace slag
GLA	Geopolymer lightweight aggregates
GMT	Gold mine tailings
GS	Geothermal silica
IMT	Iron ore mine tailings
LKD	Lime kiln dust
LS	Lithium slag
LZMT	Lead-zinc mine tailings
MCA	Maize cob ash
MK	Metakaolin
MSA	Maize stalk ash
MSW	Municipal solid waste
MSWI BA	Municipal solid waste incinerated bottom ash
MSWI FA	Municipal solid waste incinerated fly ash
N-A-S-H	Sodium-aluminum-silicate-hydrate
NORMs	Naturally occurring radioactive materials
NS	Nickel slag
OBA	Olive stone biomass ash
OPC	Ordinary Portland cement
PS	Paper sludge
RH	Relative humidity
RHA	Rice husk ash
RM	Red mud
SCM	Supplementary cementitious material
SEM	Scanning electron microscopy
SF	Silica fume
SP	Superplasticizer
SR	Silica residue
s/agg	Solid-to-aggregate ratio
VT	Vanadium tailings
WBA	Wood biomass ash
WG	Waste glass
w/b	Water-to-binder ratio
w/s	Water-to-solid ratio
XRD	X-ray diffraction

Chemical symbols/formulae

^{226}Ra	Radium series
^{232}Th	Thorium series
^{40}K	Potassium
Al_2O_3	Aluminum oxide
$Al(OH)_3$	Aluminum hydroxide
$Al_2Si_2O_7$	Metakaolin
$Al_2SiO_5(OH)_4$	Kaolinite
$Ba(OH)_2$	Barium hydroxide
$Ba(OH)_2{\cdot}8H_2O$	Barium hydroxide octahydrate
$C_6H_{11}NaO_7$	Sodium gluconate
Ca	Calcium
$CaCl_2$	Calcium chloride
$CaCO_3$	Calcium carbonate
CaO	Calcium oxide

$Ca(OH)_2$	Calcium hydroxide
Cl	Chlorine
CO_2	Carbon dioxide
Fe_2O_3	Iron oxide
H	Hydrogen
HNO_3	Nitric acid
H_2O	Water
H_2O_2	Hydrogen peroxide
H_2SO_4	Sulfuric acid
H_3PO_4	phosphoric acid
K	Potassium
K_2CO_3	Potassium carbonate
K_2O	Potassium oxide
K_2SiO_3	Potassium silicate
KOH	Potassium hydroxide
Li_2CO_3	Lithium carbonate
LiOH	Lithium hydroxide
Mg	Magnesium
MgO	Magnesium oxide
$Mg(OH)_2$	Magnesium hydroxide
$MgSO_4$	Magnesium sulphate
Na	Sodium
$NaAlO_2$	Sodium aluminate
$NaHCO_3$	Sodium bicarbonate
NaOH	Sodium hydroxide
$Na_2B_4O_7{\cdot}10H_2O$	Sodium tetraborate decahydrate-borax
Na_2CO_3	Sodium carbonate
Na_2O	Sodium oxide
$Na_5P_3O_{10}$	Sodium triphosphate
$Na_2Si_2O_5$	Sodium disilicate
Na_2SiO_3	Sodium silicates
$Na_2SiO_3{\cdot}5H_2O$	Sodium metasilicate pentahydrate
$Na_2SiO_3{\cdot}9H_2O$	Sodium metasilicate nonahydrate
Na_2SO_4	Sodium sulphate
OH	Hydroxide
SiO_2	Silicon dioxide
SO_3	Sulphur trioxide
Symbols	
C_{226Ra}	Concentrations of ^{226}Ra in Bq/kg
C_{232Th}	Concentrations of ^{232}Th in Bq/kg
C_{40K}	Concentrations of ^{40}K in Bq/kg
d_{50}	Median particle size
f_c	Compressive strength
$f_{c,pred}$	Predicted compressive strength
$f_{c,test}$	Test compressive strength
f_f	Flexural strength
f_{sp}	Splitting tensile strength
M_s	Modulus of silicates
Q_A	Alkali-quality coefficient

1. Introduction

The motivation for much of the current research on alkali-activated materials (AAMs) is to tackle the environmental impact of ordinary Portland cement (OPC) production. The latter, a main constituent material in concrete, is responsible for nearly 5–7% of all carbon dioxide (CO_2) emissions worldwide [1]. Conventional AAMs typically consist of an aluminosilicate precursor, also known as a starting material or source material, mixed with an alkaline solution [2]. The precursors can be obtained from natural sources, such as metakaolin (MK); or from waste streams such as fly ash (FA), ground granulated blast furnace slag (GGBS), and red mud (RM). These starting materials have chemical compositions that are attractive from a cementitious point of view, comprising silicon dioxide (SiO_2), aluminum oxide (Al_2O_3) and often calcium oxide (CaO). Alkaline solutions employed in AAMs include alkali-hydroxides (i.e.,

sodium/potassium hydroxides), non-silicic salts (sodium/potassium carbonates) or silicic salts (sodium/potassium silicates) [3]. AAMs are attractive as they not only avoid OPC usage, but also provide a valorisation path for industrial and agricultural waste. However, the caustic nature of the alkaline solutions has hampered their wide acceptance [4,5].

As an alternative, researchers considered one-part 'just-add-water' AAMs, where a solid aluminosilicate precursor is mixed with a solid alkaline activator as a first step, and then water is added to initiate the reaction. Real interest in one-part AAMs, as indicated by research articles published on the topic, has increased substantially in recent years. The research community tinkered with different precursors, solid activators, and admixtures to synthesize one-part AAMs with real practical potential. Much of the research on one-part AAMs after 2010 was mainly focused on the microstructural level, highlighting binding phases, microscopic characteristics, and compressive strength of different combinations of constituent materials. In the past four years, research on one-part AAMs has grown rapidly with different motivations, including valorising more waste materials as aluminosilicate precursors, or finding more sustainable solid activators. Also, the rise in research studies on one-part AAMs has brought with it more understanding of the fresh, mechanical and durability properties.

This review is undertaken to assess the advancement in knowledge on one-part AAMs, particularly in the past four years. The review initially highlights the variety of precursors, solid activators, aggregates, water type and admixtures used to form one-part AAMs. Different pre-treatment methods used in one-part AAMs are also reviewed, followed by a discussion on the mixing method, curing regimes and 3D-printing. The reaction mechanisms and resulting binding phases of one-part alkali-activation are highlighted briefly, followed by an in-depth discussion on the fresh, mechanical and durability characteristics. Given the wide scope of precursors and activators used in one-part AAMs, as well as the varying water and aggregate contents adopted, predictive equations are proposed as a general guide for common one-part AAMs. A comparison between the fresh, mechanical and durability characteristics of one-part and two-part AAMs is given as well, followed by a discussion on design standards for AAMs and health and environmental aspects associated with their use. The review finally identifies gaps in the literature requiring further investigation, by covering potential niche applications, availability of precursors in the future, sustainability of solid activators, the need for structural level testing, and the importance of developing performance-based design standards.

2. Constituent materials

2.1. Aluminosilicate precursors

Precursors in AAMs are generally derived from waste streams or natural sources. Their selection has broadened in recent years, mainly to find alternative sources to well-established but limited precursors or to provide a valorisation path for a range of waste products. Fig. 1 depicts scanning electron microscopy (SEM) images of common precursors in one-part AAMs, while Fig. 2 and Fig. 3 present a summary of the chemical composition of common precursors and their annual generation rates, respectively, as compiled from the studies reviewed in this article.

2.1.1. Industrial by-products and waste material

One of the most common industrial by-products used as a precursor in one-part AAMs is FA. Around 750–800 million tons are generated annually from thermal power plants worldwide [6]. Low-calcium FA, also known as Class F FA, is a by-product of burning bituminous coal in power plants [7], while high-calcium FA (Class C FA) is the result of burning lignite and sub-bituminous coal [8].

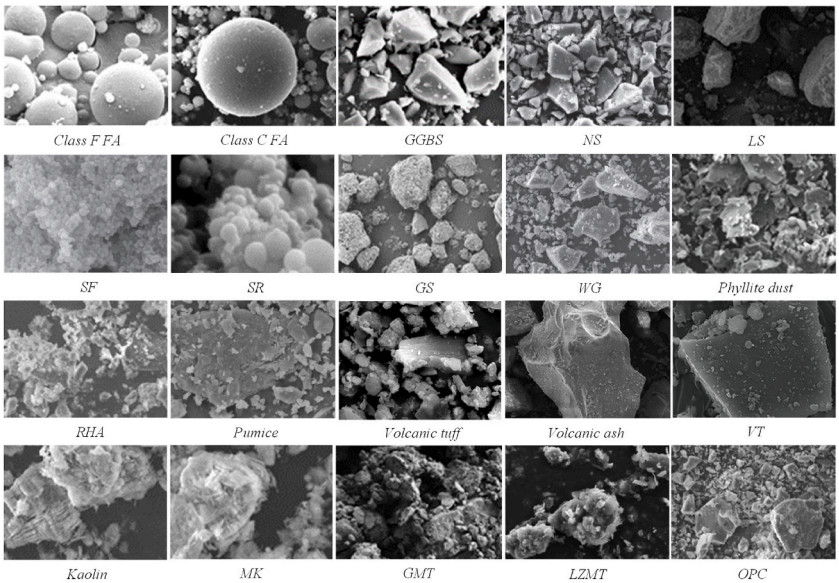

Fig. 1. SEM images of aluminosilicate precursors: Class F FA [42], *Class C FA* [90], *GGBS* [124], *NS* [31], *LS* [23], *SF* [164], *SR* [39], *GS* [209], *WG* [164], *phyllite dust* [139], *RHA* [34], *pumice* [70], *Volcanic tuff* [67], *Volcanic ash* [72], *VT* [49], *Kaolin* [210], *MK* [210], *GMT* [45], *LZMT* [48], *OPC* [117].

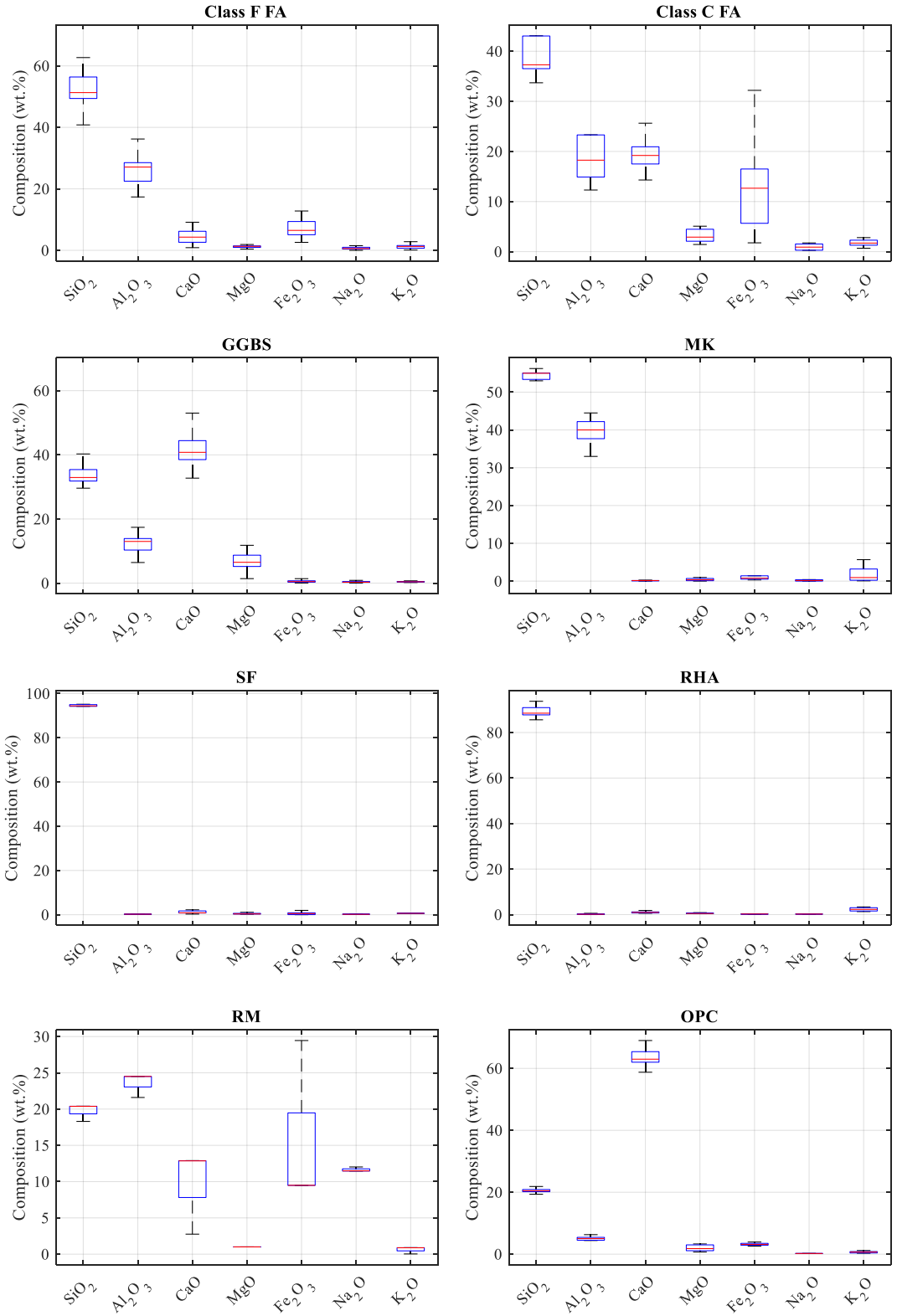

Fig. 2. Chemical composition of common aluminosilicate precursors and OPC.

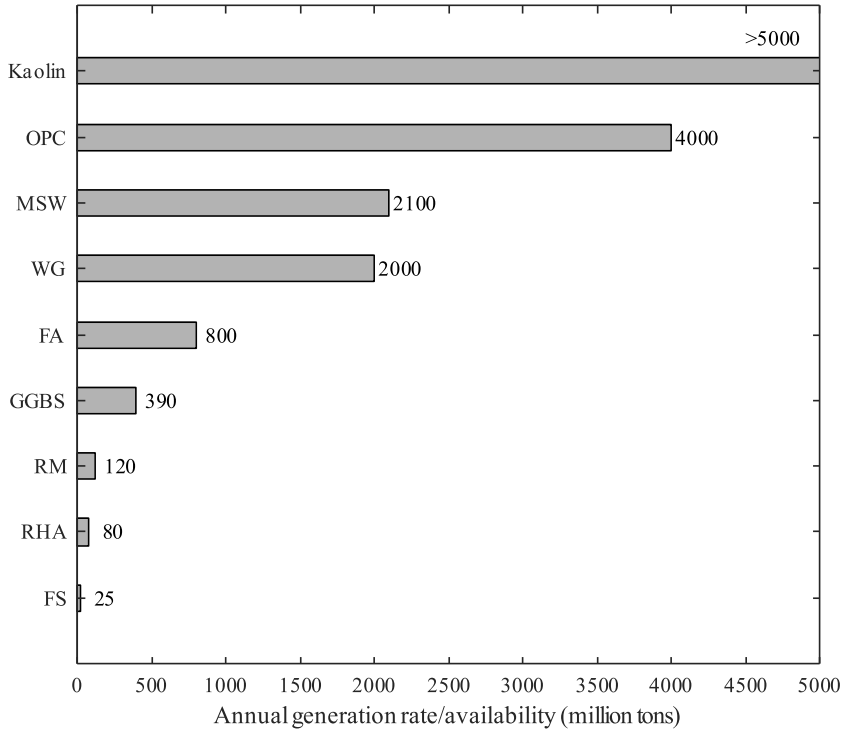

Fig. 3. Annual availability of aluminosilicate precursors.

Low-calcium FA is generally richer in SiO_2, Al_2O_3 and iron oxide (Fe_2O_3) when compared to high-calcium FA, and its CaO content is less than 15 wt%, while high-calcium FA has a CaO content in the range of 15–30 wt% (Fig. 2) [9]. FA particles are spherical in shape and consist mainly of a vitreous/glassy phase with minor crystalline peaks, including quartz, mullite and magnetite [10]. Recent studies on one-part AAMs have used fly ash sinking beads (FASB) as precursors [11–13]. Conventional FA contains spherical micro-beads which, depending on their density, can be classified as floating or sinking beads [13]. FASB particles are spherical, finer in size than conventional FA and have a more amorphous structure, making them more reactive in alkaline environments [11,12]. Despite the wide use of FA as a precursor in one-part AAMs, its production in the future is expected to reduce significantly as coal-fired power plants shut down in most developed economies and electricity production turns to greener methods [14]. Also, the wide use of FA as a supplementary cementitious material (SCM) in conventional concrete will inevitably create competitive demand pressure for its use [15]. This might indeed limit the ability of FA to act as a viable precursor for wide-scale use in one-part AAMs. Another by-product of coal-fired power plants that was recently used as a precursor to form one-part alkali-activated (AA) foamed concrete is cenospheres [16]. This by-product is characteristically lightweight with spherical and hollow particles [17,18]. The chemical composition of cenospheres is rich in SiO_2 and Al_2O_3 and their mineral phase structure is generally amorphous with distinct crystalline peaks of quartz and mullite [16].

GGBS is another industrial by-product that was used intensively in one-part AAMs and has an annual generation rate of 270–390 million tons [14]. A by-product of iron manufacturing, GGBS is formed by collecting the molten material resulting from heating iron at temperatures as high as 1600 °C in a blast furnace. This molten product is then quenched rapidly to produce GGBS with a glassy phase [19]. The chemical composition of GGBS mainly includes CaO, magnesium oxide (MgO), Al_2O_3 and SiO_2 [19]. GGBS has on average 90–95% vitreous/glassy phase with minor crystalline phases including gehlenite and akermanite [20]. The shape of GGBS particles is angular and uneven as shown in Fig. 1 [21]. Slow cooling of the molten material from which GGBS is derived results in a crystalline stone-like substance known as air-cooled slag (ACS). ACS was used in one-part AAMs as it retains similar chemical and mineralogical structures to that of GGBS; however, it is less reactive and requires thermal activation in the presence of a fluxing material, rapid quenching and crushing before use [22]. Similar to FA, GGBS is used heavily as an SCM in OPC-based conventional concrete material (CCM) and its future supply is expected to dwindle as steel production becomes cleaner [15]. This forecasted lower supply of GGBS is a key issue when considering its future use in wide-scale applications of AAMs.

Lithium slag (LS) was utilized as a precursor in recent one-part AAM studies [23,24]. It is a waste residue from lithium carbonate (Li_2CO_3) production, and estimates suggest that about 10 tons of LS are generated for each ton of Li_2CO_3 produced [25]. The chemical composition of LS mainly consists of SiO_2, Al_2O_3 and sodium oxide (Na_2O) [26]. Fayalite slag (FS) is another industrial waste slag used in one-part AAMs [27,28]. FS is a waste material from copper manufacturing and has an annual production rate of about 24.6 million tons [29]. FS mainly consists of iron silicates, zinc silicates, Al_2O_3 and CaO [30], and X-ray diffraction (XRD) patterns of FS show mainly an amorphous phase with few fayalite and magnetite crystalline features [27]. Nickel slag (NS), a waste material from nickel-alloy production, was recently used in one-part AAMs [31,32]. The chemical composition of NS mainly consists of CaO, SiO_2,

and Al_2O_3 [31]. The particle shape of NS, much like that of GGBS, is non-uniform and angular as can be seen in Fig. 1. XRD patterns show that NS is amorphous with a broad hump in the 10–40° 2θ range.

Silica fume (SF) – also known as microsilica or silica dust – is a by-product of the smelting process in silicon and ferrosilicon alloy production [33,34]. The SiO_2 content of SF is usually more than 90% (Fig. 2), and it has an amorphous phase structure with very fine and highly spherical particles (Fig. 1) [35]. Besides SF, geothermal silica (GS) was used as a supplementary SiO_2 source in one-part AAMs [36,37]. A waste material from electricity production through stream extraction from geothermal fields, GS is made up of amorphous SiO_2, has high alkali content, with angular particle shapes as shown in Fig. 1. Silica residue (SR), a waste residue from chlorosilane production, was also utilized as a source of additional SiO_2 [38,39], and its SiO_2 content is in the range of 84–89%.

Red mud (RM), a common precursor in one-part AAMs, is an industrial waste material from alumina extraction through the Bayer process. The annual global production of RM is about 120 million tons [40,41], and its high alkalinity (pH in the range of 10–12.5), together with its chemical composition (>80% of SiO_2 + Fe_2O_3 + Al_2O_3 + Na_2O + CaO), makes it suitable as both precursor and activator. The mineral phase structure of RM shows crystalline peaks of mainly hematite and boehmite, as well as gibbsite, calcite, katoite, and cancrinite [41,42]. Cement kiln dust (CKD), used as well in one-part AAMs, is an industrial waste from the cement industry [43]. CKD is recovered from the exhaust gases of calcining limestone and other clay minerals to make cement in rotary kilns [44]. The chemical composition and mineral phase structure of CKD depends largely on the calcined material and fuel type, but mainly consists of quartz, lime, portlandite and calcite crystalline peaks [44].

2.1.2. Mine tailings

Mine tailings are a waste material from the mining industry generated during the separation of valuable minerals from invaluable waste [45]. Recent investigations on one-part AAMs used gold mine tailings (GMT), iron ore mine tailings (IMT), lead-zinc mine tailings (LZMT), and vanadium tailings (VT) as precursors [46–50]. GMTs – a waste material from mining gold – mainly consist of SiO_2 and Al_2O_3, and their mineral phase structure is highly crystalline with peaks including quartz, albite, microcline, and muscovite [51]. GMT particles are irregular in shape with pointed edges as shown in Fig. 1 [52]. IMTs, meanwhile, show chemical compositions that are rich in SiO_2 and Fe_2O_3, and have a crystalline phase structure with peaks including quartz, muscovite, and hematite [47]. LZMT were mainly used as supplementary precursors in one-part AAMs and their mineral phase structure consists of quartz, as well as calcite, pyrite and dolomite [48]. The chemical composition of LZMT is mainly rich in SiO_2, sulphur trioxide (SO_3), CaO and Fe_2O_3. VT, a predominant waste from extracting vanadium, was used mainly in combination with MK [49,50,53]. VT shares a similar chemical composition to the tailings above, making it ideal as a precursor with its high SiO_2 and Al_2O_3 contents.

2.1.3. Agricultural and other waste products

Considering agricultural waste products utilized as precursors, rice husk ash (RHA) is perhaps the most common. This high SiO_2 (>85%-weight) waste product is the result of burning rice husk generated from rice paddies at a temperature of around 600–800 °C [54–56]. Nearly 70–80 million tons of RHA are generated annually worldwide [57]. RHA particles are lightweight, have a porous microstructure and large surface areas, as shown in Fig. 1. Although adequate strengths were achieved using RHA as a lone precursor in one-part AAMs (7-day strengths ~30 MPa [54]), additional alumina sources are usually provided to ensure viable Si/Al ratios for long-term stability [58].

Waste glass (WG) powder was used as a supplementary precursor in one-part AAMs [59]. This waste material has a high generation rate estimated at around 2000 million tons [14]. WG is generally rich in SiO_2 and Al_2O_3, and has an irregular particle shape (Fig. 1). It requires heat treatment to achieve the dissolution of silica and alumina in alkaline environments. Concrete waste (CoW) was also employed as a precursor after pre-treatment, either separately or in combination with other precursors [60,61]. Pre-treated CoW shows a reactive glassy phase with several crystalline peaks of dolomite and quartz. Its chemical composition is mainly made of SiO_2, Al_2O_3, CaO, and Na_2O [60] and its particle shape is non-uniform with fine pores. Ceramic waste (CW), originally made of clay and other earth materials, has also found application as a precursor due to its high SiO_2 and Al_2O_3 contents [62,63]. CW represents a huge proportion of construction and demolition wastes, and their use in AAMs is usually as a supplementary source of SiO_2. Due to their highly crystalline phase structure, CW requires pre-treatment at elevated temperatures to enhance their reactivity.

Municipal solid waste incinerated fly ash (MSWI FA) and bottom ash (MSWI BA) were also used as supplementary precursors in one-part AAMs [40,56,64]. MSWI FA is recovered from the smoke resulting from the combustion of incinerated solid waste, while MSWI BA remains as residues at the bottom of the combustion furnace. Both MSWI FA and MSWI BA show high concentrations of CaO and their XRD patterns depict peaks of quartz and calcite; and calcite, portlandite, halite and periclase, respectively [56,64].

2.1.4. Natural sources of geological origins

MK was used extensively in one-part AAMs and results from the calcination of kaolinite clay at temperatures ranging from 450 to 800 °C [10,55]. The chemical composition of MK is rich in SiO_2 and Al_2O_3 as shown in Fig. 2 and its mineral phase structure shows crystalline peaks of quartz, illite, anatase and calcite [65]. The size of MK particles is usually less than 5 μm [66], and their shape is plate-like and non-uniform [67]. Another naturally derived precursor is feldspar, also known as albite. Feldspars are plentiful and form around 60% of the earth's crust. Their chemical composition contains SiO_2, Al_2O_3 and Na_2O [68]. Their mineral phase structure consists predominantly of albite, quartz and microcline and they require pre-treatment before use in AAMs [43]. Dolomite, from dolomite rocks, was also utilized as a precursor in one-part AAMs [69]. It has high concentrations of CaO, MgO and carbonates, and when calcined at high temperatures (900–1000 °C) can result in highly reactive material. XRD patterns of dolomite show peaks of calcite, lime, portlandite and periclase.

Reactive volcanic tuffs (e.g., pumice) were also used in one-part AAMs due to their high SiO_2 and Al_2O_3 content and amorphous phase structure [70]. Volcanic tuffs are igneous rocks formed from the hardening of ejected materials during a volcanic eruption. In

one-part AAM studies, volcanic tuffs used have a mean particle size of about 10 μm and are typically heated at temperatures ranging from 450 to 900 °C for 2–4 h to enhance their reactivity [67,70,71]. Volcanic ash collected during the eruption of volcanoes was also used in one-part AAMs [72]. The crystalline phase structure of volcanic ash shows traces of augite, anorthite, diopside, albite, quartz and hematite [72]. Much like volcanic tuffs, volcanic ashes require heat pre-treatment to enhance their reactivity.

2.2. Solid activators

Generally, a solid activator provides alkali cations (Na^+, K^+) or alkaline earth cations (Ca^{2+}, Mg^{2+}) that attack the Si–O–Si and Al–O–Al bonds in the precursors, causing the dissolution of silicon and aluminum and the formation of strength giving binding phases [73]. In that sense, many solid activators were employed in one-part AAMs, including synthetic activators and those derived from active waste products.

2.2.1. Synthetic solid activators

Among the well-studied synthetic activators in one-part AAMs are sodium silicates (Na_2SiO_3), commonly referred to as water glass. Commercial Na_2SiO_3 powder is white and spherical, and is produced by heating sodium carbonate (Na_2CO_3) and SiO_2 at temperatures as high as 1200 °C [74]. The resulting glass from this fusion is then dissolved in water to form a Na_2SiO_3 solution [19]. Estimates suggest that nearly 25 million tons of synthetic Na_2SiO_3 are produced annually, and for each 1 kg of Na_2SiO_3, nearly 1.2 kg of CO_2 are released into the atmosphere [75]. In one-part AAMs, several forms of granular Na_2SiO_3 were used with different amounts of chemically bound water, including sodium metasilicate anhydrous (Na_2SiO_3-anhydrous), sodium metasilicate pentahydrate ($Na_2SiO_3{\cdot}5H_2O$), and sodium metasilicate nonahydrate ($Na_2SiO_3{\cdot}9H_2O$) [76].

Sodium hydroxide (NaOH) is another synthetic activator that was used often in one-part AAMs. It is formed via the chlor-alkali process which involves the electrolysis of a sodium chloride solution, and nearly 60 million tons of NaOH are produced annually following this method [73]. The production of NaOH is energy intensive and nearly 1.1 kg of CO_2 is emitted for each 1 kg of NaOH produced [75]. Another solid activator that has received increased attention is Na_2CO_3. This activator can be obtained from natural sources, such as trona and Na_2CO_3-rich brines [73], with reserves of over 24 billion tons worldwide [77]. Sodium carbonate can be produced from several chemical processes, including the Solvay process [20], and the annual production of Na_2CO_3 stands at nearly 50 million tons [73]. Compared to Na_2SiO_3 and NaOH, Na_2CO_3 is cheaper to produce (2–3 times cheaper) and safer to handle due to its lower pH [78].

Sodium aluminate ($NaAlO_2$) is another promising solid activator. It is white in colour and formed by adding aluminium hydroxide ($Al(OH)_3$) to a 20–25% aqueous NaOH solution [79]. Due to its high alumina content, $NaAlO_2$ was mainly combined with high silica precursors, such as RHA [54], SF [38,80], SR [81], and GS [37,82], or as substitutes to a proportion of Na_2SiO_3 in FA- and GGBS-based mixes [13,83]. Sodium sulphate (Na_2SO_4) was also used as an activator due to its lower production cost and reduced handling risks [84]. However, Na_2SO_4 possesses low pH (<8) and results in mixes with a relatively lower strength [84,85].

Calcium-based solid activators, such as CaO and calcium hydroxide ($Ca(OH)_2$), were also studied in one-part AAMs. These activators are considerably cheaper than Na_2SiO_3 and NaOH (5–6 times cheaper) and easier to source [86]. Calcium oxide is white in colour and highly alkaline (pH ≈ 12.5). It is produced by heating limestone, which contains calcium carbonate ($CaCO_3$), in a lime kiln at temperatures of more than 825 °C. Meanwhile, $Ca(OH)_2$ is formed by mixing CaO with water (H_2O), which results in either white powder or colourless crystals. Other synthetic solid activators used in one-part AAMs, but to a lower extent, include barium hydroxide ($Ba(OH)_2$) [87], barium hydroxide octahydrate ($Ba(OH)_2{\cdot}8H_2O$) [88], reactive MgO [89,90], potassium silicate (K_2SiO_3) [91,92], and sodium bicarbonate ($NaHCO_3$) [93].

2.2.2. Activators derived from waste products

Given the high cost and environmental impact of synthetic activators, several studies aimed at finding alternative solid activators derived from waste products. Among such activators is paper sludge (PS), a waste material rich in CaO resulting from the treatment of recycled paper [35,94]. To ensure its reactivity, alkali-fusion is commonly used, which involves heating PS together with a small amount of NaOH at high temperature, and then milling the calcined product to a fine powder size. Alkali-fusion was used to enhance the reactivity of several waste products with favourable chemical compositions to act as activators in one-part AAMs. These include some of the precursors addressed earlier such as RM [41,42], CoW [61], VT [49,50], and WG [95].

Several biomass ashes were used as activators as well due to their high alkaline content. For instance, Maize stalk ash (MSA) and maize cob ash (MCA) from burning maize stalk and cob, respectively, were utilized as solid activators [28,96]. Both types of ash have a high pH (13–14) and high potassium oxide (K_2O) and SiO_2 contents. Olive stone biomass ash (OBA), almond-shell biomass ash (ABA), and wood biomass ash (WBA), with their high K_2O and CaO contents, were also used as solid activators [97–99]. Cotton shell ash (CSA) was used as a solid activator in MK-based one-part AAMs due to its high K_2O and MgO contents [65]. Coffee husk ash (CHA) was also used recently as an activator in GGBS-based one-part AAMs due to its high K_2O content [100]. Moreover, oyster shells, a waste product from the fishing industry, were valorised as an activator due to their high $CaCO_3$ content (>90 wt%) [101]. To ensure reactivity, oyster shells need to be calcined at high temperatures (~1000 °C), which converts them to reactive CaO. The potential of calcium carbide residue (CCR) as a solid activator in FA and GGBS-based AAMs was also investigated in several studies [102–105]. CCR is a waste material from forming acetylene gas (commonly used as fuel) by hydrolysing calcium carbide. With high pH (>12) and high CaO content (~70 wt%), CCR can act as a sustainable solid activator.

Soda residue, with its high CaO content (~40 wt%), was also investigated as a solid activator in combination with CCR to form FA and GGBS-based AAMs [103–105]. Soda residue is a waste material from sodium carbonate production using the ammonia alkali method [103]. Another CaO-rich industrial waste used as a solid activator is lime kiln dust (LKD) [67,71]. LKD is a waste material

resulting from the production of CaO. Its chemical composition shows traces of SiO_2 and Na_2O but predominantly has a CaO content of ~80 wt%. Desulphurization dust, a waste product from steel production, with its high Na_2O and CaO contents was also used as an activator in GGBS-based one-part AAMs [106]. A selection of SEM images of activators derived from waste products is shown in Fig. 4.

2.3. Aggregates

Most one-part AAM studies available in the open literature have focused on pastes (only binders) and mortars (fine aggregates only), with very few studies considering one-part alkali-activated concrete (AAC) (having both fine and coarse aggregates). Table 1 presents a summary of the mix designs of one-part AA pastes with no added admixtures from different studies available in the literature, while Table 2 presents the same for one-part AA mortars and concrete. Silicious river sand was mainly used as a source of fine natural aggregate for one-part AA mortars. This type of sand is chemically inert and has SiO_2 content of over 95 wt% [107]. Several types of coarse aggregates were used in one-part AAC, including granite [90], basalt [108], limestone [109], dolomite [110], clay granules [111], and IMT waste [103].

Several studies have attempted to use other fine aggregate sources, mainly waste material, to reduce the demand for natural river sand and a summary of those studies is given in Table 3. The sources of natural aggregate replacements include crushed bricks [112], WG [113,114], CW [62,115], waste sands [107], crumb rubber [116], and sand derived from IMT waste [103]. In a recent study, Xu et al. [117] formed geopolymer lightweight aggregates (GLA) using one-part AA technology and then used the GLA as coarse aggregates in FA- and GGBS-based one-part AAC. The GLA was formed through the reaction of FA and Na_2SiO_3-anhydrous at ambient conditions, followed by crushing to less than 20 mm size and then curing. The resulting AAC had apparent densities in the range of 1450–1750 kg/m^3 and compressive strengths of over 40 MPa.

2.4. Water

Fig. 5 presents a summary of the water contents of several one-part AA systems with different precursors and solid activators reviewed in this article (Table 1-Table 5). The water content was taken as the water-to-solid ratio (w/s) where solids accounted for both the precursor and activators. For FA-based, GGBS-based and FA- and GGBS-based one-part AAMs, the water content was usually less than 0.5 with many studies adopting a value in the range of 0.3–0.4. RM-based and RHA-based systems had a higher water demand in the range of 0.5–0.6. MK-based one-part AAMs also require greater water content to achieve workable mixes due to the plate-like nature of MK particles, and w/s ratios of $\geq$0.5 are commonly employed [71,118].

Other water sources, such as sea water and reverse osmosis reject water, were also investigated to reduce the demand for fresh water [119–121]. Reverse osmosis is a water purification procedure that is commonly used to treat seawater. Results of sea water and reverse osmosis reject water FA- and GGBS-based one-part AAMs show comparable mechanical properties to that of mixes made of fresh water with a slightly accelerated setting. The accelerated setting is due to the reaction of Cl^- in seawater with dissolved Ca^{2+} in the mix, causing the formation of calcium chloride ($CaCl_2$) which accelerates the hydration process.

2.5. Admixtures

Table 4 lists one-part AAMs from different studies employing commercial admixtures. Results of various investigations show that for FA- and GGBS-based one-part AAMs – activated via different solid activators – using lignosulfonate-based superplasticizers (SPs) in

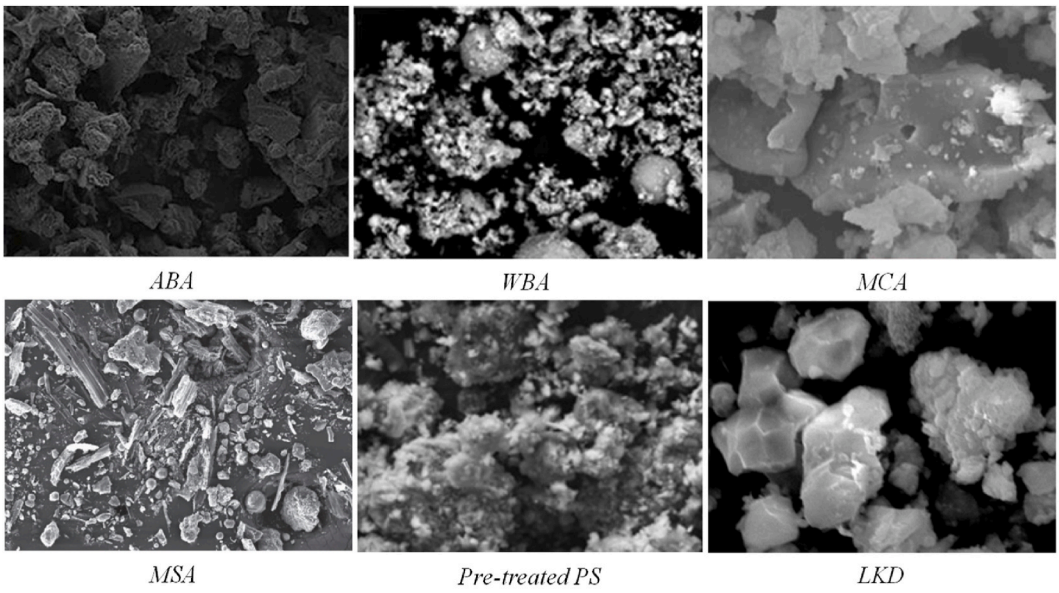

Fig. 4. SEM images of activators from waste products: ABA [98], *WBA* [118], *MCA* [211], *MSA* [212], *PS* [94], *LKD* [67].

Table 1
Details of one-part AA Pastes (with no added admixtures).

Ref.	Precursor	Solid activator	Water/Solid[a]	Calcination	Curing		28d Comp. Strength[b] (MPa)
					Temp. (°C)	RH (%)	
[42]	FA	RM, NaOH	0.34–0.56	–	60	n.r.	1.7
[193]	FA	Na_2SiO_3, NaOH	0.40	–	20 ± 2	n.r.	13.6
[213]	FA	Na_2SiO_3-anhydrous	0.25	–	25–27	n.r.	50
[78]	FA	Na_2SiO_3-anhydrous, Na_2CO_3	0.20, 0.25	–	30	n.r.	83.6
[214]	FA	Na_2SiO_3-anhydrous	0.25	–	25	n.r.	52
[215]	FA, GGBS	Na_2SiO_3-anhydrous	0.35	–	60 (24 h) Water curing (23 ± 3)	100 –	48.6
[216]	FA, GGBS	Na_2SiO_3-anhydrous	0.35	–	60 (24 h) Water curing (23 ± 3)	100 –	52.5
[161]	FA, GGBS	NaOH, KOH, Na_2SiO_3-anhydrous	0.28	–	23 ± 2	70 ± 10	40
[217]	FA, GGBS	Na_2SiO_3-anhydrous	0.25	–	n.r.	n.r.	93
[194]	FA, GGBS	$Na_2SiO_3{\cdot}5H_2O$, WG, NaOH	0.5	–	20	95	48
[83]	FA, GGBS	Na_2SiO_3-anhydrous, Na_2CO_3, $NaAlO_2$	0.36	–	25	100	97
[16]	FA, GGBS, Cenospheres	Na_2SiO_3-anhydrous	0.32	–	22 ± 2	100	14.2
[102]	FA, GGBS, SF	CCR, Hydrated lime, Hemihydrate gypsum, NaOH	0.28	–	50 (24 h) 25 ± 2	n.r.	37.5
[59]	FA, GGBS, WG	WG, NaOH	0.5	–	22 ± 1	50 ± 10	31
[36]	FA, GS	NaOH, $NaAlO_2$, Al_2O_3	0.48, 0.51	–	40	n.r.	–
[218]	FA, CW, Kaolin	NaOH, Na_2SiO_3	0.60, 0.90	800 °C (4 h)	75 (24 h)	n.r.	25
[76]	FASB, GGBS	Na_2SiO_3-anhydrous, $Na_2SiO_3{\cdot}5H_2O$, $Na_2SiO_3{\cdot}9H_2O$	0.35	–	20 ± 2	95 ± 3	76
[167]	FASB, GGBS	Na_2SiO_3-anhydrous, Na_2CO_3	0.35	–	20 ± 2	95 ± 3	76
[84]	FASB, GGBS	Na_2SiO_3-anhydrous, Na_2SO_4	0.35	–	20 ± 2	95 ± 3	77
[12]	FASB, GGBS	Na_2SiO_3-anhydrous, Na_2CO_3	0.35	–	20 ± 2	95 ± 3	76
[86]	GGBS	CaO, $Ca(OH)_2$	0.40	–	25	99	42
[219]	GGBS	NaOH	0.25	–	37 ± 2	100	63
[180]	GGBS	NaOH, $CaCO_3$	0.24–0.33	–	37 ± 2	100	69
[88]	GGBS	MgO, CaO, $Ca(OH)_2$, $Ba(OH)_2$, $Ba(OH)_2{\cdot}8H_2O$	0.40	–	23 ± 2	n.r.	42
[101]	GGBS	Oyster shell	0.40	1000 °C (3 h)	20	100	35
[98]	GGBS	ABA	0.40, 0.34	–	65	100	–
[178]	GGBS	NaOH, $Ca(OH)_2$, Na_2CO_3	0.46	–	50, 70, 90	n.r.	35
[220]	GGBS	NaOH	0.25–0.36	300–1000 °C (2 h)	23 ± 2	99 ± 1	53
[175]	GGBS	NaOH, Na_2SiO_3	~0.40	–	Water curing	100	–
[208]	GGBS	CaO, Na_2CO_3	0.4	–	n.r.	n.r.	48
[221]	GGBS	Na_2SiO_3-anhydrous	0.40	–	23 ± 2	45 ± 5	88
[169]	GGBS	$NaAlO_2$, $Na_2SiO_3{\cdot}9H_2O$	~0.30	–	20 ± 2	>50	88
[69]	GGBS, Dolomite	Na_2CO_3	0.42	1000 °C (0.5 h)	20 ± 0.5	95 ± 2	41.6
[61]	GGBS, CoW, Lead bearing sludge	NaOH	0.25–0.29	–	23 ± 2	99 ± 1	21
[222]	GGBS, Honeycomb ceramics	Na_2SiO_3, NaOH	0.45	125 °C (5 h)	20 ± 2	100	44
[164]	GGBS, WG, SF, OPC	Na_2SiO_3	~0.29	–	20 ± 5	60 ± 10	98.5
[223]	GGBS, Lead bearing sludge	NaOH, Ethylene glycol	0.25	–	23 ± 2	99 ± 1 60 ± 5	58.5
[48]	GGBS, LZMT	Na_2SiO_3	0.45	–	20 ± 2	90 ± 5	34.8
[23]	GGBS, LS	Na_2SiO_3-anhydrous	0.27	–	20 ± 3	n.r.	56
[45]	GGBS, GMT	NaOH	0.40	–	20 ± 1	≥90	33.5
[22]	ACS	Albite, NaOH	0.27	1200 °C (2 h)	23 ± 2	99 ± 1	84
[131]	RM	NaOH	0.60	800 °C (1 h)	20 ± 1	95	5.4

(*continued on next page*)

Table 1 (*continued*)

Ref.	Precursor	Solid activator	Water/Solid[a]	Calcination	Curing		28d Comp. Strength[b] (MPa)
					Temp. (°C)	RH (%)	
[41]	RM, SF	NaOH	0.65	800 °C (1 h)	20 ± 1	100	–
[40]	RM, MSWI FA	NaOH	0.50	800 °C (1 h)	20 ± 1	100	2
[54]	RHA	$NaAlO_2$	0.50	–	80	80	–
[38]	SF, SR	$NaAlO_2$	0.50	–	80	≥80	–
[80]	SF, SR	$NaAlO_2$	0.50	–	80	80	–
[209]	GS	$NaAlO_2$, Al_2O_3	n.r.	–	40	100	–
[82]	GS	$NaAlO_2$, Na_2SiO_3	n.r.	–	40	100	–
[39]	SR	$NaAlO_2$	0.60	–	70	100	–
[68]	Albite	NaOH, Na_2CO_3	0.30	850–1150 °C (0.5 h)	25	n.r.	44.2
[185]	Bentonite, Dolomite	Na_2CO_3	0.35	1100/1200 °C (3 h)	80	100	38
[224]	Bentonite	Na_2CO_3, NaOH	0.30	700–1000 °C (3 h)	80	100	32.5
[99]	Diatomite, WBA	NaOH	0.27	–	23 ± 2	99 ± 1	48
[225]	MK	NaOH, KOH	n.r.	550 °C (4 h)	≈23 100/140	n.r.	–
[226]	MK	NaOH, Na_2CO_3	0.30	650–1050 °C (3 h)	80 (72 h)	>90	–
[210]	MK, Kaolin	NaOH, Na_2SiO_3	0.22	800 °C (2 h) 900–1200 °C (24 h)	29 40–100	n.r.	10
[177]	MK, spodumene tailings, glass wool	Na_2SiO_3-anhydrous	0.25, 0.40	–	60 (24 h) 22	25	–
[47]	MK, IOT	Na_2SiO_3, NaOH	0.19, 0.15	–	n.r.	n.r.	–
[72]	Volcanic ash	Na_2SiO_3-anhydrous	0.30	–	60 (10 days)	n.r.	19.6
[50]	VT, MK	NaOH	0.28–0.44	750 °C (3 h)	20–80	n.r.	31.55
[49]	VT, MK	NaOH	0.35	750 °C (3 h)	n.r.	n.r.	–
[53]	VT, MK	NaOH	0.35	750 °C (3 h)	n.r.	n.r.	–
[60]	CoW	NaOH	0.27	1100 °C (2 h) 1200 °C (2 h)	23 ± 2	99 ± 1	79
[43]	Cement kiln dust, Feldspar	Na_2CO_3	0.29	1200 °C (3 h) 1300 °C (2–3 h)	23 ± 2	99 ± 1	52
[227]	OPC, GGBS, MK, Bentonite	Na_2CO_3	0.30, 0.50	750 °C (2 h)	22	99	–

n.r. = not reported.
[a] Water-to-solid ratio taken as the weight of water-to-total solid ratio including aluminosilicate precursors and solid activators.
[b] Maximum 28-day compressive strength is reported.

the range of 0.5–1.0% gave better fresh properties in comparison to other SPs, such as sulfonated melamine-formaldehyde, sulfonated naphthalene-formaldehyde, polycarboxylate and carboxylic acrylic ester [110,122]. Alrefaei et al. [123] stated that for FA- and GGBS-based mixes, the water-to-binder (w/b) ratio was critical, with polycarboxylate-based SPs giving better results at a w/b ratio greater than 0.36, while naphthalene-based SPs giving more favourable results at lower w/b ratios. To retard the setting of FA- and GGBS-based one-part AAMs, researchers showed that sodium tetraborate decahydrate-borax ($Na_2B_4O_7{\cdot}10H_2O$), citric acid, and sucrose gave favourable results, in comparison to other admixtures including phosphoric acid solution (H_3PO_4), sodium triphosphate ($Na_5P_3O_{10}$), and sodium gluconate ($C_6H_{11}NaO_7$) [1,89,124]. More recently, Coppola et al. [125] concluded that a combination of methylcellulose, modified starch and glycol-based shrinkage reducing admixture significantly retarded the setting of GGBS-based one-part AA pastes.

Table 5 presents a list of one-part AAMs formed with mineral admixtures and foaming agents. Among these studies, Ahmed et al. [126] investigated the effect of adding SF, MgO, MK, and cement clinker (CK) in small quantities (1.5–4.5% of binder content) to FA- and GGBS-based one-part AAMs. Results showed that these admixtures had measurable effects on the long-term strength properties, resulting in improvements of as much as 22% at 270 days when compared to the control mix. Matalkah et al. [127] observed the effects of different mineral admixtures, including gypsum powder, limestone powder and latex polymer, on the drying shrinkage of one-part AAMs made of a ternary blend of FA, GGBS and albite. The three admixtures reduced the drying shrinkage, but latex polymer was the most effective in reducing the drying shrinkage by up to 26% when compared to the control mix [127]. Aluminum powder, hydrogen peroxide (H_2O_2), and surfactant were used as admixtures to form foamed one-part AAMs [97,128]. Adding aluminum powder induces a reaction with the OH^- anions and results in the formation of hydrogen bubbles within the one-part AA mix. H_2O_2 admixtures facilitate the formation of foams within the one-part AA mix, while surfactants – also known as air entraining agents – help reduce the surface tension of liquids (i.e., allow bubbles to form easily) and often prevent different bubbles from coalescing.

Alzaza et al. [129] investigated the effect of basic oxygen furnace (BOF) submicron particles on the reactivity of one-part GGBS-based AAMs in sub-zero conditions. While the reactivity of GGBS-based AAMs is high in ambient curing conditions, a

Table 2
Details of one-part AA mortars and concretes (with no added admixtures).

Ref.	Precursor	Solid activator	Aggregates	Water/Solid[a]	Calcination	Curing		28d Comp. Strength[b] (MPa)
						Temp. (°C)	RH (%)	
[160]	FA	Na_2SiO_3, NaOH	Sand	0.30–0.39	–	40	n.r.	–
[90]	FA	NaOH, MgO, CaO	Granite aggregates, Sand	0.40	–	20 ± 2	n.r.	35
[228]	FA	Na_2SiO_3, NaOH	Silty sand	0.17	–	n.r.	n.r.	1
[179]	FA	Na_2SiO_3-anhydrous	Sand	0.30–0.40	–	n.r.	n.r.	39
[171]	FA	Na_2SiO_3-anhydrous	Sand, Coarse aggregates	0.25		23 Water curing (20 °C) Solar curing (85 °C)	35 65–70	~68
[132]	FA	Na_2SiO_3-anhydrous, KOH	Sand	0.28		22 ± 2, 70	100	62
[135]	FA, GGBS	Na_2SiO_3-anhydrous	Sand	0.5	–	23 ± 2	70 ± 5	52.5
[172]	FA, GGBS	Na_2SiO_3-anhydrous, NaOH	Sand	0.3–0.6	–	23 ± 2	70 ± 5	71.6
[136]	FA, GGBS	Na_2SiO_3-anhydrous, NaOH	Sand	0.5	–	23 ± 2	70 ± 5	49.6
[188]	FA, GGBS	Na_2SiO_3, NaOH	Sand, Coarse aggregates	0.26–0.45	–	23	100	96
[229]	FA, GGBS	Na_2SiO_3-anhydrous	Sand	0.40	–	Water curing	–	78
[189]	FA, GGBS	Na_2SiO_3, NaOH	Sand, Coarse aggregates	0.24–0.36	–	23	100	91.5
[230]	FA, GGBS	$Na_2SiO_3{\cdot}5H_2O$, KOH, Na_2CO_3	Sand	0.43	–	20–60	60	48
[170]	FA, GGBS	Na_2SiO_3, $Na_2SiO_3{\cdot}5H_2O$ Na_2CO_3, $Ca(OH)_2$	Sand	0.33–0.46	–	20	95	47.4
[119]	FA, GGBS	NaOH, Na_2SiO_3, Na_2CO_3	Sand	n.r.	–	20	100	51
[231]	FA, GGBS	Na_2SiO_3-anhydrous	Sand, Wollastonite	~0.40, ~0.33	–	60 (24 h)	n.r.	47.1
[232]	FA, GGBS	Na_2SiO_3-anhydrous, Carbonate minerals	Sand	0.40	–	60 (6 h) 23	90	60
[9]	FA, GGBS	$Na_2SiO_3{\cdot}5H_2O$, NaOH	Sand	n.r.	–	23	100	69
[233]	FA, GGBS	NaOH	Clay	n.r.	–	26 ± 2	n.r.	–
[93]	FA, GGBS	$Ca(OH)_2$, $NaHCO_3$	Sand	0.40	–	23 60	60 ± 5	39
[104]	FA, GGBS	Soda residua, CCR	Sand	0.45, 0.5. 0.55	–	Water curing (20 ± 1)	100	43.9
[163]	FA, GGBS, SF	$Na_2SiO_3{\cdot}5H_2O$	Sand	0.31–0.37	–	23	95	105
[56]	FA, RHA, MSWI FA	KOH, Na_2CO_3	Sand	0.50	–	23	90–97	–
[5]	FA, MK	Na_2SiO_3-anhydrous, Na_2SiO_3-hydrous, NaOH	Sand	0.44	–	20 ± 1	95	50.5
[234]	FA	WBA	Sand	0.34–0.42	–	Water curing	–	7.7
[11]	FASB, GGBS	Na_2SiO_3-anhydrous	Sand	0.35	–	20 ± 2	95 ± 3	57
[87]	GGBS	$Ca(OH)_2$, $Ba(OH)_2$	Sand	0.4	–	22 ± 2 Water curing	n.r.	28.5
[235]	GGBS	Na_2SiO_3-anhydrous, NaOH	Sand, Gravel	0.4	–	23 ± 2	>98	30
[94]	GGBS	PS, NaOH	Sand	0.31	–	22	75	42.3
[236]	GGBS	Na_2SiO_3	Sand	0.34	–	22	100	107
[120]	GGBS	Na_2SiO_3-anhydrous	Sand	0.34	–	22	100	104
[187]	GGBS	Na_2SiO_3-anhydrous	Sand	0.35	–	23 −5, −10, −20	100	101
[151]	GGBS	Na_2SiO_3-anhydrous	Sand	0.37	–	23 ± 2	100	60.4
[105]	GGBS	SR, CCR	Sand	0.50	–	Water curing (20 ± 1) 20–25	100 ≥50	36.9
[91]	GGBS	Na_2SiO_3, NaOH, K_2SiO_3, KOH	Sand	0.40	–	23 ± 1	>98	78
[100]	GGBS	CHA	Sand	0.60	600–800 °C (1–10 h)	60	n.r.	–
[106]	GGBS, SF	Desulphurization dust, NaOH	Sand	0.45	–	23 60	97	33

(*continued on next page*)

Table 2 (*continued*)

Ref.	Precursor	Solid activator	Aggregates	Water/Solid[a]	Calcination	Curing		28d Comp. Strength[b] (MPa)
						Temp. (°C)	RH (%)	
[34]	GGBS, SF, RHA	Na_2SiO_3-anhydrous, NaOH	Sand	0.35	–	23	60	107
[186]	GGBS, CW	Na_2SiO_3-anhydrous	Sand	0.35	–	23	100	63
[63]	GGBS, CW	Na_2SiO_3-anhydrous	Sand	0.35	–	23	35, 100	64
[27]	GGBS, FS	Na_2SiO_3-anhdrous, $Na_2Si_2O_5$	Sand	0.32–0.44 0.46	–	20	100	75
[28]	FS	MCA	Sand	0.26, 0.28	–	20	100	46.4
[237]	RHA	$NaAlO_2$	Sand	0.45–0.64	–	40	n.r.	–
[81]	SF, RHA, GGBS, SR	$NaAlO_2$	Sand	0.38–0.50	–	60, 80	80	–
[96]	MK	MCA, MSA	Sand	0.31	700–800 °C (1 h)	80	–	–
[65]	MK	CSA	Sand	0.56 0.20	700 °C (4 h) - MK 850 °C (1 h) - CSA	25 (48 h) 70 (5 days)	50	–
[118]	MK	WBA	Sand	0.49, 0.56, 0.65	700 °C	70 (24 h)	–	–
[67]	MK, Volcanic tuff	LKD	Sand	0.45, 0.55	450 °C (2 h) 950 °C (2 h)	50 (7 days)	–	27.5
[71]	MK, Volcanic tuff	LKD	Sand	0.45, 0.55	450 °C (2 h) 950 °C (2 h)	50 (7 days)	–	27.3
[64]	OPC, MSWI FA, MSWI BA	$CaSO_4$, Na_2SO_4	Sand	0.50	–	21	99	33
[238]	OPC, FA	Na_2SO_4	Sand	0.34, 0.49	–	22 ± 2	>90	52.53
[176]	OPC, GGBS, Dolomite	Na_2SO_4	Sand	~0.38	900–1000 °C	Water curing	–	52.4

n.r. = not reported.

[a] Water-to-solid ratio taken as the weight of water-to-total solid ratio including aluminosilicate precursors and solid activators.

[b] Maximum 28-day compressive strength is reported.

significant reduction in reactivity is observed when mixing is carried out in freezing conditions. BOF submicron particles are a by-product of the steel making industry, mainly composed of Fe_2O_3, and have very fine sizes (median particle size, $d_{50} < 0.5$ μm). The addition of BOF submicron particles enhanced the reactivity of GGBS-based one-part mixes cured at −5 and −10 °C, while very little enhancement was observed when curing at −20 °C [129]. This enhancement in reactivity due to the addition of BOF submicron particles was attributed in part to their very fine particle size providing additional nucleation sites for hydration products to form.

3. Preparation and curing

3.1. Pre-mixing treatment

Aluminosilicate precursors from fired sources, such as FA, GGBS, and SF, are usually mixed directly without a pre-treatment step. However, precursors derived from other sources typically require pre-treatment to ensure adequate reactivity when added in alkaline environments. In one-part AAMs, four main pre-treatment methods were applied, and these include: 1) thermal treatment/calcination, 2) thermal activation, 3) hydrothermal activation, and 4) mechanochemical treatment.

3.1.1. Thermal treatment

Thermal treatment is commonly applied to precursors of geological origins, most notably kaolinite. During such treatment, the crystalline phase structure of the precursor is broken down and transformed into an amorphous glassy phase that is highly reactive [67]. The optimum calcination temperature differs depending on the source material. For instance, the calcination of kaolinite clay ($Al_2SiO_5(OH)_4$) is typically carried out at a temperature in the range of 700–800 °C. This results in its dehydroxylation, loss of long-range silica and alumina layers, and the transformation of alumina from octahedral to tetrahedral coordination, forming as a result highly reactive MK ($Al_2Si_2O_7$) [67]. XRD patterns of MK show the disappearance of certain crystalline peaks, including mullite and illite, and a reduction in quartz and clinoptilolite peaks in the 30–60° 2θ range. While considering the 7-day compressive strength of one-part AAMs, Peys et al. [96] reported that the optimum calcination temperature for MK was 700 °C (7-day strength = 22 MPa). Increasing the calcination temperature further to 750 °C and 800 °C caused the strength to drop to 15.5 MPa and 15.0 MPa, respectively, [96]. Thermal treatment was also applied to certain activators, generally from waste products, to enhance their reactivity. For example, Kadhim et al. [67,71] showed that calcining LKD at 950 °C to activate MK-based one-part AAMs helped enhance the compressive strength remarkably. Similarly, Balo et al. [65] noticed an increase in the strength of MK-based one-part AAMs activated using CSA by calcining the latter at 850 °C for 1 h.

Table 3
Details of one-part AAMs with waste aggregates.

Ref.	Precursor	Solid activator	Aggregates	Admixture	Water/Solid[a]	Calcination	Curing		28d Comp. Strength[b] (MPa)
							Temp. (°C)	RH (%)	
[112]	FA	NaOH	Sand, Red bricks	–	~0.20, ~0.30	–	85 (24 h)	n.r.	–
[113]	FA, GGBS	Na_2SiO_3-anhydrous	Sand, WG	–	0.38	–	n.r.	100	58
[184]	FA, GGBS	Na_2SiO_3-anhydrous	Sand, WG	Foaming agent	0.38	–	23.3 22 ± 2	60 100	58
[117]	FA, GGBS	Na_2SiO_3-anhydrous	Sand, GLA	Polycarboxylate	0.35	–	20	n.r.	67
[115]	FA, GGBS	Na_2SiO_3-anhydrous	CW, Sand	–	0.35	–	23	60	~100
[103]	FA, GGBS	Soda residue, CCR	Sand, IMT sand, Gravel, IMT coarse aggregates	Polycarboxylate	0.50, 0.55, 0.6	–	Water curing (20 ± 1) 60, 75	n.r	38.6
[116]	FA, GGBS, SF	Na_2SiO_3-anhydrous	Sand, Crumb rubber	Polycarboxylate	0.41	–	16–20	60–65	53.5
[107]	GGBS	Na_2SiO_3-anhydrous	Sand, Exhausted waste sand	–	0.29–0.35	–	n.r.	n.r.	89
[62]	GGBS, CW	Na_2SiO_3-anhydrous	CW	–	0.35	–	23 60 (3 h)	100	24
[114]	GGBS, Lime	$Na_2SiO_3{\cdot}5H_2O$, KOH, Na_2CO_3	Sand, WG	Air entraining agent, Methylcellulose, Modified starch, shrinkage reducing admixture	0.60	–	20	60	15.03
[182]	GGBS, OPC	K_2CO_3	Sand, Crumb rubber	Silica aerogel	0.40	–	23 ± 2 Water curing	n.r.	34.13

n.r. = not reported.
[a] Water-to-solid ratio taken as the weight of water-to-total solid ratio including aluminosilicate precursors and solid activator.
[b] Maximum 28-day compressive strength is reported.

3.1.2. Thermal activation

Thermal activation involves calcining a low-reactivity precursor with an alkaline activator for a specific duration, and then milling the resulting product to a fine powder. For example, Feng et al. [68] heated albite powder with NaOH/Na_2CO_3 at temperatures ranging from 850 °C to 1150 °C for a period of 30 min. After calcination, the heated material was allowed to cool down to room temperature and was then pulverised in a ring mill. Findings show that heating the albite with the alkaline solid activators resulted in reasonable strength development at 28-days of over 40 MPa. However, mixing thermally treated albite (without any solid activator) with water showed little strength development of just over 2 MPa at 28 days [68]. Almalkawi et al. [70] performed thermal activation and mechanochemical processing to enhance the reactivity of volcanic tuffs (pumice) by heating it with Na_2SO_4 and Na_2CO_3 at 700 °C for 4 h, followed by cooling and grinding to fine powder size. This transformed the raw materials into highly reactive hydraulic cements that can be used directly in one-part AA mixes.

Thermal activation was also carried out on CKD (60 wt%) and feldspar (40 wt%), by calcining them at 1200/1300 °C for 2–3 h in the presence of Na_2CO_3 (0–20 wt% of CKD + feldspar) [43]. The solid blend was then milled to pass a 50 μm sieve. XRD patterns showed that the thermal activation of CKD and feldspar caused crystalline peaks of quartz, calcite and lime to fade, with a generally lower degree of crystallinity and the formation of an amorphous calcium silicate phase. Ababneh et al. [130] used thermal activation to pre-treat kaolinite clay in the presence of CaO, Na_2CO_3 and $Na_2SiO_3{\cdot}5H_2O$. A heating temperature of 950 °C was held for 1 h, and the thermally treated blend was then allowed to cool down to room temperature and subsequently milled to pass a 75 μm sieve.

Alkali-fusion – a form of thermal activation which involves calcining the precursor with NaOH – has also gained traction in recent years. Ke et al. [131] and Ye et al. [33] performed alkali-fusion to enhance the reactivity of RM by heating it with NaOH at 800 °C for 1 h. The resulting product was then pulverised into fine particles smaller than 0.315 mm. Abdel-Gawwad et al. [22] carried out alkali-fusion to enhance the reactivity of ACS by heating it with NaOH (5% and 10% by weight of ACS) at 1200 °C for 2 h. This was followed by rapid quenching and milling to less than 75 μm particle size. In another study, Abdel-Gawwad et al. [60] performed alkali-fusion on CoW by heating it with NaOH (5–15%) at temperatures of 1100/1200 °C for 2 h. The calcined material was then allowed to cool down and subsequently pulverised to pass 75 μm sieve size. Alkali-fusion of CoW resulted in improvement in the mineralogical phase structure, forming a semi-amorphous phase with crystalline peaks of lower intensity to those of the untreated CoW.

3.1.3. Hydrothermal activation

Hydrothermal activation is a relatively new form of pre-treatment in one-part AAMs. It aims to avoid the high calcination

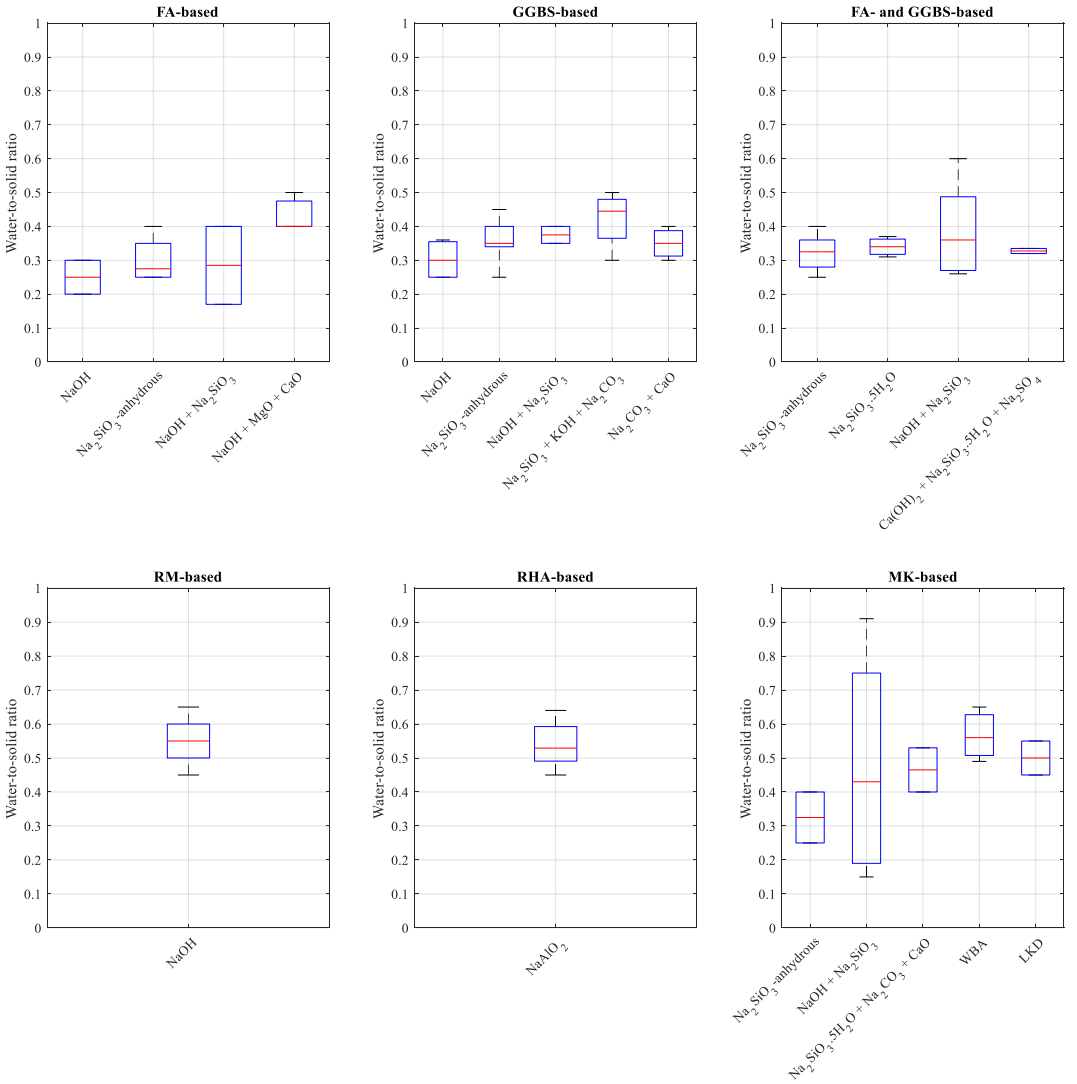

Fig. 5. Water contents of one-part alkali-activated systems with different precursors and solid activators.

temperatures of thermal activation and involves mixing the aluminosilicate precursor with a NaOH solution, and then heating the product at a temperature of usually less than 200 °C for a specific duration, followed by drying and crushing to form a fine solid blend. This blend can then be used directly with water and aggregates (if any) to form one-part AAMs. Liu et al. [45] performed hydrothermal activation on GMTs by mixing them with a NaOH solution, and allowing the mixture to react in an oven at temperatures of around 150–200 °C. This was followed by drying the mixture to a constant weight at 100 °C, and then pulverising the solid product to less than 74 μm. XRD patterns of the treated GMT showed reduced crystallinity and enhanced disordered structure of the pre-treated GMT.

Abdel-Gawwad et al. [61] used hydrothermal activation by mixing CoW powder with NaOH (5–20 wt% of CoW), and tap water (35 wt% of CoW powder) was added to the blend and heating was conducted at 60 °C for 18 h. The treated solid material was then ground to a reactive fine powder. Hydrothermal activation transformed CoW into an active precursor with enhanced $Ca(OH)_2$ and magnesium hydroxide ($Mg(OH)_2$) formations. Hydrothermal activation was also used to produce a solid activator for one-part AAMs [59]. This was done by mixing 52 wt% WG powder (high SiO_2 content) with 48 wt% NaOH micro-pearls ($Na_2O/SiO_2 \approx 1$). A small amount of water ($w/s = 0.1$) was added, and thorough mixing of the blends was performed. Heating at 150 °C was then carried out in an oven for 2 h, and the mixture was then crushed to pass 600 μm sieve size [59]. Activating WG powder with NaOH results in crystalline Na_2SiO_3 which can be used as an activator, although at a lower efficiency than the commonly used synthetic Na_2SiO_3.

3.1.4. Mechanochemical treatment

Mechanochemical treatment is conducted by grinding the precursors and the solid activators together in a ball mill for a certain duration of time. This causes a deformation of the crystalline structure of the precursors through the application of mechanical stresses at high rates [56] and is generally viewed as a 'green' pre-treatment method. Matalkah et al. [90] carried out mechanochemical

Table 4
Details of one-part AAMs with commercial superplasticizers and retarders.

Ref.	Precursor	Solid activator	Aggregates	Admixture	Water/Solid[a]	Calcination	Curing		28d Comp. Strength[b] (MPa)
							Temp. (°C)	RH (%)	
[239]	FA	$Ca(OH)_2$, Na_2SiO_3-GD	–	Polycarboxylate	0.20	–	60 (24 h) 23 ± 3	100	13.6
[89]	FA	NaOH, MgO, CaO	Sand	Sodium tetraborate borax, Citric acid, Phosphoric acid (H_3PO_4)	0.40–0.50	–	–	–	–
[4]	FA, GGBS	$Ca(OH)_2$, Na_2SiO_3-anhydrous, $Na_2SiO_3{\cdot}5H_2O$, Na_2SiO_3-GD, NaOH	–	Polycarboxylate	0.20–0.36	–	60 (24 h) 23 ± 3	n.r.	36.9
[159]	FA, GGBS	Na_2SiO_3	–	Hydrophosphate	0.28–0.30	–	n.r.	n.r.	80.1
[124]	FA, GGBS	Na_2SiO_3-anhydrous	–	Sodium tetraborate decahydrate-borax ($Na_2B_4O_7{\cdot}10H_2O$), Sodium triphosphate ($Na_5P_3O_{10}$), Polycarboxylate, Sodium gluconate ($C_6H_{11}NaO_7$), Sodium lignosulphonate, Calcium lignosulphonate	0.26–0.30	–	23 ± 2	70 ± 10	44
[123]	FA, GGBS	Na_2SiO_3-anhydrous	–	Naphthalene, Melamine, Polycarboxylate	0.30–0.36	–	Water curing	–	74.4
[138]	FA, GGBS	Na_2SiO_3-anhydrous	–	Polycaroxylate	0.39	–	n.r.	100	63
[1]	FA, GGBS	Na_2SiO_3-anhydrous, Na_2SiO_3-GD	–	Polycarboxylate, Naphthalene, Sucrose, Anhydrous borax, MasterSet RT 122	0.367	–	60 (24 h)	–	51.5
[168]	FA, GGBS	Na_2SiO_3-GD, $Ca(OH)_2$, K_2CO_3, LiOH, Na_2O	–	Polycarboxylate	0.2–0.4	–	20–23	65 ± 10	38
[165]	FA, GGBS	Na_2SiO_3-anhydrous	Sand	Sodium tetraborate decahydrate-borax ($Na_2B_4O_7{\cdot}10H_2O$)	0.27–0.28	–	30, 20, 65	n.r.	94
[240]	FA, GGBS	Na_2SiO_3-anhydrous	Sand	Sodium tetraborate decahydrate-borax ($Na_2B_4O_7{\cdot}10H_2O$)	0.28	–	25 ± 2	70 ± 10	45
[21]	FA, GGBS	$Ca(OH)_2$, Na_2SO_4, Na_2SiO_3-anhydrous	–	Naphthalene, Melamine, Polycarboxylate	0.36, 0.24	–	Water curing	–	74.4
[134]	FA, GGBS	Na_2SiO_3-anhydrous	–	Polycarboxylate	~0.36, ~0.27	–	Water curing	–	83
[241]	FA, GGBS	$Ca(OH)_2$, $Na_2SiO_3{\cdot}5H_2O$, Na_2SO_4	–	Polycarboxylate	0.35	–	23 ± 3	95 ± 5	56.3
[242]	FA, GGBS	$Ca(OH)_2$, Na_2SiO_3-G, Na_2SiO_3-GD, $Na_2SiO_3{\cdot}5H_2O$, Na_2SO_4	–	Polycarboxylate, Naphthalene	0.35–0.375	–	23 ± 3	95 ± 5	56.3
[243]	FA, GGBS	$Ca(OH)_2$, $Na_2SiO_3{\cdot}5H_2O$, Na_2SO_4	Sand	Polycarboxylate	0.32, 0.335	–	23 ± 3	95 ± 5	42.6
[244]	FA, GGBS	$Ca(OH)_2$, $Na_2SiO_3{\cdot}5H_2O$, Na_2SO_4	Sand	Polycarboxylate	0.32, 0.335	–	23 ± 3	95 ± 5	42.6
[93]	FA, GGBS	$Ca(OH)_2$, $NaHCO_3$	Sand	Shrinkage reducing admixture	0.40	–	23, 60	60 ± 5	39
[13]	FA, GGBS, FASB	Na_2SiO_3, $NaAlO_2$	Sand	Polycarboxylate	0.23	–	20 ± 2	95 ± 3	63
[245]	FA, GGBS, Albite	NaOH, Na_2SiO_3, CaO	Sand	Sodium tetraborate-borax	0.45–0.50	–	20 ± 2	>95	36
[246]	GGBS	$Ca(OH)_2$, Na_2SO_4	–	SP, Viscosity modifying agent, Antifoamer	0.26–0.38	–	Water curing (23 ± 3)	–	54.8

(*continued on next page*)

Table 4 (*continued*)

Ref.	Precursor	Solid activator	Aggregates	Admixture	Water/Solid[a]	Calcination	Curing		28d Comp. Strength[b] (MPa)
							Temp. (°C)	RH (%)	
[111]	GGBS	Na_2SiO_3-anhydrous	Sand, Clay granules	Polycarboxylate	0.4–0.6	–	22 ± 2	n.r.	53.8
[125]	GGBS	Na_2SiO_3, KOH, Na_2CO_3	Sand	Methylcellulose, Modified starch, CaO-based expansive agent, Ethylene glycol-based shrinkage reducing admixture	0.30, 0.50	–	20	60	102.1
[247]	GGBS	Na_2SiO_3-anhydrous	Sand	Polycarboxylate-based	0.45	–	23	35	83
[248]	GGBS, Lime	Na_2SiO_3	Sand, Coarse aggregates	Naphthalene sulphonates, Lignosulphonates	0.5	–	n.r.	n.r.	51
[110]	GGBS, SF	Na_2CO_3, CaO	Dolomite stone, Dolomite sand	Lignosulphonate	0.30, 0.35	–	25, 85	>90	85
[122]	GGBS, SF	NaOH	Sand	Melamine, Naphthalene, Lignosulfonate Polycarboxylate, Carboxylic acrylic acid	0.35	–	22	100	40
[109]	GGBS, SF	$Na_2SiO_3{\cdot}5H_2O$	Sand, Crushed limestone	Polycarboxylate	0.50–0.54	–	23 ± 3	50	65.4
[139]	GGBS, SF, Phyllite dust	Na_2SiO_3-anhydrous	Sand	Lignosulphonate	0.25–0.35	–	20	100	145
[31]	NS	Na_2SiO_3-anhydrous, NaOH, Na_2CO_3	Sand	Citric acid, Lignin-based SP	0.35	–	20 ± 2	≥95	96.02
[32]	NS	Na_2SiO_3-anhydrous	Sand	Citric acid, Lignin-based SP	0.35	–	20 ± 2	≥95	67
[33]	RM, SF	NaOH	–	Sodium lignosulphonate	0.45–0.65	800 °C (1 h)	20 ± 1	100	31.5
[24]	LS, GGBS	Na_2SiO_3	–	Polycarboxylate	0.25	–	20 ± 2	95 ± 3	32.5
[130]	Kaolin	$Na_2SiO_3{\cdot}5H_2O$, Na_2CO_3, CaO	Sand	Polycarboxylate	0.40–0.53	950 °C (1 h)	20 ± 2 80 (24 h)	>95	–
[249]	OPC, FA, Kaolin	NaOH, $Ca(OH)_2$	Sand	Polycarboxylate	0.35	650 °C (140 min)	n.r.	n.r.	29
[250]	OPC, FA, Kaolin	NaOH, KOH, $Ca(OH)_2$	Sand	Polycarboxylate	0.26–0.52	650 °C (140 min)	n.r.	n.r.	42.3
[251]	OPC, FA, Kaolin	NaOH, $Ca(OH)_2$	Sand	Polycarboxylate	0.35	650 °C (140 min)	21 ± 2	n.r.	29.5
[108]	OPC, FA, GGBS	K_2CO_3, $Ca(OH)_2$, Na_2SiO_3-anhydrous	Sand, Crushed basalt	SP, Citric acid	~0.275–0.29	–	20–23	65 ± 10	55

n.r. = not reported.

[a] Water-to-solid ratio taken as the weight of water-to-total solid ratio including aluminosilicate precursors and solid activators.

[b] Maximum 28-day compressive strength is reported.

treatment of raw materials by placing the precursor (in this case FA) and solid activators (CaO, MgO and NaOH) in a ball-mill, and grinding was performed for a period of over 2 h. The introduction of mechanical energy helped break down the structure of the precursor and introduced alkali earth cations and alkali metal cations to their microstructure, facilitating their mechanochemical restructuring and resulting in highly reactive hydraulic cement. A compressive strength of about 35 MPa at 28 days was achieved for the mechanochemically processed mixes (cured under ambient conditions), while control mixes formed by separate milling only achieved 28-day strengths of nearly 5 MPa [90]. Masi et al. [132] also showed improvement in the mechanical properties of FA-based one-part AAMs when the FA was ball milled with potassium hydroxide (KOH) and Na_2SiO_3-anhydrous for 2 h. The milling process reduced d_{50} of FA from 15.7 μm to <4.1 μm, and enhanced its reactivity. Important parameters to consider for mechanochemical treatment include: 1) the number of balls used and their size, 2) treatment time, and 3) milling rotation speed [32,133].

3.2. Mixing and curing

The mix design method for one-part AAMs generally starts by mixing the dry materials, including precursors, solid activators,

Table 5
Details of one-part AAMs with mineral admixtures and foaming agents.

Ref.	Precursor	Solid activator	Aggregates	Admixture	Water/Solid[a]	Calcination	Curing		28d Comp. Strength[b] (MPa)
							Temp. (°C)	RH (%)	
[252]	FA, GGBS	$Ca(OH)_2$, Na_2SiO_3, $Mg(NO_3)_2$	–	Foaming agent	0.4 0.375	–	22 ± 2	100	1.97
[126]	FA, GGBS	Na_2SiO_3-anhydrous	Sand	SF, MK, MgO, CK	0.31	–	20 ± 2	n.r.	49
[127]	FA, GGBS, Albite	NaOH, Na_2SiO_3, CaO	Sand, Crushed limestone	Sodium tetraborate-borax, Polyethylene glycol shrinkage reducing admixture, Gypsum powder, SF, Limestone powder, Latex polymer.	n.r.	–	22 ± 2	50 ± 4	–
[166]	GGBS	Na_2SiO_3, KOH, Na_2CO_3	–	Air entraining agent	0.43–0.46	–	20 ± 2	60 ± 5	39.1
[253]	GGBS	CaO, NaOH		Titanium dioxide, $CaCl_2$	0.35	–	23	99	54.4
[129]	GGBS	Na_2SiO_3-anhydrous	Sand	Basic oxygen furnace submicron particles	0.35	–	23 −5, −10, −20	100	55.5
[37]	GS	$NaAlO_2$	Sand	Al_2O_3, ZnO, ZrO_2	n.r.	–	40	100	–
[97]	GGBS, RHA	OBA	–	Aluminum powder, Recycled aluminum foil	~0.38	–	23	100	6.3
[128]	MK	NaOH, Na_2SiO_3	Sand	H_2O_2, Surfactant	0.64, 0.75, 0.91	–	60 (24 h)	100	–
[70]	Pumice	Na_2SO_4, Na_2CO_3	Sand	Gypsum	0.60, 0.71, 0.74	700 °C (4 h)	20 ± 2	90	22
[254]	OPC, FA, Kaolin	NaOH, $Ca(OH)_2$	Sand	Polycarboxylate, Aluminium powder, $NaBO_3$, H_2O_2	0.35	650 °C (140 min)	n.r.	n.r.	–

n.r. = not reported.
[a] Water-to-solid ratio taken as the weight of water-to-total solid ratio including aluminosilicate precursors and solid activators.
[b] Maximum 28-day compressive strength is reported.

aggregates, and any admixtures in solid form, for a few minutes (1–3 min). After that, water is added gradually to initiate the reaction and mixing is continued for another 1–5 min. If a pre-treatment step is employed, then the resulting solid blend from the pre-treatment process is mixed with any aggregates and solid admixtures first for a few minutes, and water is subsequently added to initiate the reaction and mixing is continued until a homogeneous mix is achieved. When liquid SPs were considered, the mix design approach differed slightly from one study to the other, with some adding the SPs 2–3 min after adding all the water to the one-part AA fresh mix, and then mixing continued for another 3–6 min. Other studies [21,134] have mixed the solid raw materials together with 60–80% of the mixing water for a few minutes. The remaining 20–40% of the mixing water was used to dilute the SP to ensure more dispersion, and then added to the mix and mixing continued for a few more minutes. After wet mixing, the fresh mix is cast in the prepared moulds and typically compacted to remove any entrapped air bubbles. For AAMs made of high-calcium precursors, demoulding is usually carried out 24 h after casting, whereas for AAMs synthesized using low-calcium precursors, more time is required to ensure sufficient hardening and demoulding can take place up to 3-days after casting [135,136]. Fig. 6 shows a summary of the mix design steps involved in one-part AAMs. From the several precursors used in one-part AAMs, metakaolin-based systems require special care and experience during mixing [137]. When initially wetted, metakaolin-based AAMs are difficult to mix and appear too dry. Rapid shearing of the fresh mix should be continued by the mixing machine without the addition of extra water to avoid reductions in mechanical properties and any harmful effects on durability [137]. After sufficient mixing the material becomes more homogeneous with better consistency. The fresh mix can then be poured into moulds and vibrated to form concrete specimens.

In a recent study, Alrefaei and Dai [138] examined the effect of delayed SP addition, in this case a polycarboxylate ether, on the resulting rheological and mechanical properties of FA- and GGBS-based one-part AA pastes. The mixing time extended for 30 min where the SP was initially added as usual (i.e., early SP addition), and a delayed SP addition which involved mixing the one-part AAMs with 90% of the water for 1 min, followed by a 19 min rest period, and then the SP was added with the remaining 10% of the water and mixing was continued for 3 min. Results indicated a lower drop in the 28-day compressive strength and better rheological properties as a result of delayed polycarboxylate addition [138]. In a different study, Perumal et al. [139] achieved high-strength one-part AAMs through particle packing, which entails careful selection of the content and particle sizes of constituent materials to ensure maximum packing density. The main binder used in their study was GGBS complemented by SF and phyllite dust to form ternary blends, and the mix was activated using Na_2SiO_3-anhydrous. The highest compressive strength achieved at 28-days was 145 MPa (cube specimens), and this remains the highest compressive strength reported for one-part AAMs.

One-part AAMs can be cured in ambient conditions or at elevated temperatures. Mixes made of low-calcium precursors, such as Class F FA and MK, typically require heat curing at temperatures above 40 °C to achieve reasonable strength development. Meanwhile, mixes synthesized using high-calcium precursors, such as Class C FA and GGBS, can develop appropriate strengths with curing at

Fig. 6. Mix design method for one-part AAMs.

Table 6
Details of 3D-printed one-part AAMs.

Ref.	Precursor	Solid activator	Aggregates	Admixture	Water/Solid[a]	Curing		28d Comp. Strength[b] (MPa)
						Temp. (°C)	RH (%)	
[144]	FA	Na_2SiO_3-anhydrous	Sand	–	0.315	60 (24 h) 23 ± 3	100	35
[148]	FA, GGBS	Na_2SiO_3-anhydrous	Sand	–	0.315	60 (24 h) 23 ± 3	n.r.	43.2
[92]	FA, GGBS	K_2SiO_3, KOH	Sand	–	0.35	n.r.	n.r.	26.8
[147]	FA, GGBS	Na_2SiO_3-GD, Na_2SiO_3-anhydrous	Sand	Scurose,	0.315, 0.33	60 (24 h) 23 ± 3	n.r.	55
[146]	FA, GGBS	Na_2SiO_3-anhydrous	Sand	Magnesium aluminosilicate, Sucrose		–	–	–
[145]	GGBS	$Na_2SiO_3 \cdot 5H_2O$	Sand	Nanoclay, Hydromagnesite	0.35, 0.40	–	–	–

n.r. = not reported.
[a] Water-to-solid ratio taken as the weight of water-to-total solid ratio including aluminosilicate precursors and solid activator.
[b] Maximum 28-day compressive strength is reported.

ambient temperatures (20–30 °C). Curing specimens in sealed plastic sheets or in curing rooms (relative humidity (RH) > 90%) is desirable to limit moisture loss and ion leaching [12]. Water curing is usually avoided to prevent activator leaching [73,126].

3.3. 3D printing

In recent years, 3D printing technology/digital construction has gained increased interest, particularly due to the expected savings in construction time, material and labour with such technology and the potential for increased geometrical freedom [140–142]. 3D-printed concrete materials are placed layer by layer in the absence of formwork [143] and few studies developed viable 3D-printed one-part AAMs as can be seen in Table 6 [92,144–148]. The preparation steps involved in producing extrusion-based 3D printed one-part AAMs include pre-mixing preparation, mixing, pumping, extrusion and building [142,146]. Pre-mixing preparation entails preparing a 3D model of the object to be printed in a CAD platform. A G-Code is also prepared using slicing software which basically defines the printing sequence. The G-Code is run by a controller which gives commands to a gantry printer or a robotic arm with a nozzle/extruder for laying the 3D printed concrete. The printing device is connected to a concrete pump to pump out the fresh mix. The fresh mix in 3D-printed one-part AAMs is prepared using the 'just-add-water' approach described in section 3.2, and is placed layer-by-layer until the required shape is attained [92]. Prior to pumping, it is important to ensure full dissolution of the solid activator. Muthukrishnan et al. [146] recommend a fresh mixing time of at least 15 min for FA- and GGBS-based one-part AAC activated using Na2SiO3-anhydrous.

Fresh material that can be pumped easily and have good thixotropic properties (i.e., ability to lose viscosity with shear stress application and the recovery of such viscosity upon the removal of shear stress) are best suited for extrusion-based 3D printing [142]. One-part AAMs generally exhibit good pumpability and thixotropic characteristics [146]. The mechanical properties of the resulting 3D-printed one-part AAM depend on several print related parameters, such as printing layer height and printing speed [92]. Other important parameters to consider for 3D-printed one-part AAMs is conformity and dimensional stability, load carrying capacity (also known as buildability), and the directional mechanical strength. As with the case of other printed material, 3D-printed one-part AAMs exhibit anisotropic properties. Panda et al. [92] showed that 50 × 50 × 50 mm cubes of 3D-printed FA- and GGBS-based one-part AAMs loaded at 28 days along their three major axis achieved strengths of 28.3, 25.9 and 24.3 MPa, with such anisotropic behaviour being attributed to motion patterns during printing. Bong et al. [147] reported that the 28-day compressive strength of 3D-printed FA- and GGBS-based one-part AAMs was 10–27% lower than that of normal mould-cast specimens. This was observed in several 3D-concrete-printing studies [149,150] and is likely due to the higher porosity of printed materials in comparison to mould-cast specimens. These voids are inevitably introduced due to the layer-by-layer placement nature of 3D-printed materials.

In a recent study, the rheological behaviour of 3D-printed GGBS-based one-part AAMs was investigated [145]. Findings showed that small additions of nanoclay (0.4 wt%) significantly improved the yield stress of the fresh mix, and thereby the printability of the GGBS-based mixes [145]. The addition of hydromagnesite nucleation seeds by 2 wt% of GGBS content also led to rapid strength development and better buildability of performance [145]. In a different study, the addition of sucrose to 3D-printed FA- and GGBS-based one-part AAMs led to slower development of yield strength in the fresh mix, allowing more time for pumping and placement of the material [146]. However, sucrose did not have a significant impact on the viscosity of the fresh mix [146].

4. Reaction mechanisms and fresh properties

4.1. Reaction mechanisms and hydration products

As water is added to the dry one-part mix, the dissolution of the solid activator takes place which is an exothermic reaction [11]. Precursor wetting and dissolution of amorphous phases occur concurrently as well. Heat evolution curves in conduction calorimetry studies show this by an initial peak taking place immediately after water is added to the dry one-part mix [5,11,91,151]. This initial peak is typically followed by a dormant period, known as the induction period, and then a second peak is observed, also known as the acceleration peak, corresponding to the formation of hydration products [5,11,86]. As such, the reaction process of one-part AAMs in most cases can be divided into four stages: a) pre-induction period, b) induction period, c) acceleration period and d) deceleration period [11,13,94]. The resulting hydration products depend largely on whether low-calcium or high-calcium precursors are used. Using low-calcium precursors leads to the formation of 3-dimensional tetrahedrally interlinked N-A-S-H (sodium-aluminum-silicate-hydrate) gels [10,152], whereas high-calcium precursors result in the formation of tobermorite-like C-A-S-H (calcium-aluminum-silicate-hydrate) gels [152–155]. Blending low-calcium and high-calcium binders in one-part AAMs leads to the development of cross-linked N-A-S-H and C-A-S-H gels [10,139,156].

The silica solubility of the activator used has a marked influence on the reaction of one-part AAMs, including how and when the heat evolution peaks occur in calorimetric studies [34]. Dakhane and Neithalath [91] investigated in depth the reaction kinetics of GGBS-based one-part AAMs and reported that the solubility of silicate-based powders decreases with increasing the alkalinity of the system (i.e., increasing the alkali hydroxide content). The solubility of sodium silicate powders was determined to be less than that of potassium silicate powders, mainly due to the smaller hydration sphere of potassium ions [91,157,158]. For Na_2SiO_3 activated GGBS-based one-part pastes, increasing the modulus of silicate, M_s, of the activator (SiO_2/Na_2O), increases the silicate solubility, which in turn results in a higher dissolution peak, a shorter induction period and a lower acceleration peak [91].

Meanwhile, potassium silicate activated GGBS-based systems showed similar behaviour with the exception of a longer induction period with an increase in the M_s (SiO_2/K_2O) of the activator [91]. The cumulative heat released, measured after 80 h, was noticed to be lower with higher activator M_s due to the lower alkalinity of the system [91]. Wang et al. [159] noticed a higher dissolution peak in the heat profile of GGBS-based one-part AAMs activated via Na_2SiO_3 with an increase in activator content due to higher alkali concentration. Higher dissolution and acceleration peaks are noticed as well for GGBS-based and GGBS- and FASB-based one-part AAMs

activated using Na_2SiO_3-anhydrous in comparison to mixes activated with $Na_2SiO_3{\cdot}5H_2O$ or $Na_2SiO_3{\cdot}9H_2O$ [76]. The use of Na_2SO_4 in combination with Na_2SiO_3 to activate GGBS-based or GGBS- and FASB-based one-part AAMs led to longer induction periods and lower acceleration peaks in heat evolution curves [84].

Heat flow profiles of FA- and MK-based one-part AAMs activated with a combination of hydrous Na_2SiO_3 and NaOH or Na_2SiO_3-anhydrous showed higher reaction heat with an increase in the activator intensity or a reduction in the activator modulus (i.e., higher reaction heat with higher alkalinity) [5]. The heat released from mixes activated with Na_2SiO_3-anhydrous was higher than that of mixes activated with hydrous Na_2SiO_3 and NaOH despite having the same M_s value [5]. Also, the heat release from mixes activated with Na_2SiO_3-anhdyrous started slightly later than their Na_2SiO_3 and NaOH counterparts, indicating that the dissolution of the granular Na_2SiO_3-anhdyrous is comparatively slower [5]. In a comparative study between one-part and two-part AAMs, Ren et al. [151] showed that GGBS-based one-part AAMs activated via Na_2SiO_3-anhydrous had a lower acceleration peak in isothermal studies and developed comparatively lower C-A-S-H gels. Similarly, Hajimohammadi and van Deventer [160] highlighted that certain zeolite phases observed in FA-based two-part AAMs did not appear in FA-based one-part AAMs.

4.2. Initial flow and rate of flow loss

The initial flow and rate of flow loss of one-part AAMs are affected largely by the physicochemical properties of the aluminosilicate precursors. Precursors with irregular particles and higher CaO content usually result in lower initial flow and a higher rate of flow loss. For instance, the initial flow of GGBS-based one-part AAMs is generally lower than that of FA-based mixes [93,136,161]. Moreover, the flow loss of GGBS-based mixes with time is considerably higher than their FA-based counterparts [162]. The addition of LS to GGBS-based one-part AA pastes activated via Na_2SiO_3 reduced initial flow [23,24]. This reduction in flow was attributed to the high water demand of LS, as well as their irregular particle shape and high surface area. On the contrary, adding a small quantity of SF to GGBS-based one-part AAMs led to an improvement in initial flow, and caused a change in the shear stress-shear rate relationship by increasing the yield stress of the fresh mix and reducing the viscosity [163,164].

The type and dosage of the solid activator also play a major role on the fresh properties. A Comparative study on FA- and GGBS-based one-part AA pastes activated using NaOH, KOH and Na_2SiO_3-anhydrous showed that NaOH activated mixes achieved the lowest flowability and higher rate of flow loss [161]. Shah et al. [165] reported a higher initial flow in FA- and GGBS-based one-part AAMs with an increase in Na_2SiO_3-anhydrous dosage from 8 to 10% of binder content. This occurs as small dosages of Na_2SiO_3 help plasticize the mix and reduce the yield stress [166]. Meanwhile, Guo et al. [13] reported a drop in the fluidity of FA-, FASB- and GGBS-based one-part AA mortars, as the Na_2SiO_3 dosage increased from 10 to 30% (in 5% increments). This might suggest that there is an optimal value for the Na_2SiO_3 dosage in one-part mixes when considering initial flow, beyond which the consistency of the mix reduces.

> Replacing a proportion of Na_2SiO_3 with either Na_2CO_3, $NaAlO_2$ or $Ca(OH)_2$ in FA- and GGBS-based one-part mixtures caused a reduction in flow [83,167–169]. Ouyang et al. [170] combined silicate-based activators (either quick-dissolving Na_2SiO_3 or $Na_2SiO_3{\cdot}5H_2O$) with either Na_2CO_3 or $Ca(OH)_2$ to activate FA- and GGBS-based one-part mixtures and showed a higher reduction in workability with $Ca(OH)_2$ replacement as opposed to Na_2CO_3. Adding potassium carbonate (K_2CO_3) to Na_2SiO_3-GD and $Ca(OH)_2$ in FA-based one-part mixes caused a further reduction in workability [168]. Meanwhile, adding either lithium hydroxide (LiOH) or Na_2O to Na_2SiO_3-GD and $Ca(OH)_2$, as partial or full replacements of the latter, caused an increase in the relative slump [168]. The use of $NaHCO_3$ to activate FA- and GGBS-based one-part AAMs was shown to lead to slightly higher flow values as compared to using $Ca(OH)_2$ as activator [93]

The w/b and aggregate/binder ratios have also a major influence on the workability of the one-part mix. Generally, a higher w/b and a lower aggregate/binder ratios result in higher initial flow [164,171]. Goncalves et al. [107] showed that increasing the w/b content in GGBS-based one-part AAMs from 0.29 to 0.31 and 0.33 resulted in an increase in initial flow by 57% and 106%, respectively. Meanwhile, Yang et al. [172] showed a sharp reduction in the flow of FA- and GGBS-based one-part AA mortars as the sand/binder ratio increased above 2.5.

4.3. Setting time

The setting of AAMs depends largely on the rate of their reaction mechanism. Rapid setting typically occurs with higher CaO content in the precursor. The faster dissolution rate of CaO in comparison to SiO_2 and Al_2O_3 provides nucleation sites at an early age. This in turn causes short setting and rapid hardening [173]. For that reason, GGBS-based AA mixes tend to set more rapidly than other AA mixtures (e.g., FA-based and MK-based systems) [161,174]. It was identified that the setting process of low-CaO and high-CaO precursors differs in alkaline environments, where the former usually sets through a gel percolation approach, while the latter sets through localized precipitation of C-A-S-H gels [174]. An increase in the fineness of GGBS caused significantly shorter setting times [175], while the addition of SF to GGBS-based one-part AAC caused as much as 30 min delay in setting [110]. LS-based one-part mixes activated using Na_2SiO_3-anhydrous had very long initial (310 min) and final setting times (840 min) [23]. The addition of GGBS (40%) in combination with LS (60%) as precursors helped shorten the initial (140 min) and final setting times (480 min) to more reasonable levels. Jeon et al. [176] reported a reduction in setting times of GGBS-based one-part AAMs with an increase in calcined dolomite content due to its high reactivity. MK- and volcanic tuff-based one-part AAMs activated using LKD showed initial and final setting times in the range of 61–87 min and 78–110 min, respectively, where setting time was reduced with an increase in LKD content [67].

Considering the effect of activator type on setting, Ouyang et al. [170] showed that mixes activated using $Na_2SiO_3{\cdot}5H_2O$ had shorter setting times than mixes activated via quick-dissolving Na_2SiO_3. Also, a combination of sodium silicates and $Ca(OH)_2$ resulted

in shorter setting times than a combination of sodium silicates and Na_2CO_3 in FA- and GGBS-based one-part mixes, potentially due to the additional soluble Ca^{2+} supplied by $Ca(OH)_2$ [170]. Similarly, FA- and GGBS-based one-part AAMs show more rapid setting when activated using $Ca(OH)_2$ as compared to $NaHCO_3$ [93]. Replacing a proportion of Na_2SiO_3 with either Na_2CO_3, or $NaAlO_2$ in FA- and GGBS-based one-part systems caused a delay in setting [83,167]. A higher replacement of Na_2SiO_3 reduces the pH of the mix, causing a more moderate reaction rate [167,174]. Also, the delay in setting due to $NaAlO_2$ addition occurs as aluminate species coagulate the silicate species in Na_2SiO_3 and absorb to the precursor particles, which could generate negative charge sites that repel the OH^- responsible for catalysing the dissolution of aluminosilicate species [169]. A high solid activator dosage typically leads to shorter setting times. For instance, Li et al. [164] showed a reduction in the setting times of GGBS-based one-part AAMs activated via Na_2SiO_3 as the activator-to-binder dosage increased from 0.10 to 0.25.

5. Mechanical properties

The mechanical properties of one-part AAMs were mostly discussed in terms of the compressive strength, and less frequently in terms of the flexural strength and splitting tensile strength. As would be expected, different precursors, solid activators, water contents, binder-to-aggregate ratios, and curing conditions had a measurable effect on the resulting strengths, which are discussed here.

5.1. Precursor type and content

The compressive strength of one-part AAMs tends to be higher when calcium-rich precursors are used. For instance, Yang et al. [135] reported that the 28-day compressive strength of GGBS-based AA mortars (21.5–52.5 MPa) was higher than that of FA-based counterparts (0.57–9.45 MPa) using the same solid activator and cured in the same environment. Lemougna et al. [177] also reported lower 7-day compressive strength of MK-based one-part pastes (~20 MPa) activated with Na_2SiO_3-anhydrous in comparison to GGBS-based one-part AA pastes (~62 MPa). The substitution of a proportion of low-calcium precursors with high-calcium ones could result in significant improvements in the compressive strength. The fineness of the source material plays an important role in the resulting compressive strength, with finer precursors often resulting in improved compressive strength development [110,136]. Moreover, for a given activator dosage and water content, there appears to be an optimum precursor content for optimised mechanical properties. This differs from one mix to the other, depending on the constituents and curing conditions. Very little precursor content could lead to insufficient formation of binding phases, whereas excess content could result in many unreacted particles and excessive shrinkage [163].

5.2. Activator type and dosage

It is generally observed that sodium silicates are the most effective when it comes to compressive strength development in one-part AAMs. Even among the sodium silicates, the anhydrous type with a modulus of silicates ($M_s = SiO_2/Na_2O$) of around 0.9 typically outperforms the others, including $Na_2SiO_3{\cdot}5H_2O$ ($M_s \approx 1.04$), $Na_2SiO_3{\cdot}9H_2O$ ($M_s \approx 1.03$), Na_2SiO_3-GD ($M_s = 2.0$), quick-dissolving Na_2SiO_3 ($M_s \approx 2.86$) and sodium disilicate ($Na_2Si_2O_5$) ($M_s \approx 1.98$) [4,5,27,84,170]. Replacing a proportion of Na_2SiO_3 with either NaOH, Na_2CO_3, $NaAlO_2$ or Na_2SO_4 caused a reduction in the compressive strength of one-part AA systems [83,84,167,172]. Sodium hydroxides, despite their higher pH, usually come second to Na_2SiO_3 when considering compressive strength development [172]. Feng et al. [68] noted that Na_2CO_3 was less effective when compared to NaOH in activating albite-based one-part mixes. More recently, however, Zhou et al. [178] showed that combining Na_2CO_3 with $Ca(OH)_2$ to activate GGBS-based one-part mixes could attain compressive strengths that are 60% higher than the same mixes activated using NaOH. As for calcium-based activators, Kim et al. [86] highlighted that CaO was twice as effective when compared to $Ca(OH)_2$ in GGBS-based one-part AA pastes. Also, the use of $Ca(OH)_2$ in FA-based one-part AAMs was less effective than $NaHCO_3$ when considering the 28-day compressive strength [93]; however, the opposite was noticed when considering GGBS-based one-part mixtures where $Ca(OH)_2$ activated mortars had slightly higher 28-day compressive strengths [93].

The fineness of the activator also affects the strength of the hardened one-part AA mix. Having finer $Na_2SiO_3{\cdot}5H_2O$ particles was shown to result in higher compressive strength in FA- and GGBS-based mixes [163]. The large voids left behind after the dissolution of coarse activator particles was detrimental to the resulting compressive strength. As for the activator content, the compressive strength of one-part AA mixes tends to increase with higher activator dosage (more specifically, a higher Na_2O content) up to an optimum value, after which the compressive strength decreases. This optimum dosage of Na_2O varied from one study to the other but most often was in the range of 4–8 wt% [161,163,179]. Beyond this optimum value, excess Na_2O inhibits the formation of binding phases, increases the likelihood of activator leaching and efflorescence, which all contribute to matrix degeneration and strength loss. For MK-based one-part systems activated via biomass ashes, the compressive strength depended largely on the potassium-to-aluminum (K/Al) molar ratio [65,118]. For instance, Balo et al. [65] showed an increase in the compressive strength of CSA-activated MK-based one-part AAMs as the K/Al molar ratio increased from 1 to 5, with a drop in compressive strength afterwards as K/Al increased to 6.

5.3. Water content

The water content in one-part AAMs is dictated by the amount necessary to ensure full dissolution of the activator and any excess water beyond such limit results in strength deterioration. Dong et al. [163] experimented with several w/s ratios for FA- and GGBS-based one-part AA mixes in the range of 0.31–0.37 and concluded that optimum compressive strengths are recorded at a w/s ratio of 0.31. Oderji et al. [124] concluded an optimum w/s ratio of 0.28 for FA- and GGBS-based mixes activated using Na_2SiO_3-anhydrous while considering a range of values from 0.26 to 0.3. Abdel-Gawwad and Abo-El-Enein [180] investigated GGBS-based one-part AA pastes activated using a combination of NaOH and $CaCO_3$ with a range of w/s within 0.24–0.33 and

concluded that a value of 0.27 gave the best compressive strength results. Perumal et al. [139] investigated ternary blends of GGBS, phyllite dust and SF-based one-part mixes, with w/s in the range of 0.25–0.35 and noticed high compressive strength at a w/s of 0.30. This shows that for FA- and GGBS-based one-part mixes, optimum w/s ratios are likely in the range of 0.27–0.31.

5.4. Aggregate type and content

Aggregates act as nucleating sites for the formation of hydration products, with typically higher strengths observed in concretes, followed by mortars, and then pastes [168]. The strength of one-part AAC can be 16–20% higher than that of mortars having similar compositions [139,181]. The optimal content of aggregates in one-part AAMs was not thoroughly investigated, but Yang et al. [172] reported an increase in the compressive strength of GGBS-based one-part AA mortars with an increase in the sand-to-binder ratio up to a value of 2.5, after which a reduction in strength was observed. Replacing natural aggregates with other aggregate sources can result in lower or higher strength depending on the aggregate type. For instance, higher replacement of natural sand with lightweight expanded clay granules or crumb rubber particles resulted in a proportional reduction in the compressive strength of one-part AA mortars [111,116,182]. This reduction is due to the lower strength and elastic modulus of lighter aggregates, causing stress concentrations within the concrete matrix and the formation of microcracks [183]. The use of IMT aggregates instead of natural sand and gravel in FA- and GGBS-based one-part AAC resulted in lower compressive strength development [103]. Meanwhile, replacing a proportion of sand particles with either CW or WG fine aggregates in FA- and GGBS-based one-part AAMs resulted in an increase in the compressive strength [113,115,184]. Such improvement is attributed to the participation of CW and WG aggregates in the reaction, imparting additional silica and alumina to the mix and absorbing some of the available water, causing an increase in pH concentration and a higher dissolution of aluminosilicate species.

5.5. Admixture type and dosage

Few studies reported that adding sodium tetraborate decahydrate-borax to FA- and GGBS-based one-part AAMs (dosages in the range of 2–8% of precursor content) caused a reduction in strength in proportion with the dosage added [124,165]. Bong et al. [1] showed that adding polycarboxylate- and naphthalene-based SPs at 1% of precursor contents to FA- and GGBS-based one-part mixes activated via different types of sodium silicates caused a slight reduction in the compressive strength. The addition of sucrose (1% of precursor content) also negatively impacted the resulting compression strength [1].

The addition of a small dosage of SF to GGBS-based one-part mixes often improves the compressive strength. Compressive strengths of over 100 MPa at 28 days were recorded for GGBS-based one-part AAMs with small dosages of SF [34,139]. In GGBS-based mixes, the presence of SF causes the formation of cross-linked and non-cross-linked C-A-S-H gels, together with N-A-S-H gels, while the absence of SF results in the formation of non-cross-linked C-A-S-H gels [139]. Dong et al. [163] noted that adding SF to FA- and GGBS-based mixes resulted in a reduction in the compressive strength. This occurs as SF reduces the reactivity of FA in the mix.

5.6. Curing conditions

Heat curing of one-part AAMs made from different precursor bases, including GGBS, MK, volcanic tuff, bentonite and dolomite, was seen to contribute to significant improvement in the compressive strength [71,103,110,185]. This becomes more crucial when low-calcium precursors are used. For instance, Peng et al. [185] showed that for calcined bentonite- and dolomite-based one-part mixes activated using Na_2CO_3, heat curing at 80 °C for 3 days caused the compressive strength at 28 days to increase from less than 5 MPa (ambient curing) to 38.3 MPa. The effect of water curing on the compressive strength as reported in different studies was less conclusive. Yang et al. [87] reported that water curing of GGBS-based one-part mixes activated via a combination of $Ca(OH)_2$ and $Ba(OH)_2$ resulted in significantly higher strengths (as much as 201% increase) than ambient air curing. Abdollahnejad et al. [186] noted that water curing had a greater impact on improving the compressive strength of GGBS- and CW-based one-part mortars activated via Na_2SiO_3-anhydrous than sealed curing.

Meanwhile, other studies on FA-based and FA- and GGBS-based one-part AAMs have shown lower compressive strength development when water curing was employed as opposed to ambient curing [126,171]. This might suggest that when C-A-S-H gels are the primary hydration products, water curing could be beneficial for compressive strength development, while the opposite is the case when N-A-S-H gels are predominant. Sub-zero curing temperatures were also investigated for one-part AAMs [129,187], and findings showed that one-part AAMs performed better than OPC-based CCM cured at the same temperature. For instance, GGBS-based one-part AAMs cured at −5 °C were able to achieve a 56-day compressive strength of nearly 68 MPa, while OPC-based CCM mixes cured at the same temperature resulted in a 56-day strength of about 10 MPa [187]. Not only that, but one-part mixes showed greater strength recovery/increase when the sub-zero curing was followed by curing at ambient temperatures of 23 °C [187].

5.7. Predictive equations

Yang et al. [135] introduced an alkali-quality coefficient, Q_A, to help infer the compressive strength from the precursor and activator compositions (by weight) as given by Eq. (1), where s stands for the total weight of solids (precursor + activator). This coefficient can be expanded to account for the w/s and solid/aggregate (s/agg) ratios. General trends show that the compressive strength, f_c, reduces with a higher w/s ratio and improves with a greater s/agg ratio. As such, predictive expressions are proposed to correlate f_c with the constituent materials of pastes and mortars as given by Eq. (2). The parameter λ in Eq. (2) is a regression coefficient determined from the corresponding dataset.

Table 7
Summary of data points for Eq. (2).

Ref.	Precursor	Activator	Aggregates	n_{mixes}	$f_{c,test}/f_{c,pred}$	
					Average	COV
Pastes – 28-days						
[172]	FA, GGBS	Na_2SiO_3-anhydrous NaOH	–	4	0.74	0.16
[217]	FA, GGBS	Na_2SiO_3-anhydrous	–	13	1.04	0.16
[213]	FA	Na_2SiO_3-anhydrous	–	4	1.03	0.09
[48]	GGBS, LZMT	Na_2SiO_3	–	5	1.25	0.05
[78]	FA	Na_2SiO_3-anhydrous	–	2	0.92	0.32
[101]	GGBS	Oyster shells	–	1	0.96	0.00
[214]	FA	Na_2SiO_3-anhydrous	–	5	1.16	0.13
[107]	GGBS	Na_2SiO_3-anhydrous	–	3	0.95	0.08
Total				37	1.04	0.195
Mortars – 7-days						
[135]	GGBS	Na_2SiO_3-anhydrous	Sand	5	0.92	0.12
[172]	FA, GGBS	Na_2SiO_3-anhydrous NaOH	Sand	31	0.97	0.21
[136]	FA, GGBS	Na_2SiO_3-anhydrous NaOH	Sand	11	0.96	0.12
[34]	GGBS, SF, RHA	Na_2SiO_3-anhydrous NaOH	Sand	17	1.00	0.28
[170]	FA, GGBS	Na_2SiO_3 $Na_2SiO_3{\cdot}5H_2O$	Sand	2	1.16	0.42
[63]	GGBS, CW	Na_2SiO_3-anhydrous	Sand	8	1.07	0.21
[107]	GGBS	Na_2SiO_3-anhydrous	Sand	1	0.92	0.00
[187]	GGBS	Na_2SiO_3-anhydrous	Sand	1	1.56	0.00
[151]	GGBS	Na_2SiO_3-anhydrous	Sand	1	1.00	0.00
Total				77	1.00	0.24
Mortars – 28-days						
[135]	GGBS	Na_2SiO_3-anhydrous	Sand	5	0.97	0.12
[172]	FA, GGBS	Na_2SiO_3-anhydrous NaOH	Sand	33	1.09	0.22
[136]	FA, GGBS	Na_2SiO_3-anhydrous NaOH	Sand	12	1.17	0.11
[34]	GGBS, SF, RHA	Na_2SiO_3-anhydrous NaOH	Sand	2	0.79	0.02
[170]	FA, GGBS	Na_2SiO_3 $Na_2SiO_3{\cdot}5H_2O$	Sand	1	1.27	0.00
[163]	FA, GGBS, SF	$Na_2SiO_3{\cdot}5H_2O$	Sand	5	0.88	0.10
[63]	GGBS, CW	Na_2SiO_3-anhydrous	Sand	4	0.89	0.02
[151]	GGBS	Na_2SiO_3-anhydrous	Sand	1	1.01	0.00
Total				63	1.06	0.20
Mortars – 90-days						
[135]	GGBS	Na_2SiO_3-anhydrous	Sand	5	1.00	0.09
[172]	FA, GGBS	Na_2SiO_3-anhydrous NaOH	Sand	39	1.09	0.21
[136]	FA, GGBS	Na_2SiO_3-anhydrous NaOH	Sand	11	1.18	0.15
[34]	GGBS, SF, RHA	Na_2SiO_3-anhydrous NaOH	Sand	2	0.79	0.03
[163]	FA, GGBS, SF	$Na_2SiO_3{\cdot}5H_2O$	Sand	6	0.98	0.23
[151]	GGBS	Na_2SiO_3-anhydrous	Sand	1	0.96	0.00
Total				64	1.08	0.20

n_{mixes} = number of mixes; $f_{c,test}$ = test compressive strength; $f_{c,pred}$ = predicted compressive strength.

$$Q_A = \frac{\left(\frac{Na_2O}{(SiO_2)^2} \,.\, Al_2O_3 \,.\, CaO\right)}{s} \text{ (by weight)} \tag{1}$$

$$f_c = \lambda \times \frac{Q_A}{w/s} \cdot (\text{MPa}) \rightarrow (\text{pastes}) \tag{2a}$$

$$f_c = \lambda \times \frac{Q_A}{w/s} \times (s/agg) \cdot (\text{MPa}) \rightarrow (\text{mortars}) \tag{2b}$$

$$\lambda = \begin{cases} 1100.6 \rightarrow \textit{pastes at } 28 \textit{ days} \\ 2078 \rightarrow \textit{mortars at } 7 \textit{ days} \\ 2209.7 \rightarrow \textit{mortars at } 28 \textit{ days} \\ 2599.3 \rightarrow \textit{mortars at } 90 \textit{ days} \end{cases} \tag{2c}$$

A database of one-part AA pastes and mortars was assembled from the literature as given in Table 7. This dataset includes mixes from different studies of which the chemical composition of the precursors and solid activators, and mix design details were fully reported. To eliminate the effect of different admixtures and specimen size on f_c, only cube specimens with no added chemical admixtures were considered. Also, as the curing environment affects f_c, the database only included specimens cured under ambient temperatures in the range of 20–30 °C. As can be seen from Table 7, the dataset included mostly mixes with FA and GGBS as the main precursors and Na_2SiO_3-anhydrous and NaOH as the main solid activators. Few studies considered in the dataset used other precursors either separately or in combination with FA and GGBS, such as RHA, SF, CW, and LZMT. For mixes activated with sodium silicates, the determination of Q_A was straightforward as Na_2O and SiO_2 were usually reported. For mixes activated with NaOH, the amount of Na_2O was calculated by assuming 1 mol of NaOH contains 0.5 mol of Na_2O as suggested by Yang and Song [136]. The results are shown in Fig. 7 and Fig. 8 for one-part AA pastes and mortars, respectively. Due to limited one-part AA paste results, correlations at 28 days are only shown, whereas for one-part AA mortars, results up to 90-days are given.

Findings show that Eq. (2a) for the 28-day f_c of one-part AA pastes gives an average test-to-predicted value of 1.04 and a coefficient of variation (COV) of 19.5%. Eq. (2b) for the 7-day, 28-day and 90-day f_c of one-part AA mortars gives an average test-to-predicted value of 0.996, 1.06 and 1.08, respectively, and a COV of 23.6%, 20.3% and 19.8%, accordingly. It should be noted, however, that Eq. (2) is in no way replacing the need for physical tests for a given blend of constituent materials as they do not capture the effect of optimal water contents, aggregate/binder ratios, or the effect of certain admixtures. Also, the determination of Q_A using weight ratios of chemical compositions of precursors and activators has its limitations, as certain crystalline phases in the precursors which show on the chemical compositions do not participate in the reaction. However, the predictive equations can provide a good guide to estimate the compressive strength for a given blend of constituent materials and narrow down potential mixes for optimal f_c.

The flexural strength, f_f, and splitting tensile strength, f_{sp}, of one-part AAMs are generally controlled by the same factors that affect f_c. Both Neupane [188] and Neupane et al. [189] suggest Eq. (3) to predict f_{sp} from f_c for FA- and GGBS-based AAC activated using a mixture of Na_2SiO_3 and NaOH. Parameter A in Eq. (3) is a factor taken as 0.67 by Neupane [188] and 0.70 by Neupane et al. [189].

$$f_{sp} = A \times (f_c)^{0.5} \tag{3}$$

6. Durability

The durability of AAMs has been the subject of much investigation and interest, to the point that some researchers argue that their superior durability performance to that of OPC-based CCM, drawing reference to existing ancient roman structures made of concrete

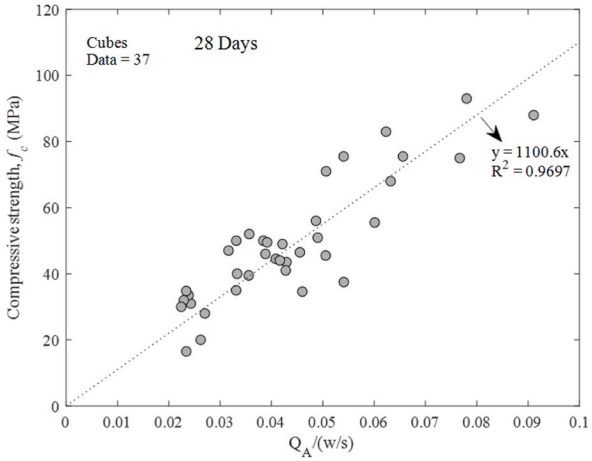

Fig. 7. 28-day compressive strength of one-part AA pastes.

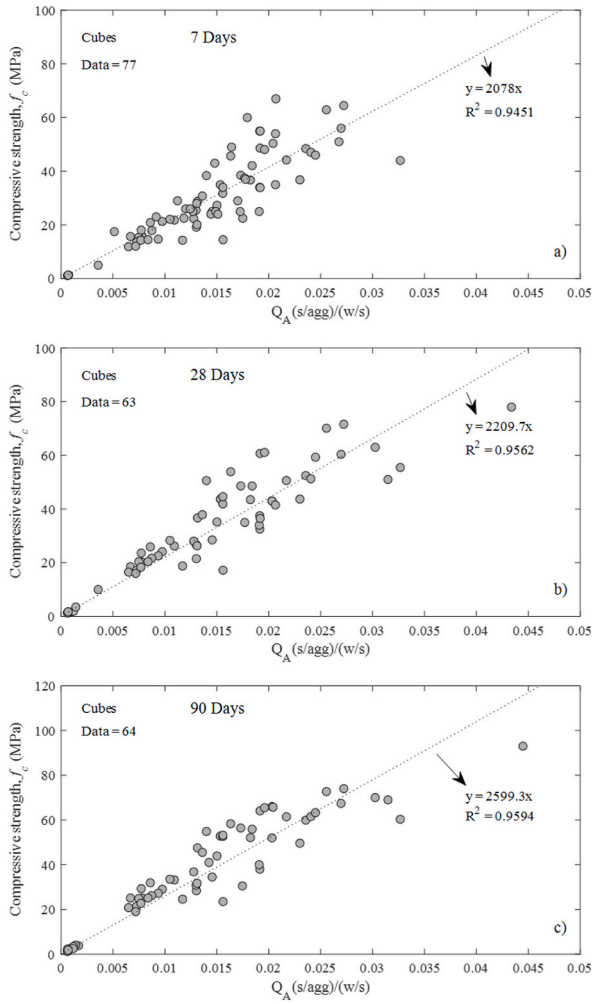

Fig. 8. Compressive strength of one-part AA mortars: a) 7 days, b) 28 days, c) 90 days.

with similar blends, merit their use as alternative construction material [156]. In this section, the durability performance of one-part AAMs, including their porosity and water absorption, efflorescence, acid resistance, and shrinkage, is reviewed.

6.1. *Porosity and water absorption*

The porosity and water absorption of one-part AAMs are generally influenced by the precursors used, activator type and dosage, and water content. For instance, GGBS-based mixtures tend to have a more compact pore structure when compared to sole FA-based mixes [190], binary GGBS- and FASB-based pastes [12,167] or binary LS- and GGBS-based systems [23] due to the nature of hydration products formed. Findings also show that while incorporating FASB in GGBS-based one-part AAMs causes an increase in the overall pore volume, it improves the pore structure by reducing the amount of harmful pores (size between 20 and 200 nm) and increasing the amount of harmless pores (size <20 nm) [167]. The incorporation of LZMT by up to 10% in GGBS-based one-part AAMs was reported to reduce the total porosity and improve particle packing [48].

Investigating the effect of different sodium silicates on the pore structure of GGBS- and FASB-based one-part AA pastes, Ma et al. [76] showed that $Na_2SiO_3{\cdot}5H_2O$ resulted in the highest volume of pores followed by $Na_2SiO_3{\cdot}9H_2O$ and then Na_2SiO_3-anhydrous. These results were consistent with the observed compressive strengths. Using Na_2SiO_3-anhydrous as a sole activator in GGBS- and FASB-based mixes resulted in lower porosity than using it in combination with either Na_2CO_3 or Na_2SO_4 [12,84,167]. Zhou et al. [178] showed that the porosity of GGBS-based one-part AA pastes was lower for mixes activated using a combination of Na_2CO_3 and $Ca(OH)_2$ than mixes activated using NaOH. Porosity and water absorption also depend on the water content of the mix. For instance, the water absorption of GGBS-based one-part pastes activated using a combination of NaOH and $CaCO_3$ decreased as the w/s ratio increased from 0.24 to 0.27 and then increased again with a further increase in w/s up to 0.33 [180].

6.2. *Efflorescence*

Efflorescence occurs when free alkalis from the activator leach out to the surface as water evaporates and react with the

atmospheric CO_2, forming as a result white deposits of carbonate salt (Na_2CO_3) [57]. Efflorescence in AAMs does not slow down with time, unlike that for OPC systems, and can have serious durability ramifications. Dong et al. [163] carried out a thorough investigation (up to 90 days) to see the effect of several factors; including the type and dosage of activator, binder content, and water content, on the efflorescence of FA- and GGBS- based one-part AA mortars. Their findings point to the importance of controlling the activator dosage, especially the Na_2O content, which had a directly proportional relationship with efflorescence. It is suggested that for effective efflorescence control, the Na_2O content should be limited to 3–6% of the total binder weight [163]. Increasing the proportion of FA in the binder (i.e., reducing GGBS content) caused a significant reduction in efflorescence, potentially indicating the higher susceptibility of GGBS-based mixtures to efflorescence [163]. Increasing the Al content in the mix could help control efflorescence by ensuring a certain extent of reaction at an early stage [19,153]. Moreover, a higher water content was also seen to increase efflorescence due to the likelihood of a more porous microstructure [23]. Sealed curing or curing at an RH $\geq$ 95% could help reduce the intensity of efflorescence [3].

6.3. Sulphate and acid resistance

Resistance of one-part AAMs to aggressive solutions depends mainly on their porosity as well as the nature of their hydration products [191]. The immersion of GGBS-based and FA- and GGBS-based one-part AAMs – activated using Na_2SiO_3-anhydrous – in Na_2SO_4 solutions for up to 270 days show good residual strengths of around 90% [11,126]. Immersion of one-part AAMs in an Na_2SO_4 solution can help with further dissolution of aluminosilicate species and results in strength improvements [11]. Mixes with higher FA/FASB content showed higher Na_2SO_4 resistance as indicated by their residual strengths [11]. Exposing FA and GGBS- based one-part AAMs – activated using Na_2SiO_3-anhydrous either separately or in combination with Na_2CO_3 – to acidic solutions, including nitric acid (HNO_3) and sulfuric acid (H_2SO_4) caused a reduction in their residual strength in direct proportion to the immersion time [11,12,126]. This consistent reduction in strength can be attributed to the destructive effect of H^+ cations on C-A-S-H and N-A-S-H gels, causing a weakened microstructure. Here again, the mixes with higher FA/FASB content experienced a lower drop in compressive strength with longer acid immersion time in comparison to GGBS-based mixes [11]. Higher calcium content in the precursor causes the formation of expansive products, such as gypsum and ettringite, when in contract with aggressive solutions, which could further damage the microstructure of one-part AAMs [81]. Adding mineral admixtures, such as SF, MgO and MK, by up to 4.5% to FA- and GGBS-based one-part mixes resulted in improved resistance to Na_2SO_4 and H_2SO_4 solutions [126].

Noticing the possible structural evolution in one-part AAMs due to exposure to Na_2SO_4, Coppola et al. [166] investigated the sulphate resistance of GGBS-based one-part AAMs by partially immersing 28-day cured prisms in 10 wt% magnesium sulphate ($MgSO_4$) solution for up to 130 days. Results showed severe mass loss and a significant reduction in strength due to the formation of expansive products and the breaking of C-A-S-H gels. The authors also investigated the effect of immersion in 30 wt% $CaCl_2$ solution to observe the effect of calcium chloride ingress in the one-part mixes. GGBS-based one-part mixes had excellent residual strength (change in strength $<$8%) and very minimal mass loss [166].

6.4. Shrinkage

In AAMs, autogenous and drying shrinkage could indeed pose a challenge to their wide-scale use. Autogenous shrinkage is the volumetric reduction in concrete due to water demand for hydration, which causes capillary pores with surface tension responsible for length reduction [192]. Drying shrinkage, on the other hand, is the volumetric change in concrete due to the loss of water as concrete is stored in unsaturated air [192]. In such cases, as the concrete dries, free water in the pores moves to the surface and evaporates. This causes hydrostatic tension to develop in the capillary pores and may lead to microcracks. The development of microcracks due to autogenous and drying shrinkage could be detrimental to the durability of AAMs.

In one-part AAMs, shrinkage depends on the precursor type, activator used, water content, aggregates, and curing conditions. FA-based one-part AA mortars had lower drying shrinkage values when compared to their GGBS-based counterparts using the same activator and cured in the same environment [93]. The finer pore structure of GGBS-based mixtures, compared to FA-based systems, causes higher capillary stresses, and this ultimately results in higher drying shrinkage values [93,109]. It was shown recently that the drying shrinkage of GGBS-based one-part AAC was about 3.5–5.5 times that of OPC-based CCM [109], while the drying shrinkage of FA-, GGBS- and albite-based one-part AA paste was twice that of OPC-based pastes [127]. The addition of SF by 15% of binder weight to GGBS-based one-part AAC led to a significant reduction in the drying shrinkage by as much as 32% [109]. Meanwhile, the addition of 5 wt% SF to a ternary blend of FA, GGBS and albite-based one-part AAM led to a slight increase in the drying shrinkage [127]. Increasing the LS content in the mix was also associated with higher drying shrinkage values [23].

As for activator type, it was shown that for GGBS-based one-part AAMs, the drying shrinkage increased when Na_2SiO_3-anhydrous was used in comparison to a combination of NaOH and Na_2CO_3 [3] or sole Na_2SO_4 [84]. Higher drying shrinkage values were observed for FA- and GGBS-based one-part AA mortars when activated with $Ca(OH)_2$ as compared to $NaHCO_3$ [93]. Replacing a proportion of soda residue with CCR to activate GGBS-based AA mortars led to lower drying shrinkage values [104]. Furthermore, a higher content of activator in FA- and GGBS-based mixtures was associated with higher drying shrinkage [93,94]. Similarly, an increase in the water-to-binder ratio in GGBS-based one-part AAMs resulted in higher drying shrinkage [109].

The incorporation of natural aggregates in the mix caused a reduction in the drying shrinkage of one-part AAMs [115,184]. Also, using CW as fine aggregates helped reduce the drying shrinkage of FA- and GGBS-based one-part mixes when compared to control mixes with natural sand [115]. Similarly, using WG as fine aggregates caused the shrinkage of FA- and GGBS-based mixtures to reduce in comparison to mixes with natural sand [184]. This is due to the participation of CW and WG in the reaction with time, forming hydration products at the surface of the aggregates and forming a strong interfacial transition zone which restrained the drying shrinkage. The incorporation of lightweight and unreactive clay granules as a replacement for natural sand in GGBS-based one-part

AAC caused an increase in the drying shrinkage, which was proportional to the increase in replacement level [111]. This occurs as lightweight aggregates have greater water absorption and induce more voids when compared to ordinary natural aggregates, increasing as a result of the drying shrinkage. Also, a higher content of lightweight aggregates causes a reduction in the elastic modulus, which makes specimens less stiff to resist a reduction in length due to drying [192]. Curing of one-part AAMs at elevated temperatures (i.e., oven curing) caused a significant reduction in the drying shrinkage of FA- and GGBS-based one-part AAMs when compared to ambient curing [93]. High temperature curing causes rapid strength development, which increases the stiffness of the concrete matrix, resulting in greater resistance to drying shrinkage [93]. Sealed curing for 7 days proved to be less effective than water curing for reducing the drying shrinkage of GGBS-based AAC [109].

The autogenous shrinkage of one-part AAMs is comparatively less discussed. Generally, similar trends were noticed for autogenous shrinkage, where higher values are reported for GGBS-based one-part mixtures in comparison to their FA-based counterparts [93]. Also, $Ca(OH)_2$ activated FA- and GGBS-based one-part AA mortars had higher autogenous shrinkage than $NaHCO_3$ activated counterparts [93]. The autogenous shrinkage increased as well with higher activator dosage, and reduced when oven curing was employed [93].

7. One-part vs. two-part AAMs

The change in production method from the conventional two-part to the one-part 'just-add-water' method affects the fresh properties, mechanical strength, and durability characteristics. Saedi et al. [175] and Ren et al. [151] showed more rapid setting in GGBS-based two-part AAMs when compared to their one-part counterparts. Longer setting in GGBS-based one-part systems was partly attributed to the additional time needed for the solid activators to dissolve [151]. Also, as the activator dissolves upon water addition, heat is released which causes part of the GGBS to react more rapidly. This rapid partial reaction of the GGBS forms a hard reaction gel around other unreacted GGBS particles, causing in the process longer setting times [151]. Partial reaction of GGBS particles was not observed in two-part AAMs [151]. Alhamdan [93] also reported a much quicker setting of FA- and GGBS-based two-part AAMs when compared to their one-part counterparts. The workability of one-part and two-part AAMs (FA-based or GGBS-based) was generally comparable, with a slightly higher flow in one-part systems [4,5,93,151]. The higher viscosity of the alkaline activator in two-part AAMs could be responsible for comparatively lower flow values [93].

Comparing the compressive strength of two-part AAMs to that of similar one-part systems, the former usually develops a relatively higher compressive strength [193,194]. For example, Nematollahi et al. [4] showed a drop in the compressive strength by nearly 31% when the production method changed from two-part to one-part. Zhang et al. [5] synthesized FA- and MK-based one-part and two-part mixes and noticed that the compressive strength of the one-part mixes was in the range of 65–95% of their two-part counterparts. This occurs as the alkaline activator in two-part systems fully dissolves in the solution and participates in the reaction process which causes higher development of hydration products.

The strength development of ambient cured one-part and two-part AA specimens seems to differ as well, with two-part systems developing almost 90% of the 28 days strength within the first 7 days. On the contrary, one-part systems exhibited an increase in strength of more than 30% between 7 and 28 days for the ambient cured samples [5]. This again is due to the rapid dissolution induced by the fully dissolved activator in two-part systems, causing a relatively faster formation of binding phases. In a different study, Ren et al. [151] showed a similar strength development in two-part and one-part GGBS-based AAMs in the first 7 days; however, one-part AA mixes continued to show lower strength development after 7 days and up to 90 days. At 90 days, one-part mixes achieved a compressive strength of 67.4 MPa, while the two-part counterparts had a compressive strength of 70.8 MPa.

Considering the durability of one-part and two-part AAMs, results of GGBS-based systems suggest higher porosity and water absorption of the former group accompanied by greater proneness to efflorescence [151]. The autogenous and drying shrinkage of FA- and GGBS-based one-part AA mortars were reported to be significantly lower than that of their two-part counterparts, with generally similar trends on the effects of precursor, activator dosage and curing conditions on the shrinkage characteristics [93].

8. Design standards for AAMs

Design standards for concrete materials typically prescribe mix design rules and test methods, and outline the mechanical and durability characteristics of such materials. Their main objective is to allow commerce while also ensuring reliability and safety. The prescriptive nature of such standards limits the materials that can be used in the mix design process, and this has long been identified as an issue with existing concrete design standards and guidelines [195,196]. For AAMs, the issue of developing design standards becomes more critical due to the wide scope of aluminosilicate precursors and activators that are currently available and which are constantly being discovered. Several efforts have been made to develop design-standards for AAMs to allow their use for practical applications. Among such efforts is the publication of a performance-based design standard for AAMs in the UK [197], which allows the activator to be added in an aqueous state (two-part AAMs) or in a solid form blended with the precursors and other constituents (one-part AAMs). The specification sets requirements on the precursor components and activators, and stipulates ways to assess their performance and durability.

Other design standards for AAMs are underway, including an Indian design standard for two-part AAMs used in precast concrete [198]. This design standard lists several precursors, including FA, GGBS, SF, MK, and RHA, and several activators, including NaOH, KOH, Na_2SiO_3, K_2SiO_3, Na_2CO_3 and K_2CO_3, for possible use. The Indian design standard stipulates guidelines for precursor and activator contents, water-to-solid ratio, aggregates content, and target strengths [198]. In addition, ongoing work by RILEM experts to publish a durability performance-based standard for AAMs titled "Durability Testing of Alkali-activated Materials-Technical committee 247-DTA," are also underway [199]. Concrete guidelines specifying durability testing methods often approach the subject with

the chemistry of OPC-based systems in mind. The RILEM durability performance-based standard takes into account the chemistry of AAMs and focuses mainly on chloride penetration, carbonation, sulphate attack, freeze-and-thaw resistance, and alkali-aggregate reactions [199].

In a recent publication, van Deventer et al. [200] set out a framework for future performance-based design standards to ensure their wide-scale deployment. This includes the development of standards with no restrictions on the constituents used, whether precursors, activators, aggregates, or admixtures. The authors also argue that performance and durability test methods should take into account the nature of AAMs, including their chemistry and service life conditions. Such suggestions could indeed inform and widen the scope of future performance-based standards for AAMs, including one-part AAMs.

9. Health and environmental aspects

Due to the industrial process involved in generating some of the precursors and activators used in one-part AAMs, some constituents may be considered as naturally occurring radioactive materials (NORMs). Their natural radioactivity, as such, should be determined to ensure their safety and to avoid any health and environmental issues. Constituents identified as NORMs include FA, GGBS, ACS, FS, SF, RM, volcanic tuff, and WG, to name a few [201]. Their radioactivity is determined from the concentration of natural radionuclide content, mainly ^{226}Ra (radium series), ^{232}Th (thorium series) and ^{40}K (potassium) [202]. The concentration of natural radionuclides in building constituent materials usually varies between 1 and 4000 Bq/kg, where Bq (becquerel) is the unit used to estimate radionuclides activity [202].

Recent European legislation concerned with the safety against exposure to radiation stipulates that the indoor gamma-radiation of building materials formed using NORMs should be determined [203]. As a reference, the gamma-radiation emitted by building materials should be restrained to $\leq$1 mSv per year, where mSv is a millisievert used to measure whole-body radiation dose. This gamma-radiation of building materials, or their constituents, is typically determined using an activity concentration index (ACI) given by Eq. (4), where C_{226Ra}, C_{232Th} and C_{40K} are the concentrations of ^{226}Ra, ^{232}Th and ^{40}K in Bq/kg [201]. The ACI is a helpful screening tool for building materials using NORMs to give insights into their gamma-radiation. For materials used predominantly or partially (e.g., walls, basements), an ACI value of 0.5 or less indicates a radiation dose of about 0.3 mSv, while an ACI value of 1 indicates a dose of 1 mSv [202]. The ACI index is not applicable directly to raw constituent materials, but in case used, an appropriate partitioning factor should be employed.

$$ACI = \frac{C_{226_{Ra}}}{300} + \frac{C_{232_{Th}}}{200} + \frac{C_{40_K}}{3000} \quad (4)$$

The natural radioactivity of FA generally depends on the coal from which it is derived, the combustion process and its particle size [204]. FA generally has an ACI value of over 1, but when used to form AAMs, the ACI value of the resulting product is usually less than 1. For instance, Nuccetelli et al. [205] showed that the ACI value for different FA-based two-part AAMs was consistently less than 1. The same was also noticed by Puertas et al. [202], where ACI values of less than 1 were reported for FA-based two-part AAMs. As for GGBS, its natural radioactivity depends on the iron ore used in blast furnaces [206]. ACI values of lower than 1 are commonly reported for GGBS, and their natural radioactivity was less than that of FA [201]. GGBS-based AAMs tend to show ACI values of less than 1 as well [202]. Red mud, with its high alkalinity and toxicity, consistently shows ACI values of over 1 [204]. In addition, AAMs with red mud accounting for over 60% by content typically show ACI values of over 1 [204]. Certain biomass ashes, used as both precursors and activators, have ACI values of over 1 due to their high ^{40}K content. WG, used either as a precursor, activator or aggregates, poses very little natural radioactivity threat due to their consistently low ACI values [201].

10. Directions for future research

Future studies on one-part AAMs are needed to enable wide-scale deployment. AAMs can be used in niche applications in which they offer better results than that of OPC-based CCMs and help tackle pressing environmental issues. It was shown that one-part AAMs can provide a valorisation path for waste products from the industrial, mining, and agricultural sectors. This in itself is a compelling reason for the use of AAMs, particularly when considering the rising amount of waste, declining landfill spaces and other waste management challenges. The application of one-part AAMs in 3D-printing seems very promising as well. Sub-zero curing is another area where one-part AAMs have shown superior performance to OPC-based CCM [129,187]. Furthermore, GGBS-based one-part AAMs showed significantly better resistance to $CaCl_2$ solutions when compared to OPC-based CCM [166], and this merits their use in structures in contact with $CaCl_2$ de-icing salts. Early studies also show superior thermal stability of one-part AAMs to that of OPC-based mixes [177] which might allow their use as fire-resistant construction materials.

Finding alternative precursors to FA and GGBS, as well as improving the sustainability of solid activators will be important questions to tackle in the years ahead. Future studies can build on the work available for other feasible precursors to find suitable mix designs with excellent fresh, mechanical and durability characteristics. Moreover, commercial synthetic solid activators, particularly those produced at high purity, can constitute up to 80% of the overall production cost of one-part AAMs [207]. The production of synthetic activators is also energy-intensive, and their wide scale use can present environmental challenges. Future studies can find ways to clean up the production of synthetic solid activators. For instance, a recent study on GGBS-based one-part mixes activated using CaO used solid activators for carbon capture with promising results [208]. Alternatively, solid activators from waste products can be used. While the currently available research on waste-derived solid activators is in its early stages, several candidates including WG and biomass ashes have shown significant potential.

Much of the available work on one-part AAMs has been concerned with pastes and mortars. Concrete-level studies, constituting

both fine and coarse aggregates, are necessary as well to shed light on their fresh properties, mechanical strength, and durability characteristics. Understanding the material-level properties of one-part AA concrete could promote more structural-level studies, a precursor to any real-world application. Structural-level studies on one-part AAMs have been lacking to date, unlike that for two-part AAMs, and future research effort should be made in that direction. Concrete-level studies with a focus on more sustainable aggregate types is also important and much needed. A number of these studies have been discussed in this review, including replacing natural aggregates with WG aggregates, CW, and crumb rubber. Establishing workable mix designs for one-part AA concretes with sustainable aggregates, as well as a comprehensive understanding of their mechanical and durability properties, is very much needed.

Most studies on one-part AAMs have mostly examined the compressive strength and often the flexural and splitting strengths. Studies on the elastic modulus, crushing strains, and full stress-strain response of one-part AAMs are lacking. Quantifying such properties for design purposes is very important and future studies can fill this research gap. Another important parameter for design is the creep, or the deformation under sustained loading, of one-part AAMs. This has not been addressed and is particularly important when considering the long-term behaviour of concrete structures. Shi et al. [174] noted that while the early-age creep of conventional AAMs might be similar to OPC-based CCM, the long-term creep of such materials can be more dramatic and must be taken into consideration in the design process. Other durability related parameters, such as carbonation depth, sorptivity, abrasion resistance, and freeze-and-thaw resistance, were not assessed thoroughly and further studies, particularly those using precursors other than FA and GGBS, are much needed.

To ensure the sustainability of AAMs, constituent materials should be sourced locally. This calls for the development of performance-based design standards as developing prescriptive design codes for a varied range of potentially suitable precursors is near impossible. As discussed in this article, several design standards are being developed for AAMs, but most of them are geared towards conventional two-part AAMs. Performance-based design standards for one-part AAMs are needed to allow for their commercial use and wide-scale deployment. Furthermore, the natural radioactivity of one-part AAMs, and the myriad constituents used to form them, should be determined to ensure their safety and compliance with existing building requirements.

11. Conclusions

This paper reviewed recent studies on one-part alkali-activated materials (AAMs), with focus on the constituent materials, preparation methods, fresh properties, mechanical properties, and durability characteristics, as well as the internal reaction mechanisms and resulting binding phases. The influence of different precursors and solid activators with varying chemical compositions on the mechanical properties, was examined, and predictive expressions were proposed. The review shows that one-part AAMs are a viable alternative to conventional concrete with the advantage of making use of existing production methods and supply chains. With appropriate mix proportioning, high strength AAM concrete with good durability performance, suitable for structural applications, can be achieved. Based on the discussion points made, several concluding remarks are outlined below.

- A range of aluminosilicate precursors were used in one-part AAMs including industrial by-products and waste, mine tailings, agricultural waste, commercial and construction waste, and sources of geological origins. However, both fly ash (FA) and ground granulated blast furnace slag (GGBS) remain the two most predominant precursors used.
- Among the synthetic activators used in one-part AAMs, sodium silicate is the most common and the most effective in terms of compressive strength development. Solid activators from waste streams, such as pre-treated paper sludge, lime kiln dust and various biomass ashes, were also investigated.
- Several sources of fine natural aggregate replacements were employed in one-part AAMs, including waste glass, ceramic waste, waste sand and crumb rubber. The addition of waste glass and ceramic waste was promising, resulting in slightly higher strengths due to their reactivity in alkaline media. Meanwhile, the addition of softer aggregates, like crumb rubber particles and lightweight clay, resulted in a reduction in strength.
- The water content of FA- and GGBS-based one-part AAMs differs depending on the constituent materials, but a range of water-to-solid ratios of 0.27–0.31 were proven to provide optimal results. Clay-based one-part mixes typically need higher water contents of over 0.4 to achieve standard consistency.
- One-part AAMs made from precursors having high calcium contents and activated using aggressive solid activators (i.e. high pH) tend to have a higher rate of flow loss and short setting times. The fresh flow of one-part AAMs seems to be controlled largely by the surface morphology of the precursors and the surface tension induced by the activators. Precursors with smooth and spherical surfaces and activators imparting lower surface tension result in high flowability mixes.
- One-part AAMs made of high-calcium precursors and activated using aggressive solid activators usually develop higher compressive strengths when compared with low-calcium-based one-part AAMs or those activated with solid activators with low pH.
- Considering the different types of precursors and solid activators, limiting the Na_2O content in the activator to 6 wt% seems a good starting point for finding the optimum activator dosage for improved compressive strength and limited efflorescence.
- The porosity and water absorption of one-part AAMs have an indirectly proportional relationship with the compressive strength depending mainly on the precursors, solid activators, and water content used.
- Immersion of one-part AAMs in Na_2SO_4 and $CaCl_2$ solutions had very little effect on the residual strength. Meanwhile, immersion in HNO_3 and $MgSO_4$ solutions for extended periods, particularly GGBS-based one-part AAMs, caused severe mass loss and significant reduction in residual strength.
- GGBS-based and LS-based one-part AAMs tended to develop greater drying shrinkage in comparison to FA/FASB-based one-part AAMs.

- Future studies on one-part AAMs need to focus on synthesising one-part AAMs made from precursors other than FA and GGBS, and to examine thoroughly their fresh, mechanical and durability properties, as well as reducing or replacing synthetic solid activators.
- Structural level testing of one-part AAMs is lacking, and further studies in this direction are needed. Development of performance-based design standards is also important to ensure flexibility in proportioning one-part AAMs to local conditions.

Declaration of competing interest

The authors declare that they have no known competing financial interests or personal relationships that could have appeared to influence the work reported in this paper.

Acknowledgements

The first author acknowledges the funding provided by the President's PhD Scholarship at Imperial College London for his research.

References

[1] S.H. Bong, B. Nematollahi, A. Nazari, M. Xia, J. Sanjayan, Efficiency of different superplasticizers and retarders on properties of "one-part" fly ash-slag blended geopolymers with different activators, Materials 12 (2019), https://doi.org/10.3390/ma12203410.
[2] M. Amran, R. Alyousef, H. Alabduljabbar, M. El-Zeadani, Clean production and properties of geopolymer concrete; A review, J. Clean. Prod. 251 (2020), https://doi.org/10.1016/j.jclepro.2019.119679, 119679.
[3] S.D. Wang, X.C. Pu, K.L. Scrivener, P.L. Pratt, Alkali-activated slag cement and concrete: a review of properties and problems, Adv. Cement Res. 7 (1995) 93–102, https://doi.org/10.1680/adcr.1995.7.27.93.
[4] B. Nematollahi, J. Sanjayan, F.U.A. Shaikh, Synthesis of heat and ambient cured one-part geopolymer mixes with different grades of sodium silicate, Ceram. Int. 41 (2015) 5696–5704, https://doi.org/10.1016/j.ceramint.2014.12.154.
[5] H.Y. Zhang, J.C. Liu, B. Wu, Mechanical properties and reaction mechanism of one-part geopolymer mortars, Construct. Build. Mater. 273 (2021), 121973, https://doi.org/10.1016/j.conbuildmat.2020.121973.
[6] N. Shyamananda Singh, S. Thokchom, R. Debbarma, Properties of fly ash and rice husk ash blended geopolymer with sodium aluminate as activator solution, Eng. Appl. Sci. Res. 48 (2021) 92–101, https://doi.org/10.14456/easr.2021.11.
[7] M. Amran, M. Gutierrez, R. Alyousef, M. El-Zeadani, H. Alabduljabbar, V. Aune, Performance investigation of high-proportion Saudi- fly-ash-based concrete, Results Eng 6 (2020), 100118, https://doi.org/10.1016/j.rineng.2020.100118.
[8] X. Guo, H. Shi, X. Wei, Pore properties, inner chemical environment, and microstructure of nano-modified CFA-WBP (class C fly ash-waste brick powder) based geopolymers, Cem. Concr. Compos. 79 (2017) 53–61, https://doi.org/10.1016/j.cemconcomp.2017.01.007.
[9] V. Wong, W. Jervis, B. Fishburn, T. Numata, W. Joe, A. Rawal, C.C. Sorrell, P. Koshy, Long-term strength evolution in ambient-cured solid-activator geopolymer compositions, Minerals 11 (2021) 1–22, https://doi.org/10.3390/min11020143.
[10] I. Garcia-Lodeiro, A. Palomo, A. Fernández-Jiménez, An Overview of the Chemistry of Alkali-Activated Cement-Based Binders, Woodhead Publishing Limited, 2015, https://doi.org/10.1533/9781782422884.1.19.
[11] S. Zhou, C. Ma, G. Long, Y. Xie, A novel non-Portland cementitious material : mechanical properties , durability and characterization, Construct. Build. Mater. 238 (2020), 117671, https://doi.org/10.1016/j.conbuildmat.2019.117671.
[12] T. Wei, H. Zhao, C. Ma, A comparison of water curing and standard curing on one-part alkali- activated fly ash sinking beads and slag : properties , microstructure and mechanisms, Construct. Build. Mater. 273 (2021), 121715, https://doi.org/10.1016/j.conbuildmat.2020.121715.
[13] S. Guo, C. Ma, G. Long, Y. Xie, Cleaner one-part geopolymer prepared by introducing fly ash sinking spherical beads : properties and geopolymerization mechanism, J. Clean. Prod. 219 (2019) 686–697, https://doi.org/10.1016/j.jclepro.2019.02.116.
[14] N.R. Rakhimova, Recent advances in blended alkali-activated cements: a review, Eur. J. Environ. Civ. Eng. (2020) 1–23, https://doi.org/10.1080/19648189.2020.1858170.
[15] M.C.G. Juenger, R. Snellings, S.A. Bernal, Supplementary cementitious materials: new sources, characterization, and performance insights, Cement Concr. Res. 122 (2019) 257–273, https://doi.org/10.1016/j.cemconres.2019.05.008.
[16] A. Hajimohammadi, T. Ngo, J.L. Provis, T. Kim, J. Vongsvivut, High strength/density ratio in a syntactic foam made from one-part mix geopolymer and cenospheres, Compos. B Eng. 173 (2019), 106908, https://doi.org/10.1016/j.compositesb.2019.106908.
[17] F. Blanco, P. Garciéa, P. Mateos, J. Ayala, Characteristics and properties of lightweight concrete manufactured with cenospheres, Cement Concr. Res. 30 (2000) 1715–1722, https://doi.org/10.1016/S0008-8846(00)00357-4.
[18] A. Hanif, S. Diao, Z. Lu, T. Fan, Z. Li, Green lightweight cementitious composite incorporating aerogels and fly ash cenospheres - mechanical and thermal insulating properties, Construct. Build. Mater. 116 (2016) 422–430, https://doi.org/10.1016/j.conbuildmat.2016.04.134.
[19] J.L. Provis, S.A. Bernal, Geopolymers and related alkali-activated materials, Annu. Rev. Mater. Res. 44 (2014) 299–327, https://doi.org/10.1146/annurev-matsci-070813-113515.
[20] C. Shi, P.V. Krivenko, D. Roy, Alkali-activated Cements and Concretes, first ed., CRC Press, London, 2003 https://doi.org/10.1201/9781482266900.
[21] Y. Alrefaei, Y.S. Wang, J.G. Dai, Q.F. Xu, Effect of superplasticizers on properties of one-part Ca(OH)2/Na2SO4 activated geopolymer pastes, Construct. Build. Mater. 241 (2020), 117990, https://doi.org/10.1016/j.conbuildmat.2019.117990.
[22] H.A. Abdel-Gawwad, S.R.V. García, H.S. Hassan, Thermal activation of air cooled slag to create one-part alkali activated cement, Ceram. Int. 44 (2018) 14935–14939, https://doi.org/10.1016/j.ceramint.2018.05.089.
[23] S.F. Ali Shah, B. Chen, M.R. Ahmad, M.A. Haque, Development of Cleaner One-part geopolymer from lithium slag, J. Clean. Prod. 291 (2021), 125241, https://doi.org/10.1016/j.jclepro.2020.125241.
[24] Q. Luo, Y. Wang, S. Hong, F. Xing, B. Dong, Properties and microstructure of lithium-slag-based geopolymer by one- part mixing method, Construct. Build. Mater. 273 (2021), 121723, https://doi.org/10.1016/j.conbuildmat.2020.121723.
[25] Z.H. He, S.G. Du, D. Chen, Microstructure of ultra high performance concrete containing lithium slag, J. Hazard Mater. 353 (2018) 35–43, https://doi.org/10.1016/j.jhazmat.2018.03.063.
[26] J. Lu, Z. Yu, Y. Zhu, S. Huang, Q. Luo, S. Zhang, Effect of lithium-slag in the performance of slag cement mortar based on least-squares support vector machine prediction, Materials 12 (2019) 1–16, https://doi.org/10.3390/ma12101652.
[27] P.N. Lemougna, N. Dilissen, G.M. Hernandez, F. Kingne, J. Gu, H. Rahier, Effect of sodium disilicate and metasilicate on the microstructure and mechanical properties of one-part alkali-activated copper slag/ground granulated blast furnace slag, Materials 14 (2021), https://doi.org/10.3390/ma14195505.
[28] A. Peys, L. Arnout, B. Blanpain, H. Rahier, K. Van Acker, Y. Pontikes, Mix-design parameters and real-life considerations in the pursuit of lower environmental impact inorganic polymers, Waste and Biomass Valorization 9 (2018) 879–889, https://doi.org/10.1007/s12649-017-9877-1.
[29] Z. Deng, Z. Huang, F. He, A. Zheng, G. Wei, J. Meng, Z. Zhao, H. Li, Evaluation of calcined copper slag as an oxygen carrier for chemical looping gasification of sewage sludge, Int. J. Hydrogen Energy 44 (2019) 17823–17834, https://doi.org/10.1016/j.ijhydene.2019.05.039.
[30] H. Shi, Characterization and Modification of the Secondary Copper Smelting Slag for Smooth Operation and Slag Valorization, KU Leuven, 2017.
[31] L. Xu, X. Wang, C. Guan, W. Wu, L. Zhang, The effect of activators on the mechanical properties and microstructure of alkali-activated nickel slag, Adv. Civ. Eng. (2020), https://doi.org/10.1155/2020/1764108.

[32] X. Wang, W. Wu, L. Zhang, L. Fu, X. Li, Preparation of one-part alkali-activated nickel slag binder using an optimal ball milling process, Construct. Build. Mater. 322 (2022), 125902, https://doi.org/10.1016/j.conbuildmat.2021.125902.

[33] N. Ye, J. Yang, S. Liang, Y. Hu, J. Hu, B. Xiao, Q. Huang, Synthesis and strength optimization of one-part geopolymer based on red mud, Construct. Build. Mater. 111 (2016) 317–325, https://doi.org/10.1016/j.conbuildmat.2016.02.099.

[34] T. Luukkonen, Z. Abdollahnejad, J. Yliniemi, P. Kinnunen, M. Illikainen, Comparison of alkali and silica sources in one-part alkali-activated blast furnace slag mortar, J. Clean. Prod. 187 (2018) 171–179, https://doi.org/10.1016/j.jclepro.2018.03.202.

[35] E. Adesanya, P. Perumal, T. Luukkonen, J. Yliniemi, K. Ohenoja, P. Kinnunen, M. Illikainen, Opportunities to improve sustainability of alkali-activated materials: a review of side-stream based activators, J. Clean. Prod. 286 (2021), 125558, https://doi.org/10.1016/j.jclepro.2020.125558.

[36] A. Hajimohammadi, J.L. Provis, J.S.J. Van Deventer, Effect of alumina release rate on the mechanism of geopolymer gel formation, Chem. Mater. 22 (2010) 5199–5208, https://doi.org/10.1021/cm101151n.

[37] A. Hajimohammadi, J.L. Provis, J.S.J. van Deventer, Time-resolved and spatially-resolved infrared spectroscopic observation of seeded nucleation controlling geopolymer gel formation, J. Colloid Interface Sci. 357 (2011) 384–392, https://doi.org/10.1016/j.jcis.2011.02.045.

[38] P. Sturm, S. Greiser, G.J.G. Gluth, C. Jäger, H.J.H. Brouwers, Degree of reaction and phase content of silica-based one-part geopolymers investigated using chemical and NMR spectroscopic methods, J. Mater. Sci. 50 (2015) 6768–6778, https://doi.org/10.1007/s10853-015-9232-5.

[39] G.J.G. Gluth, C. Lehmann, K. Rübner, H.C. Kühne, Geopolymerization of a silica residue from waste treatment of chlorosilane production, Mater. Struct. Constr. 46 (2013) 1291–1298, https://doi.org/10.1617/s11527-012-9972-5.

[40] N. Ye, Y. Chen, J. Yang, S. Liang, Y. Hu, B. Xiao, Q. Huang, Y. Shi, J. Hu, X. Wu, Co-disposal of MSWI fly ash and Bayer red mud using an one-part geopolymeric system, J. Hazard Mater. 318 (2016) 70–78, https://doi.org/10.1016/j.jhazmat.2016.06.042.

[41] N. Ye, Y. Chen, J. Yang, S. Liang, Y. Hu, J. Hu, S. Zhu, W. Fan, B. Xiao, Transformations of Na, Al, Si and Fe species in red mud during synthesis of one-part geopolymers, Cement Concr. Res. 101 (2017) 123–130, https://doi.org/10.1016/j.cemconres.2017.08.027.

[42] H. Choo, S. Lim, W. Lee, C. Lee, Compressive strength of one-part alkali activated fly ash using red mud as alkali supplier, Construct. Build. Mater. 125 (2016) 21–28, https://doi.org/10.1016/j.conbuildmat.2016.08.015.

[43] H.A. Abdel-Gawwad, K.A. Khalil, Application of thermal treatment on cement kiln dust and feldspar to create one-part geopolymer cement, Construct. Build. Mater. 187 (2018) 231–237, https://doi.org/10.1016/j.conbuildmat.2018.07.161.

[44] S.K. Kaliyavaradhan, T.C. Ling, K.H. Mo, Valorization of waste powders from cement-concrete life cycle: a pathway to circular future, J. Clean. Prod. 268 (2020), 122358, https://doi.org/10.1016/j.jclepro.2020.122358.

[45] Q. Liu, X. Li, M. Cui, J. Wang, X. Lyu, Preparation of eco-friendly one-part geopolymers from gold mine tailings by alkaline hydrothermal activation, J. Clean. Prod. 298 (2021), 126806, https://doi.org/10.1016/j.jclepro.2021.126806.

[46] T. Mashifana, J. Sebothoma, T. Sithole, Alkaline activation of basic oxygen furnace slag modified gold mine tailings for building material, Adv. Civ. Eng. (2021), https://doi.org/10.1155/2021/9984494.

[47] R.A.M. Figueiredo, A.B.M. Silveira, E.L.P. Melo, G.Q.G. Costa, P.R.G. Brandão, M.T.P. Aguilar, A.B. Henriques, D.B. Mazzinghy, Mechanical and chemical analysis of one-part geopolymers synthesised with iron ore tailings from Brazil, J. Mater. Res. Technol. 14 (2021) 2650–2657, https://doi.org/10.1016/j.jmrt.2021.07.153.

[48] W. Chen, R. Peng, C. Straub, B. Yuan, Promoting the performance of one-part alkali-activated slag using fine lead-zinc mine tailings, Construct. Build. Mater. 236 (2020), 117745, https://doi.org/10.1016/j.conbuildmat.2019.117745.

[49] Y. Luo, S. Bao, Y. Zhang, Preparation of one-part geopolymeric precursors using vanadium tailing by thermal activation, J. Am. Ceram. Soc. 103 (2020) 779–783, https://doi.org/10.1111/jace.16835.

[50] Y. Luo, S. Bao, Y. Zhang, Y. Yuan, Recycling vanadium-bearing shale leaching residue for the production of one-part geopolymers, Mater. Res. Express 6 (2019), https://doi.org/10.1088/2053-1591/ab3755.

[51] S. Mabroum, S. Moukannaa, A. El Machi, Y. Taha, M. Benzaazoua, R. Hakkou, Mine wastes based geopolymers: a critical review, Clean. Eng. Technol. 1 (2020), 100014, https://doi.org/10.1016/j.clet.2020.100014.

[52] J.P.J. Aseniero, E.M. Opiso, M.H.T. Banda, C.B. Tabelin, Potential utilization of artisanal gold-mine tailings as geopolymeric source material: preliminary investigation, SN Appl. Sci. 1 (2019) 1–9, https://doi.org/10.1007/s42452-018-0045-4.

[53] S. Bao, Y. Luo, Y. Zhang, Fabrication of green one-part geopolymer from silica-rich vanadium tailing via thermal activation and modification, Int. J. Miner. Metall. Mater. 29 (2022) 177–184.

[54] P. Sturm, G.J.G. Gluth, H.J.H. Brouwers, H.C. Kühne, Synthesizing one-part geopolymers from rice husk ash, Construct. Build. Mater. 124 (2016) 961–966, https://doi.org/10.1016/j.conbuildmat.2016.08.017.

[55] P. Cong, Y. Cheng, Advances in geopolymer materials: a comprehensive review, J. Traffic Transp. Eng. (English Ed. 8 (2021) 283–314, https://doi.org/10.1016/j.jtte.2021.03.004.

[56] A.T. Almalkawi, A. Balchandra, P. Soroushian, Potential of using industrial wastes for production of geopolymer binder as green construction materials, Construct. Build. Mater. 220 (2019) 516–524, https://doi.org/10.1016/j.conbuildmat.2019.06.054.

[57] L.Y. Ming, O.W. En, H.C. Yong, M.M.A.B. Abdullah, O.S. Ween, Characteristic of one-Part Geopolymer as building materials, in: Sustain. Waste Util. Bricks, Concr. Cem. Mater. Charact. Prop. Performance, Appl., 2021, pp. 97–118.

[58] W.K. Part, M. Ramli, C.B. Cheah, An overview on the influence of various factors on the properties of geopolymer concrete derived from industrial by-products, Construct. Build. Mater. 77 (2015) 370–395, https://doi.org/10.1016/j.conbuildmat.2014.12.065.

[59] M.H. Samarakoon, P.G. Ranjith, W. Hui Duan, A. Haque, B.K. Chen, Extensive use of waste glass in one-part alkali-activated materials: towards sustainable construction practices, Waste Manag. 130 (2021) 1–11, https://doi.org/10.1016/j.wasman.2021.04.060.

[60] H.A. Abdel-Gawwad, E. Heikal, H. El-Didamony, F.S. Hashim, A.H. Mohammed, Recycling of concrete waste to produce ready-mix alkali activated cement, Ceram. Int. 44 (2018) 7300–7304, https://doi.org/10.1016/j.ceramint.2018.01.042.

[61] H.A. Abdel-Gawwad, A.M. Rashad, M. Heikal, Sustainable utilization of pretreated concrete waste in the production of one-part alkali-activated cement, J. Clean. Prod. 232 (2019) 318–328, https://doi.org/10.1016/j.jclepro.2019.05.356.

[62] Z. Abdollahnejad, T. Luukkonen, M. Mastali, P. Kinnunen, M. Illikainen, Development of one-Part Alkali-activated ceramic/slag binders containing recycled ceramic aggregates, J. Mater. Civ. Eng. 31 (2019), 04018386, https://doi.org/10.1061/(asce)mt.1943-5533.0002608.

[63] Z. Abdollahnejad, T. Luukkonen, M. Mastali, C. Giosue, O. Favoni, M.L. Ruello, P. Kinnunen, M. Illikainen, Microstructural analysis and strength development of one-Part Alkali-activated slag/ceramic binders under different curing regimes, Waste and Biomass Valorization 11 (2020) 3081–3096, https://doi.org/10.1007/s12649-019-00626-9.

[64] I. Garcia-Lodeiro, V. Carcelen-Taboada, A. Fernández-Jiménez, A. Palomo, Manufacture of hybrid cements with fly ash and bottom ash from a municipal solid waste incinerator, Construct. Build. Mater. 105 (2016) 218–226, https://doi.org/10.1016/j.conbuildmat.2015.12.079.

[65] A.M. Balo, H. Rahier, A. Mobili, A. Katsiki, N. Fagel, U.M. Chinje, D. Njopwouo, Metakaolin-based inorganic polymer synthesis using cotton shell ash as sole alkaline activator, Construct. Build. Mater. 191 (2018) 1011–1022, https://doi.org/10.1016/j.conbuildmat.2018.10.047.

[66] P. Duxson, A.F. Jiménez, J.L. Provis, G.C. Lukey, A. Palomo, J.S.J. van Deventer, Geopolymer technology : the current state of the art, J. Mater. Sci. 42 (2007) 2917–2933, https://doi.org/10.1007/s10853-006-0637-z.

[67] A. Kadhim, M. Sadique, R. Al-Mufti, K. Hashim, Long-term performance of novel high-calcium one-part alkali-activated cement developed from thermally activated lime kiln dust, J. Build. Eng. 32 (2020), 101766, https://doi.org/10.1016/j.jobe.2020.101766.

[68] D. Feng, J.L. Provis, J.S.J. Van Deventer, Thermal activation of albite for the synthesis of one-part mix geopolymers, J. Am. Ceram. Soc. 95 (2012) 565–572, https://doi.org/10.1111/j.1551-2916.2011.04925.x.

[69] T. Yang, Z. Zhang, H. Zhu, W. Zhang, Y. Gao, X. Zhang, Q. Wu, Effects of calcined dolomite addition on reaction kinetics of one-part sodium carbonate-activated slag cements, Construct. Build. Mater. 211 (2019) 329–336, https://doi.org/10.1016/j.conbuildmat.2019.03.245.

[70] A.T. Almalkawi, S. Hamadna, P. Soroushian, One-part alkali activated cement based volcanic pumice, Construct. Build. Mater. 152 (2017) 367–374, https://doi.org/10.1016/j.conbuildmat.2017.06.139.
[71] A. Kadhim, M. Sadique, R. Al-Mufti, K. Hashim, Developing one-part alkali-activated metakaolin/natural pozzolan binders using lime waste, Adv. Cement Res. 33 (2021) 342–356, https://doi.org/10.1680/jadcr.19.00118.
[72] R. Çetintaş, S. Soyer-Uzun, Relations between structural characteristics and compressive strength in volcanic ash based one–part geopolymer systems, J. Build. Eng. 20 (2018) 130–136, https://doi.org/10.1016/j.jobe.2018.07.011.
[73] J.L. Provis, Alkali-activated materials, Cement Concr. Res. 114 (2018) 40–48, https://doi.org/10.1016/j.cemconres.2017.02.009.
[74] R. Vinai, M. Soutsos, Production of sodium silicate powder from waste glass cullet for alkali activation of alternative binders, Cement Concr. Res. 116 (2019) 45–56, https://doi.org/10.1016/j.cemconres.2018.11.008.
[75] A. Mellado, C. Catalán, N. Bouzón, M.V. Borrachero, J.M. Monzó, J. Payá, Carbon footprint of geopolymeric mortar: study of the contribution of the alkaline activating solution and assessment of an alternative route, RSC Adv. 4 (2014) 23846–23852, https://doi.org/10.1039/c4ra03375b.
[76] C. Ma, G. Long, Y. Shi, Y. Xie, Preparation of cleaner one-part geopolymer by investigating different types of commercial sodium metasilicate in China, J. Clean. Prod. 201 (2018) 636–647, https://doi.org/10.1016/j.jclepro.2018.08.060.
[77] A.F. Abdalqader, F. Jin, A. Al-Tabbaa, Development of greener alkali-activated cement: utilisation of sodium carbonate for activating slag and fly ash mixtures, J. Clean. Prod. 113 (2016) 66–75, https://doi.org/10.1016/j.jclepro.2015.12.010.
[78] O. Wan-en, L. Yun-ming, H. Li-ngee, M. Mustafa, A. Bakri, The effect of sodium carbonate on the fresh and hardened properties of fly ash-based one-Part Geopolymer, IOP Conf. Ser. Mater. Sci. Eng. 864 (2020), https://doi.org/10.1088/1757-899X/864/1/012197.
[79] T. Luukkonen, Z. Abdollahnejad, J. Yliniemi, P. Kinnunen, M. Illikainen, One-part alkali-activated materials: a review, Cement Concr. Res. 103 (2018) 21–34, https://doi.org/10.1016/j.cemconres.2017.10.001.
[80] P. Sturm, G.J.G. Gluth, S. Simon, H.J.H. Brouwers, H.C. Kühne, The effect of heat treatment on the mechanical and structural properties of one-part geopolymer-zeolite composites, Thermochim. Acta 635 (2016) 41–58, https://doi.org/10.1016/j.tca.2016.04.015.
[81] P. Sturm, G.J.G. Gluth, C. Jäger, H.J.H. Brouwers, H.C. Kühne, Sulfuric acid resistance of one-part alkali-activated mortars, Cement Concr. Res. 109 (2018) 54–63, https://doi.org/10.1016/j.cemconres.2018.04.009.
[82] A. Hajimohammadi, J.L. Provis, J.S.J. Van Deventer, The effect of silica availability on the mechanism of geopolymerisation, Cement Concr. Res. 41 (2011) 210–216, https://doi.org/10.1016/j.cemconres.2011.02.001.
[83] Y.S. Wang, Y. Alrefaei, J.G. Dai, Roles of hybrid activators in improving the early-age properties of one-part geopolymer pastes, Construct. Build. Mater. 306 (2021), 124880, https://doi.org/10.1016/j.conbuildmat.2021.124880.
[84] C. Ma, B. Zhao, L. Wang, G. Long, Y. Xie, Clean and low-alkalinity one-part geopolymeric cement : effects of sodium sulfate on microstructure and properties, J. Clean. Prod. 252 (2020), https://doi.org/10.1016/j.jclepro.2019.119279, 119279.
[85] H. Ye, L. Huang, Z. Chen, Influence of activator composition on the chloride binding capacity of alkali-activated slag, Cem. Concr. Compos. 104 (2019), 103368, https://doi.org/10.1016/j.cemconcomp.2019.103368.
[86] M.S. Kim, Y. Jun, C. Lee, J.E. Oh, Use of CaO as an activator for producing a price-competitive non-cement structural binder using ground granulated blast furnace slag, Cement Concr. Res. 54 (2013) 208–214, https://doi.org/10.1016/j.cemconres.2013.09.011.
[87] K.H. Yang, J. Il Sim, S.H. Nam, Enhancement of reactivity of calcium hydroxide-activated slag mortars by the addition of barium hydroxide, Construct. Build. Mater. 24 (2010) 241–251, https://doi.org/10.1016/j.conbuildmat.2009.09.001.
[88] Y. Jeong, S.H. Kang, Y. Du, J. Moon, Local Ca-structure variation and microstructural characteristics on one-part activated slag system with various activators, Cem. Concr. Compos. 102 (2019) 1–13, https://doi.org/10.1016/j.cemconcomp.2019.04.009.
[89] W. Wu, F. Matalkah, P. Soroushian, A. Almalkawi, X. Wang, L. Xu, Influence of admixtures on rheological properties and heat of hydration of alkali aluminosilicate cement, Adv. Cement Res. 29 (2017) 397–403, https://doi.org/10.1680/jadcr.16.00181.
[90] F. Matalkah, L. Xu, W. Wu, P. Soroushian, Mechanochemical synthesis of one-part alkali aluminosilicate hydraulic cement, Mater. Struct. Constr. 50 (2017) 1–12, https://doi.org/10.1617/s11527-016-0968-4.
[91] A. Dakhane, N. Neithalath, Reaction kinetics and characterization of slag-based , high strength , " just -add- water " type (one -part) alkali-activated binders, Recent Prog. Mater. 4 (2022), 2202006, https://doi.org/10.21926/rpm.2202006.
[92] B. Panda, G.B. Singh, C. Unluer, M.J. Tan, Synthesis and characterization of one-part geopolymers for extrusion based 3D concrete printing, J. Clean. Prod. 220 (2019) 610–619, https://doi.org/10.1016/j.jclepro.2019.02.185.
[93] A. Alhamdan, Shrinkage Behaviour of One and Two Part Alkali-Activated Mortars: Factors and Mitigation Techniques, Concordia University, 2018.
[94] E. Adesanya, K. Ohenoja, T. Luukkonen, P. Kinnunen, M. Illikainen, One-part geopolymer cement from slag and pretreated paper sludge, J. Clean. Prod. 185 (2018) 168–175, https://doi.org/10.1016/j.jclepro.2018.03.007.
[95] M. Abdulkareem, J. Havukainen, J. Nuortila-Jokinen, M. Horttanainen, Environmental and economic perspective of waste-derived activators on alkali-activated mortars, J. Clean. Prod. 280 (2021), 124651, https://doi.org/10.1016/j.jclepro.2020.124651.
[96] A. Peys, H. Rahier, Y. Pontikes, Potassium-rich biomass ashes as activators in metakaolin-based inorganic polymers, Appl. Clay Sci. 119 (2016) 401–409, https://doi.org/10.1016/j.clay.2015.11.003.
[97] A. Font, L. Soriano, M.M. Tashima, J. Monzó, M.V. Borrachero, J. Payá, One-part eco-cellular concrete for the precast industry: functional features and life cycle assessment, J. Clean. Prod. 269 (2020), https://doi.org/10.1016/j.jclepro.2020.122203.
[98] L. Soriano, A. Font, M.M. Tashima, J. Monzó, M.V. Borrachero, J. Payá, One-part blast furnace slag mortars activated with almond-shell biomass ash: a new 100% waste-based material, Mater. Lett. 272 (2020), 127882, https://doi.org/10.1016/j.matlet.2020.127882.
[99] H.S. Hassan, H.A. Abdel-Gawwad, S.R. Vasquez-Garcia, I. Israde-Alcantara, N. Flores-Ramirez, J.L. Rico, M.S. Mohammed, Cleaner production of one-part white geopolymer cement using pre- treated wood biomass ash and diatomite, J. Clean. Prod. 209 (2019) 1420–1428, https://doi.org/10.1016/j.jclepro.2018.11.137.
[100] F.S. Lima, T.C.F. Gomes, J.C.B. de Moraes, Novel one-part alkali-activated binder produced with coffee husk ash, Mater. Lett. 313 (2022) 2–5, https://doi.org/10.1016/j.matlet.2022.131733.
[101] B. Yang, J.G. Jang, Environmentally benign production of one-part alkali-activated slag with calcined oyster shell as an activator, Construct. Build. Mater. 257 (2020), 119552, https://doi.org/10.1016/j.conbuildmat.2020.119552.
[102] P. Cong, L. Mei, Using silica fume for improvement of fly ash/slag based geopolymer activated with calcium carbide residue and gypsum, Construct. Build. Mater. 275 (2021), 122171, https://doi.org/10.1016/j.conbuildmat.2020.122171.
[103] W. Guo, Z. Zhang, Z. Xu, J. Zhang, Y. Bai, Q. Zhao, Y. Qiu, Mechanical properties and compressive constitutive relation of solid waste-based concrete activated by soda residue-carbide slag, Construct. Build. Mater. 333 (2022), 127352, https://doi.org/10.1016/j.conbuildmat.2022.127352.
[104] W. Guo, Z. Zhang, Y. Bai, G. Zhao, Z. Sang, Q. Zhao, Development and characterization of a new multi-strength level binder system using soda residue-carbide slag as composite activator, Construct. Build. Mater. 291 (2021), 123367, https://doi.org/10.1016/j.conbuildmat.2021.123367.
[105] W. Guo, S. Wang, Z. Xu, Z. Zhang, C. Zhang, Y. Bai, Q. Zhao, Mechanical performance and microstructure improvement of soda residue – carbide slag – ground granulated blast furnace slag binder by optimizing its preparation process and curing method, Construct. Build. Mater. 302 (2021), 124403, https://doi.org/10.1016/j.conbuildmat.2021.124403.
[106] E. Adesanya, K. Ohenoja, A. Di Maria, P. Kinnunen, M. Illikainen, Alternative alkali-activator from steel-making waste for one-part alkali-activated slag, J. Clean. Prod. 274 (2020), 123020, https://doi.org/10.1016/j.jclepro.2020.123020.
[107] M. Gonçalves, I.S. Vilarinho, M. Capela, A. Caetano, R.M. Novais, J.A. Labrincha, M.P. Seabra, Waste-based one-part alkali activated materials, Materials 14 (2021) 1–17, https://doi.org/10.3390/ma14112911.
[108] M. Askarian, Z. Tao, G. Adam, B. Samali, Mechanical properties of ambient cured one-part hybrid OPC-geopolymer concrete, Construct. Build. Mater. 186 (2018) 330–337, https://doi.org/10.1016/j.conbuildmat.2018.07.160.

[109] G. Sadeghian, K. Behfarnia, M. Teymouri, Drying shrinkage of one-part alkali-activated slag concrete, J. Build. Eng. 51 (2022), 104263, https://doi.org/10.1016/j.jobe.2022.104263.
[110] M. Kovtun, E.P. Kearsley, J. Shekhovtsova, Dry powder alkali-activated slag cements, Adv. Cement Res. 27 (2015) 447–456.
[111] K.H. Yang, J.K. Song, J.S. Lee, Properties of alkali-activated mortar and concrete using lightweight aggregates, Mater. Struct. Constr. 43 (2010) 403–416, https://doi.org/10.1617/s11527-009-9499-6.
[112] O. Tsioulou, A. Lampropoulos, K. Neocleous, N. Kyriakides, T. Polydorou, Development of an innovative one part green concrete, IABSE Congr. Christchurch 2020 Resilient Technol, Sustain. Infrastruct. - Proc. (2020) 874–880, https://doi.org/10.2749/christchurch.2021.0874.
[113] A. Hajimohammadi, T. Ngo, A. Kashani, Glass waste versus sand as aggregates: the characteristics of the evolving geopolymer binders, J. Clean. Prod. 193 (2018) 593–603, https://doi.org/10.1016/j.jclepro.2018.05.086.
[114] L. Coppola, D. Coffetti, E. Crotti, A. Marini, C. Passoni, T. Pastore, Lightweight cement-free alkali-activated slag plaster for the structural retrofit and energy upgrading of poor quality masonry walls, Cem. Concr. Compos. 104 (2019), https://doi.org/10.1016/j.cemconcomp.2019.103341.
[115] Z. Abdollahnejad, M. Mastali, B. Woof, M. Illikainen, High strength fiber reinforced one-part alkali activated slag/fly ash binders with ceramic aggregates: microscopic analysis, mechanical properties, drying shrinkage, and freeze-thaw resistance, Construct. Build. Mater. 241 (2020), 118129, https://doi.org/10.1016/j.conbuildmat.2020.118129.
[116] A. Abdelmonim, D.V. Bompa, Mechanical and Fresh Properties of Multi-Binder Geopolymer Mortars Incorporating Recycled Rubber Particles, Infrastructure vol. 6 (2021), https://doi.org/10.3390/infrastructures6100146.
[117] L.Y. Xu, L.P. Qian, B.T. Huang, J.G. Dai, Development of artificial one-part geopolymer lightweight aggregates by crushing technique, J. Clean. Prod. 315 (2021), 128200, https://doi.org/10.1016/j.jclepro.2021.128200.
[118] A. Mobili, F. Tittarelli, H. Rahier, One-part alkali-activated pastes and mortars prepared with metakaolin and biomass ash, Appl. Sci. 10 (2020), https://doi.org/10.3390/app10165610.
[119] W. Lv, Z. Sun, Z. Su, Study of seawater mixed one-part alkali activated GGBFS-fly ash, Cem. Concr. Compos. 106 (2020), 103484, https://doi.org/10.1016/j.cemconcomp.2019.103484.
[120] T. Luukkonen, J. Yliniemi, P. Kinnunen, M. Illikainen, Sustainable batching water options for one-part alkali-activated slag mortar: sea water and reverse osmosis reject water, PLoS One 15 (2020) 1–17, https://doi.org/10.1371/journal.pone.0242462.
[121] Z. Sun, One-part Alkali-Activated Concrete with Seawater, LTD, 2022, https://doi.org/10.1016/B978-0-323-85469-6.00010-6, 12.
[122] T. Luukkonen, Z. Abdollahnejad, K. Ohenoja, P. Kinnunen, M. Illikainen, Suitability of commercial superplasticizers for one-part alkali-activated blast-furnace slag mortar, J. Sustain. Cem. Mater. 8 (2019) 244–257, https://doi.org/10.1080/21650373.2019.1625827.
[123] Y. Alrefaei, Y.S. Wang, J.G. Dai, The effectiveness of different superplasticizers in ambient cured one-part alkali activated pastes, Cem. Concr. Compos. 97 (2019) 166–174, https://doi.org/10.1016/j.cemconcomp.2018.12.027.
[124] S.Y. Oderji, B. Chen, C. Shakya, M.R. Ahmad, S.F.A. Shah, Influence of superplasticizers and retarders on the workability and strength of one-part alkali-activated fly ash/slag binders cured at room temperature, Construct. Build. Mater. 229 (2019), 116891, https://doi.org/10.1016/j.conbuildmat.2019.116891.
[125] L. Coppola, D. Coffetti, E. Crotti, S. Candamano, F. Crea, G. Gazzaniga, T. Pastore, The combined use of admixtures for shrinkage reduction in one-part alkali activated slag-based mortars and pastes, Construct. Build. Mater. 248 (2020), 118682, https://doi.org/10.1016/j.conbuildmat.2020.118682.
[126] M.R. Ahmad, B. Chen, S.F.A. Shah, Influence of different admixtures on the mechanical and durability properties of one-part alkali-activated mortars, Construct. Build. Mater. 265 (2020), 120320, https://doi.org/10.1016/j.conbuildmat.2020.120320.
[127] F. Matalkah, T. Salem, M. Shaafaey, P. Soroushian, Drying shrinkage of alkali activated binders cured at room temperature, Construct. Build. Mater. 201 (2019) 563–570, https://doi.org/10.1016/j.conbuildmat.2018.12.223.
[128] A. Hajimohammadi, T. Ngo, P. Mendis, T. Nguyen, A. Kashani, J.S.J. van Deventer, Pore characteristics in one-part mix geopolymers foamed by H2O2: the impact of mix design, Mater. Des. 130 (2017) 381–391, https://doi.org/10.1016/j.matdes.2017.05.084.
[129] A. Alzaza, K. Ohenoja, M. Illikainen, Enhancing the mechanical and durability properties of subzero-cured one-part alkali-activated blast furnace slag mortar by using submicron metallurgical residue as an additive, Cem. Concr. Compos. 122 (2021), 104128, https://doi.org/10.1016/j.cemconcomp.2021.104128.
[130] A. Ababneh, F. Matalkah, R. Aqel, Synthesis of kaolin-based alkali-activated cement: carbon footprint, cost and energy assessment, J. Mater. Res. Technol. 9 (2020) 8367–8378, https://doi.org/10.1016/j.jmrt.2020.05.116.
[131] X. Ke, S.A. Bernal, N. Ye, J.L. Provis, J. Yang, One-part geopolymers based on thermally treated red Mud/NaOH blends, J. Am. Ceram. Soc. 98 (2015) 5–11, https://doi.org/10.1111/jace.13231.
[132] G. Masi, A. Filipponi, M.C. Bignozzi, Fly ash-based one-part alkali activated mortars cured at room temperature: effect of precursor pre-treatments, Open Ceram 8 (2021), 100178, https://doi.org/10.1016/j.oceram.2021.100178.
[133] F. Matalkah, A.H. Alomari, P. Soroushian, Case Studies in Construction Materials Scaled-up production of alkali-activated cement in the presence of carbon dioxide for concrete construction, Case Stud. Constr. Mater. 13 (2020), e00463, https://doi.org/10.1016/j.cscm.2020.e00463.
[134] Y. Alrefaei, Y.S. Wang, J.G. Dai, Effect of mixing method on the performance of alkali-activated fly ash/slag pastes along with polycarboxylate admixture, Cem. Concr. Compos. 117 (2021), 103917, https://doi.org/10.1016/j.cemconcomp.2020.103917.
[135] K.H. Yang, J.K. Song, A.F. Ashour, E.T. Lee, Properties of cementless mortars activated by sodium silicate, Construct. Build. Mater. 22 (2008) 1981, https://doi.org/10.1016/j.conbuildmat.2007.07.003. –1989.
[136] K.-H. Yang, J.-K. Song, Workability loss and compressive strength development of cementless mortars activated by combination of sodium silicate and sodium hydroxide, J. Mater. Civ. Eng. 21, 21 (2009), https://doi.org/10.1061/(asce)0899-1561, 2009, 119, 3, 127, 119.
[137] J.L. Provis, P. Duxson, J.S.J. van Deventer, The role of particle technology in developing sustainable construction materials, Adv. Powder Technol. 21 (2010) 2–7, https://doi.org/10.1016/j.apt.2009.10.006.
[138] Y. Alrefaei, J. Dai, Effects of delayed addition of polycarboxylate ether on one-part alkali-activated fly ash/slag pastes : adsorption , reaction kinetics , and rheology, Construct. Build. Mater. 323 (2022), 126611, https://doi.org/10.1016/j.conbuildmat.2022.126611.
[139] P. Perumal, H. Sreenivasan, T. Luukkonen, A.M. Kantola, V. Telkki, P. Kinnunen, M. Illikainen, High strength one-part alkali-activated slag blends designed by particle packing optimization, Construct. Build. Mater. 299 (2021), 124004, https://doi.org/10.1016/j.conbuildmat.2021.124004.
[140] Y.W.D. Tay, B. Panda, S.C. Paul, N.A. Noor Mohamed, M.J. Tan, K.F. Leong, 3D printing trends in building and construction industry: a review, Virtual Phys. Prototyp. 12 (2017) 261–276, https://doi.org/10.1080/17452759.2017.1326724.
[141] R.A. Buswell, W.R. Leal de Silva, S.Z. Jones, J. Dirrenberger, 3D printing using concrete extrusion: a roadmap for research, Cement Concr. Res. 112 (2018) 37–49, https://doi.org/10.1016/j.cemconres.2018.05.006.
[142] H. Zhong, M. Zhang, 3D printing geopolymers: a review, Cem. Concr. Compos. 128 (2022), 104455, https://doi.org/10.1016/j.cemconcomp.2022.104455.
[143] M. Amran, H.S. Abdelgader, A.M. Onaizi, R. Fediuk, T. Ozbakkaloglu, R.S.M. Rashid, G. Murali, 3D-printable alkali-activated concretes for building applications: a critical review, Construct. Build. Mater. 319 (2022), 126126, https://doi.org/10.1016/j.conbuildmat.2021.126126.
[144] B. Nematollahi, M. Xia, S.H. Bong, J. Sanjayan, Hardened Properties of 3D Printable 'One-Part' Geopolymer for Construction Applications, RILEM Bookseries, 2019, pp. 190–199, https://doi.org/10.1007/978-3-319-99519-9_12.
[145] B. Panda, S. Ruan, C. Unluer, M. Jen, Investigation of the properties of alkali-activated slag mixes involving the use of nanoclay and nucleation seeds for 3D printing, Compos. Part B. 186 (2020), 107826, https://doi.org/10.1016/j.compositesb.2020.107826.
[146] S. Muthukrishnan, S. Ramakrishnan, J. Sanjayan, Effect of alkali reactions on the rheology of one-part 3D printable geopolymer concrete, Cem. Concr. Compos. 116 (2021), 103899, https://doi.org/10.1016/j.cemconcomp.2020.103899.
[147] S.H. Bong, M. Xia, B. Nematollahi, C. Shi, Ambient temperature cured ' just-add-water ' geopolymer for 3D concrete printing applications, Cem. Concr. Compos. 121 (2021), 104060, https://doi.org/10.1016/j.cemconcomp.2021.104060.
[148] B. Nematollahi, S.H. Bong, M. Xia, J. Sanjayan, Digital fabrication of 'just-add-water' geopolymers: effects of curing condition and print-time interval, in: Second RILEM Int. Conf. Concr. Digit. Fabr., 2020, pp. 93–102, https://doi.org/10.1007/978-3-030-49916-7_4.

[149] R.J.M. Wolfs, F.P. Bos, T.A.M. Salet, Cement and Concrete Research Hardened properties of 3D printed concrete : the influence of process parameters on interlayer adhesion, Cement Concr. Res. 119 (2019) 132–140, https://doi.org/10.1016/j.cemconres.2019.02.017.
[150] T.T. Le, S.A. Austin, S. Lim, R.A. Buswell, R. Law, A.G.F. Gibb, T. Thorpe, Cement and Concrete Research Hardened properties of high-performance printing concrete 42 (2012) 558–566, https://doi.org/10.1016/j.cemconres.2011.12.003.
[151] J. Ren, H. Sun, Q. Li, Z. Li, L. Ling, X. Zhang, Y. Wang, F. Xing, Experimental comparisons between one-part and normal (two-part) alkali-activated slag binders, Construct. Build. Mater. 309 (2021), 125177, https://doi.org/10.1016/j.conbuildmat.2021.125177.
[152] D. Khale, R. Chaudhary, Mechanism of geopolymerization and factors influencing its development: a review, J. Mater. Sci. 42 (2007) 729–746, https://doi.org/10.1007/s10853-006-0401-4.
[153] J.L. Provis, Geopolymers and other alkali activated materials: Why, how, and what? Mater. Struct. Constr. 47 (2014) 11–25, https://doi.org/10.1617/s11527-013-0211-5.
[154] C. Shi, A.F. Jiménez, A. Palomo, New cements for the 21st century: the pursuit of an alternative to Portland cement, Cement Concr. Res. (2011), https://doi.org/10.1016/j.cemconres.2011.03.016.
[155] M. Torres-Carrasco, F. Puertas, Alkaline activation of different aluminosilicates as an alternative to Portland cement: alkali activated cements or geopolymers, Rev. Ing. Construcción. 32 (2017) 5–12, https://doi.org/10.4067/S0718-50732017000200001.
[156] A. Palomo, P. Krivenko, I. Garcia-Lodeiro, E. Kavalerova, O. Maltseva, A. Fernández-Jiménez, A review on alkaline activation: new analytical perspectives, Mater. Construcción 64 (2014), https://doi.org/10.3989/mc.2014.00314.
[157] T.T.H. Bach, E. Chabas, I. Pochard, C. Cau Dit Coumes, J. Haas, F. Frizon, A. Nonat, Retention of alkali ions by hydrated low-pH cements: mechanism and Na+/K+ selectivity, Cement Concr. Res. 51 (2013) 14–21, https://doi.org/10.1016/j.cemconres.2013.04.010.
[158] J.L. Provis, J.S.J. van Deventer, Geopolymerisation kinetics. 1. In situ energy-dispersive X-ray diffractometry, Chem. Eng. Sci. 62 (2007) 2309–2317, https://doi.org/10.1016/j.ces.2007.01.027.
[159] K. tuo Wang, L. qiu Du, X. sen Lv, Y. He, X. min Cui, Preparation of drying powder inorganic polymer cement based on alkali-activated slag technology, Powder Technol. 312 (2017) 204–209, https://doi.org/10.1016/j.powtec.2017.02.036.
[160] A. Hajimohammadi, J.S.J. van Deventer, Characterisation of one-Part Geopolymer binders made from fly ash, Waste and Biomass Valorization 8 (2017) 225–233, https://doi.org/10.1007/s12649-016-9582-5.
[161] S.Y. Oderji, B. Chen, M.R. Ahmad, S.F.A. Shah, Fresh and hardened properties of one-part fly ash-based geopolymer binders cured at room temperature: effect of slag and alkali activators, J. Clean. Prod. 225 (2019) 1–10, https://doi.org/10.1016/j.jclepro.2019.03.290.
[162] N. Ismail, H. El-Hassan, Development and characterization of fly ash–slag blended geopolymer mortar and lightweight concrete, J. Mater. Civ. Eng. 30 (2018), 04018029, https://doi.org/10.1061/(asce)mt.1943-5533.0002209.
[163] M. Dong, M. Elchalakani, A. Karrech, Development of high strength one-part geopolymer mortar using sodium metasilicate, Construct. Build. Mater. 236 (2020), 117611, https://doi.org/10.1016/j.conbuildmat.2019.117611.
[164] L. Li, J.X. Lu, B. Zhang, C.S. Poon, Rheology behavior of one-part alkali activated slag/glass powder (AASG) pastes, Construct. Build. Mater. 258 (2020), 120381, https://doi.org/10.1016/j.conbuildmat.2020.120381.
[165] S.F.A. Shah, B. Chen, S.Y. Oderji, M.A. Haque, M.R. Ahmad, Improvement of early strength of fly ash-slag based one-part alkali activated mortar, Construct. Build. Mater. 246 (2020), 118533, https://doi.org/10.1016/j.conbuildmat.2020.118533.
[166] L. Coppola, D. Coffetti, E. Crotti, G. Gazzaniga, T. Pastore, The durability of one-Part Alkali-activated slag-based mortars in different environments, Sustainability 12 (2020).
[167] C. Ma, B. Zhao, S. Guo, G. Long, Y. Xie, Properties and characterization of green one-part geopolymer activated by composite activators, J. Clean. Prod. 220 (2019) 188–199, https://doi.org/10.1016/j.jclepro.2019.02.159.
[168] M. Askarian, Z. Tao, B. Samali, G. Adam, R. Shuaibu, Mix composition and characterisation of one-part geopolymers with different activators, Construct. Build. Mater. 225 (2019) 526–537, https://doi.org/10.1016/j.conbuildmat.2019.07.083.
[169] B. Chen, J. Wang, J. Zhao, Effect of sodium aluminate dosage as a solid alkaline activator on the properties of alkali-activated slag paste, Adv. Mater. Sci. Eng. 2021 (2021), https://doi.org/10.1155/2021/6658588.
[170] S. Ouyang, W. Chen, Z. Zhang, X. Li, W. Zhu, Experimental study of one-part geopolymer using different alkali sources, J. Phys. Conf. Ser. 1605 (2020), https://doi.org/10.1088/1742-6596/1605/1/012155.
[171] S. Haruna, B.S. Mohammed, M.M.A. Wahab, M.S. Liew, Effect of paste aggregate ratio and curing methods on the performance of one-part alkali-activated concrete, Construct. Build. Mater. 261 (2020), 120024, https://doi.org/10.1016/j.conbuildmat.2020.120024.
[172] K.H. Yang, J.K. Song, K.S. Lee, A.F. Ashour, Flow and compressive strength of alkali-activated mortars, ACI Mater. J. 106 (2009) 50–58, https://doi.org/10.14359/56316.
[173] S. Pangdaeng, T. Phoo-ngernkham, V. Sata, P. Chindaprasirt, Influence of curing conditions on properties of high calcium fly ash geopolymer containing Portland cement as additive, Mater. Des. 53 (2014) 269–274, https://doi.org/10.1016/j.matdes.2013.07.018.
[174] C. Shi, B. Qu, J.L. Provis, Cement and concrete research recent progress in low-carbon binders, Cement Concr. Res. 122 (2019) 227–250, https://doi.org/10.1016/j.cemconres.2019.05.009.
[175] M. Saedi, K. Behfarnia, H. Soltanian, The e ff ect of the blaine fi neness on the mechanical properties of the alkali- activated slag cement, vol. 26, 2019, https://doi.org/10.1016/j.jobe.2019.100897.
[176] I.K. Jeon, J.S. Ryou, S.H. Jakhrani, H.G. Kim, Effects of light-burnt dolomite incorporation on the setting, strength, and drying shrinkage of one-part alkali-activated slag cement, Materials 12 (2019) 1–16, https://doi.org/10.3390/ma12182874.
[177] P.N. Lemougna, A. Adediran, J. Yliniemi, A. Ismailov, E. Levanen, P. Tanskanen, P. Kinnunen, J. Roning, M. Illikainen, Thermal stability of one-part metakaolin geopolymer composites containing high volume of spodumene tailings and glass wool, Cem. Concr. Compos. 114 (2020), 103792, https://doi.org/10.1016/j.cemconcomp.2020.103792.
[178] S. Zhou, C. Tan, Y. Gao, Y. Li, S. Guo, One-part alkali activated slag using Ca(OH)2 and Na2CO3 instead of NaOH as activator : more excellent compressive strength and microstructure, Mater. Res. Express 8 (2021), 085501.
[179] S. Haruna, B.S. Mohammed, M.M.A. Wahab, A. Haruna, Compressive strength and workability of high calcium one-part alkali activated mortars using response surface methodology, IOP Conf. Ser. Earth Environ. Sci. 476 (2020), https://doi.org/10.1088/1755-1315/476/1/012018.
[180] H.A. Abdel-Gawwad, S.A. Abo-El-Enein, A novel method to produce dry geopolymer cement powder, HBRC J 12 (2016) 13–24, https://doi.org/10.1016/j.hbrcj.2014.06.008.
[181] T. Luukkonen, J. Yliniemi, Z. Abdollahnejad, 4 - alkali-activated dry-mix concretes, in: Handb. Adv. Alkali-Activated Concr., Woodhead Publishing Series in Civil and Structural Engineering, 2022, pp. 67–88, https://doi.org/10.1016/B978-0-323-85469-6.00008-8.
[182] L. Bostanci, Synergistic effect of a small amount of silica aerogel powder and scrap rubber addition on properties of alkali-activated slag mortars, Construct. Build. Mater. 250 (2020), 118885, https://doi.org/10.1016/j.conbuildmat.2020.118885.
[183] M. Elzeadani, D.V. Bompa, A.Y. Elghazouli, Preparation and properties of rubberised geopolymer concrete: a review, Construct. Build. Mater. 313 (2021), 125504, https://doi.org/10.1016/j.conbuildmat.2021.125504.
[184] A. Hajimohammadi, T. Ngo, A. Kashani, Sustainable one-part geopolymer foams with glass fines versus sand as aggregates, Construct. Build. Mater. 171 (2018) 223–231, https://doi.org/10.1016/j.conbuildmat.2018.03.120.
[185] M.X. Peng, Z.H. Wang, Q.G. Xiao, F. Song, W. Xie, L.C. Yu, H.W. Huang, S.J. Yi, Effects of alkali on one-part alkali-activated cement synthesized by calcining bentonite with dolomite and Na2CO3, Appl. Clay Sci. 139 (2017) 64–71, https://doi.org/10.1016/j.clay.2017.01.020.
[186] Z. Abdollahnejad, M. Mastali, T. Luukkonen, P. Kinnunen, M. Illikainen, Fiber-reinforced one-part alkali-activated slag/ceramic binders, Ceram. Int. 44 (2018) 8963–8976, https://doi.org/10.1016/j.ceramint.2018.02.097.
[187] A. Alzaza, K. Ohenoja, M. Illikainen, One-part alkali-activated blast furnace slag for sustainable construction at subzero temperatures, Construct. Build. Mater. 276 (2021), 122026, https://doi.org/10.1016/j.conbuildmat.2020.122026.

[188] K. Neupane, Fly ash and GGBFS based powder-activated geopolymer binders: a viable sustainable alternative of portland cement in concrete industry, Mech. Mater. 103 (2016) 110–122, https://doi.org/10.1016/j.mechmat.2016.09.012.
[189] K. Neupane, D. Chalmers, P. Kidd, High-strength geopolymer concrete- properties, advantages and challenges, Adv. Mater. 7 (2018) 15, https://doi.org/10.11648/j.am.20180702.11.
[190] M. Chi, R. Huang, Binding mechanism and properties of alkali-activated fly ash/slag mortars, Construct. Build. Mater. 40 (2013) 291–298, https://doi.org/10.1016/j.conbuildmat.2012.11.003.
[191] W. Zhang, X. Yao, T. Yang, Z. Zhang, The degradation mechanisms of alkali-activated fly ash/slag blend cements exposed to sulphuric acid, Construct. Build. Mater. 186 (2018) 1177–1187, https://doi.org/10.1016/j.conbuildmat.2018.08.050.
[192] A. Neville, Properties of Concrete, fifth ed., Prentice Hall, Edinburgh, 2012.
[193] T. Suwan, M. Fan, Effect of manufacturing process on the mechanisms and mechanical properties of fly ash-based geopolymer in ambient curing temperature, Mater. Manuf. Process. 32 (2017) 461–467, https://doi.org/10.1080/10426914.2016.1198013.
[194] M.H. Samarakoon, P.G. Ranjith, W.H. Duan, V.R.S. De Silva, Properties of one-part fly ash/slag-based binders activated by thermally-treated waste glass/NaOH blends: a comparative study, Cem. Concr. Compos. 112 (2020), 103679, https://doi.org/10.1016/j.cemconcomp.2020.103679.
[195] R.D. Hooton, Bridging the gap between research and standards 38 (2008) 247–258, https://doi.org/10.1016/j.cemconres.2007.09.012.
[196] R.D. Hooton, Cement and Concrete Research Current developments and future needs in standards for cementitious materials, Cement Concr. Res. 78 (2015) 165–177, https://doi.org/10.1016/j.cemconres.2015.05.022.
[197] PAS 8820, Construction Materials. Alkali-Activated Cementitious Material and Concrete, 2016, 2016, Specification.
[198] Indian Standard 17452, Use of Alkali-Activated Concrete for Precast Products - Guidelines, 2020.
[199] Technical Committee 247-DTA, 247-DTA, Durability Testing of Alkali-Activated Materials, RILEM, 2019. https://www.rilem.net/groupe/247-dta-durability-testing-of-alkali-activated-materials-290. (Accessed 29 May 2022). accessed.
[200] J.S.J. van Deventer, C.E. White, R.J. Myers, A Roadmap for Production of Cement and Concrete with Low - CO 2 Emissions, Springer Netherlands, 2021, https://doi.org/10.1007/s12649-020-01180-5.
[201] F. Puertas, J.A. Suárez-Navarro, M.M. Alonso, C. Gascó, NORM waste, cements, and concretes, A review, Mater. Constr. 71 (2021), https://doi.org/10.3989/MC.2021.13520.
[202] F. Puertas, M.D.M. Alonso, M. Torres-Carrasco, P. Rivilla, C. Gasco, L. Yagüe, J.A. Suárez, N. Navarro, Radiological characterization of anhydrous/hydrated cements and geopolymers, Construct. Build. Mater. 101 (2015) 1105–1112, https://doi.org/10.1016/j.conbuildmat.2015.10.074.
[203] European Union, Directive 2013/59/EURATOM 5 - December 2013, 2013.
[204] T. Kovacs, G. Bator, W. Schroeyers, J. Labrincha, F. Puertas, M. Hegedus, D. Nicolaides, M.A. Sanjuán, P. Krivenko, I.N. Grubeša, Z. Sas, B. Michalik, M. Anagnostakis, I. Barisic, C. Nuccetelli, R. Trevisi, T. Croymans, S. Schreurs, N. Todorović, D. Vaiciukyniene, R. Bistrickaite, A. Tkaczyk, K. Kovler, R. Wiegers, R. Doherty, From Raw Materials to NORM By-Products, 2017, https://doi.org/10.1016/B978-0-08-102009-8.00006-2.
[205] C. Nuccetelli, R. Trevisi, I. Ignjatović, J. Dragaš, Alkali-activated concrete with Serbian fly ash and its radiological impact, J. Environ. Radioact. 168 (2017) 30–37, https://doi.org/10.1016/j.jenvrad.2016.09.002.
[206] J. Labrincha, F. Puertas, W. Schroeyers, K. Kovler, Y. Pontikes, C. Nuccetelli, P. Krivenko, O. Kovalchuk, O. Petropavlovsky, M. Komljenovic, E. Fidanchevski, R. Wiegers, E. Volceanov, E. Gunay, M.A. Sanjuán, V. Ducman, B. Angjusheva, D. Bajare, T. Kovacs, G. Bator, S. Schreurs, J. Aguiar, J.L. Provis, From NORM By-Products to Building Materials, 2017, https://doi.org/10.1016/B978-0-08-102009-8.00007-4.
[207] T. Luukkonen, Z. Abdollahnejad, J. Yliniemi, M. Mastali, P. Kinnunen, M. Illikainen, Alkali-activated soapstone waste - mechanical properties, durability, and economic prospects, Sustain. Mater. Technol. 22 (2019), e00118, https://doi.org/10.1016/j.susmat.2019.e00118.
[208] H. Zheng, Y. He, Y. Zhu, L. Liu, X. Cui, Novel procedure of CO2capture of the CaO sorbent activator on the reaction of one-part alkali-activated slag, RSC Adv. 11 (2021) 12476–12483, https://doi.org/10.1039/d1ra01353j.
[209] A. Hajimohammadi, J.L. Provis, J.S.J. Van Deventer, One-part geopolymer mixes from geothermal silica and sodium aluminate, Ind. Eng. Chem. Res. 47 (2008) 9396–9405.
[210] Y.M. Liew, C.Y. Heah, L. yuan Li, N.A. Jaya, M.M.A.B. Abdullah, S.J. Tan, K. Hussin, Formation of one-part-mixing geopolymers and geopolymer ceramics from geopolymer powder, Construct. Build. Mater. 156 (2017) 9–18, https://doi.org/10.1016/j.conbuildmat.2017.08.110.
[211] P. Suwanmaneechot, T. Nochaiya, P. Julphunthong, Improvement , characterization and use of waste corn cob ash in cement-based materials Improvement , characterization and use of waste corn cob ash in cement-based materials, IOP Conf. Ser. Mater. Sci. Eng. 103 (2015), 012023, https://doi.org/10.1088/1757-899X/103/1/012023.
[212] T. Qi, H. Wang, G. Feng, X. Du, Z. Wang, S. Zhang, Effects of corn stalk fly ash (CSFA) on the mechanical and deformation properties of cemented coal Gangue backfill, Adv. Mater. Sci. Eng. 2020 (2020).
[213] B.S. Mohammed, S. Haruna, M.M.A. Wahab, M.S. Liew, A. Haruna, Mechanical and microstructural properties of high calcium fly ash one-part geopolymer cement made with granular activator, Heliyon 5 (2019), e02255, https://doi.org/10.1016/j.heliyon.2019.e02255.
[214] S. Haruna, B.S. Mohammed, M.M.A. Wahab, M.U. Kankia, M. Amran, A.M. Gora, Long-term strength development of fly ash-based one-part alkali-activated binders, Materials 14 (2021) 1–14, https://doi.org/10.3390/ma14154160.
[215] B. Nematollahi, J. Sanjayan, J. Qiu, E.H. Yang, High ductile behavior of a polyethylene fiber-reinforced one-part geopolymer composite: a micromechanics-based investigation, Arch. Civ. Mech. Eng. 17 (2017) 555–563, https://doi.org/10.1016/j.acme.2016.12.005.
[216] B. Nematollahi, J. Sanjayan, J. Qiu, E.H. Yang, Micromechanics-based investigation of a sustainable ambient temperature cured one-part strain hardening geopolymer composite, Construct. Build. Mater. 131 (2017) 552–563, https://doi.org/10.1016/j.conbuildmat.2016.11.117.
[217] B.S. Mohammed, S. Haruna, M. Mubarak, M.S. Liew, Optimization and characterization of cast in-situ alkali-activated pastes by response surface methodology, Construct. Build. Mater. 225 (2019) 776–787, https://doi.org/10.1016/j.conbuildmat.2019.07.267.
[218] A. Galvão Souza Azevedo, K. Strecker, Kaolin, fly-ash and ceramic waste based alkali-activated materials production by the “one-part” method, Construct. Build. Mater. 269 (2021), https://doi.org/10.1016/j.conbuildmat.2020.121306.
[219] H.A. Abdel Gawwad, S. Abd El-Aleem, A.S. Ouda, Preparation and characterization of one-part non-Portland cement, Ceram. Int. 42 (2016) 220–228, https://doi.org/10.1016/j.ceramint.2015.08.096.
[220] M. Refaat, A. Mohsen, E.-S.A.R. Nasr, M. Kohail, Minimizing energy consumption to produce safe one-part alkali-activated materials, J. Clean. Prod. (2021), 129137, https://doi.org/10.1016/j.jclepro.2021.129137.
[221] M. Almakhadmeh, A.M. Soliman, Effects of mixing water temperatures on properties of one-part alkali-activated slag paste, Construct. Build. Mater. 266 (2021), 121030, https://doi.org/10.1016/j.conbuildmat.2020.121030.
[222] C. Liu, X. Yao, W. Zhang, Controlling the setting times of one-part alkali-activated slag by using honeycomb ceramics as carrier of sodium silicate activator, Construct. Build. Mater. 235 (2020), 117091, https://doi.org/10.1016/j.conbuildmat.2019.117091.
[223] H.A. Abdel-Gawwad, M.S. Mohammed, E.N. Ads, A novel eco-sustainable approach for the cleaner production of ready-mix alkali activated cement using industrial solid wastes and organic-based activator powder, J. Clean. Prod. 256 (2020), 120705, https://doi.org/10.1016/j.jclepro.2020.120705.
[224] M.X. Peng, Z.H. Wang, S.H. Shen, Q.G. Xiao, L.J. Li, Y.C. Tang, L.L. Hu, Alkali fusion of bentonite to synthesize one-part geopolymeric cements cured at elevated temperature by comparison with two-part ones, Construct. Build. Mater. 130 (2017) 103–112, https://doi.org/10.1016/j.conbuildmat.2016.11.010.
[225] D. Koloušek, J. Brus, M. Urbanova, J. Andertova, V. Hulinsky, J. Vorel, Preparation, structure and hydrothermal stability of alternative (sodium silicate-free) geopolymers, J. Mater. Sci. 42 (2007) 9267–9275, https://doi.org/10.1007/s10853-007-1910-5.
[226] M.X. Peng, Z.H. Wang, S.H. Shen, Q.G. Xiao, Synthesis, characterization and mechanisms of one-part geopolymeric cement by calcining low-quality kaolin with alkali, Mater. Struct. 48 (2015) 699–708, https://doi.org/10.1617/s11527-014-0350-3.
[227] I. Garcia-Lodeiro, A. Fernández-Jimenez, A. Palomo, Cements with a low clinker content: versatile use of raw materials, J. Sustain. Cem. Mater. 4 (2015) 140–151, https://doi.org/10.1080/21650373.2015.1040865.

[228] A.A.S. Tigue, R.A.J. Malenab, J.R. Dungca, D.E.C. Yu, M.A.B. Promentilla, Chemical stability and leaching behavior of one-part geopolymer from soil and coal fly ash mixtures, Minerals 8 (2018), https://doi.org/10.3390/min8090411.
[229] Y. Alrefaei, J.G. Dai, Tensile behavior and microstructure of hybrid fiber ambient cured one-part engineered geopolymer composites, Construct. Build. Mater. 184 (2018) 419–431, https://doi.org/10.1016/j.conbuildmat.2018.07.012.
[230] L. Coppola, D. Coffetti, E. Crotti, R. Dell'Aversano, G. Gazzaniga, The Influence of Heat and Steam Curing on the Properties of One-Part Fly Ash/Slag Alkali Activated Materials : Preliminary Results the Influence of Heat and Steam Curing on the Properties of One-Part Fly Ash/Slag Alkali Activated Materials : Prelimina, AIP Conf. Proc., 2019, 020038.
[231] S.H. Bong, B. Nematollahi, M. Xia, A. Nazari, J. Sanjayan, Properties of one-part geopolymer incorporating wollastonite as partial replacement of geopolymer precursor or sand, Mater. Lett. 263 (2020), 127236, https://doi.org/10.1016/j.matlet.2019.127236.
[232] T.H. Vu, N. Gowripalan, P. De Silva, A. Paradowska, U. Garbe, P. Kidd, V. Sirivivatnanon, Assessing carbonation in one-part fly ash/slag geopolymer mortar: change in pore characteristics using the state-of-the-art technique neutron tomography, Cem. Concr. Compos. 114 (2020), 103759, https://doi.org/10.1016/j.cemconcomp.2020.103759.
[233] Y. Min, J. Wu, B. Li, J. Zhang, Effects of fly ash content on the strength development of soft clay stabilized by one-Part Geopolymer under curing stress, J. Mater. Civ. Eng. 33 (2021), 04021274, https://doi.org/10.1061/(asce)mt.1943-5533.0003887.
[234] C.C. Ban, P.W. Ken, M. Ramli, Mechanical and durability performance of novel self-activating geopolymer mortars, Procedia Eng. 171 (2017) 564–571, https://doi.org/10.1016/j.proeng.2017.01.374.
[235] D. Ravikumar, N. Neithalath, Effects of activator characteristics on the reaction product formation in slag binders activated using alkali silicate powder and NaOH, Cem. Concr. Compos. 34 (2012) 809–818, https://doi.org/10.1016/j.cemconcomp.2012.03.006.
[236] T. Luukkonen, H. Sreenivasan, Z. Abdollahnejad, J. Yliniemi, A. Kantola, V.V. Telkki, P. Kinnunen, M. Illikainen, Influence of sodium silicate powder silica modulus for mechanical and chemical properties of dry-mix alkali-activated slag mortar, Construct. Build. Mater. 233 (2020), 117354, https://doi.org/10.1016/j.conbuildmat.2019.117354.
[237] A. Hajimohammadi, J.S.J. van Deventer, Solid reactant-based geopolymers from rice hull ash and sodium aluminate, Waste and Biomass Valorization 8 (2017) 2131–2140, https://doi.org/10.1007/s12649-016-9735-6.
[238] A. Fernández-Jiménez, I. Garcia-Lodeiro, O. Maltseva, A. Palomo, Hydration mechanisms of hybrid cements as a function of the way of addition of chemicals, J. Am. Ceram. Soc. 102 (2019) 427–436, https://doi.org/10.1111/jace.15939.
[239] B. Nematollahi, J. Sanjayan, F.U. Ahmed Shaikh, Tensile strain hardening behavior of PVA fiber-reinforced engineered geopolymer composite, J. Mater. Civ. Eng. 27 (2015), 04015001, https://doi.org/10.1061/(asce)mt.1943-5533.0001242.
[240] S.F.A. Shah, B. Chen, S.Y. Oderji, M. Aminul Haque, M.R. Ahmad, Comparative study on the effect of fiber type and content on the performance of one-part alkali-activated mortar, Construct. Build. Mater. 243 (2020), 118221, https://doi.org/10.1016/j.conbuildmat.2020.118221.
[241] D. Sood, K.M.A. Hossain, T. Manzur, M.J. Hasan, Developing geopolymer pastes using dry mixing technique, Proceedings, Annu. Conf. - Can. Soc. Civ. Eng. 2019-June (2019).
[242] D. Sood, K.M.A. Hossain, Optimizing precursors and reagents for the development of alkali-activated binders in ambient curing conditions, J. Compos. Sci. 5 (2021).
[243] D. Sood, K.M.A. Hossain, Fresh state, rheological and microstructural characteristics of alkali-activated mortars developed using novel dry mixing technique under ambient conditions, Appl. Sci. 11 (2021), https://doi.org/10.3390/app11198920.
[244] D. Sood, K.M.A. Hossain, Strength, fracture and durability characteristics of ambient cured alkali—activated mortars incorporating high calcium industrial wastes and powdered reagents, Crystals (2021) 11, https://doi.org/10.3390/cryst11101167.
[245] F. Matalkah, P. Soroushian, Synthesis and characterization of alkali aluminosilicate hydraulic cement that meets standard requirements for general use, Construct. Build. Mater. 158 (2018) 42–49, https://doi.org/10.1016/j.conbuildmat.2017.10.002.
[246] J. Il Choi, B.Y. Lee, R. Ranade, V.C. Li, Y. Lee, Ultra-high-ductile behavior of a polyethylene fiber-reinforced alkali-activated slag-based composite, Cem. Concr. Compos. 70 (2016) 153–158, https://doi.org/10.1016/j.cemconcomp.2016.04.002.
[247] Z. Abdollahnejad, M. Mastali, M. Falah, K.M. Shaad, T. Luukkonen, M. Illikainen, Durability of the reinforced one-Part Alkali-activated slag mortars with different fibers, Waste and Biomass Valorization 12 (2021) 487–501, https://doi.org/10.1007/s12649-020-00958-x.
[248] F. Collins, J.G. Sanjayan, Early age strength and workability of slag pastes activated by sodium silicates, Mag. Concr. Res. 53 (2001) 321–326, https://doi.org/10.1680/macr.2001.53.5.321.
[249] Z. Abdollahnejad, C. Jesus, F. Pacheco-Torgal, J.B. Aguiar, One-part geopolymers versus ordinary Portland cement (OPC) mortars: durability Assessment, Int. Conf. Wastes Solut. Treat. Oppor. (2013) 115–120, in: 2nd.
[250] Z. Abdollahnejada, P. Hlavacekb, S. Miraldoa, F. Pacheco-Torgala, J.L.B. de Aguiarc, Compressive strength, microstructure and hydration products of hybrid alkaline cements, Mater. Res. 17 (2014) 829–837, https://doi.org/10.4103/0972-0707.153053.
[251] Z. Abdollahnejad, F. Pacheco-Torgal, J.B. Aguiar, C. Jesus, Durability performance of fly ash based one-part geopolymer mortars, Key Eng. Mater. 634 (2015) 113–120. https://doi.org/10.4028/www.scientific.net/KEM.634.113.
[252] K. Yang, K. Lee, J. Song, M. Gong, Properties and sustainability of alkali-activated slag foamed concrete, J. Clean. Prod. 68 (2014) 226–233, https://doi.org/10.1016/j.jclepro.2013.12.068.
[253] S. Sim, D. Jeon, W.S. Yum, H. Song, D.H. Kim, J.E. Oh, Development of a clinker-free white binder of one-part CaO-activated GGBFS with TiO 2 addition, Construct. Build. Mater. 248 (2020), 118705, https://doi.org/10.1016/j.conbuildmat.2020.118705.
[254] Z. Abdollahnejad, S. Miraldo, F. Pacheco-Torgal, J.B. Aguiar, Cost-efficient one-part alkali-activated mortars with low global warming potential for floor heating systems applications, Eur. J. Environ. Civ. Eng. 21 (2017) 412–429, https://doi.org/10.1080/19648189.2015.1125392.